Chapter 7
A Bio-Physical NPZD Model to Assess Large-Scale Depletion Effects of Aquaculture

7.1 INTRODUCTION

Large scale mussel aquaculture can influence ecosystem level processes within the marine environment through the ability to filter large volumes of water, expel particulate wastes, and regenerate nutrients (Prins *et al.*, 1998; Smaal and Heral, 1998; Grant *et al.*, 2007). Cultured filter feeding mussels depend on the coastal ecosystem to supply food in the form of suspended particulate matter, and through their feeding behaviour, compete with other animals within the marine environment. This creates the potential for depleted food resources and the displacement of various components of the local food web (Gibbs, 2007). Large populations can lead to a variety of ecosystem effects, including the localised depletion of suspended matter (Incze *et al.*, 1981; Rodhouse and Roden, 1987; Dowd, 2005). In extreme cases bivalve grazing can have a significant reducing impact on primary production and even control phytoplankton biomass in a range of ecosystems (Officer *et al.*, 1982; Smaal and Prins, 1993; Prins *et al.*, 1998; Jiang and Gibbs, 2005). This 'top-down' control of the phytoplankton biomass implies that more traditional 'bottom-up' control (i.e nutrient loadings) becomes less important (Prins *et al.*, 1998).

This potential for change creates a strong need for the understanding of how bivalve culture interacts with and influences low trophic level process in its receiving environment (Gibbs, 2007). Estimating productive and ecological carrying capacities, and hence culture sustainability, is a fundamental concept. Mathematical models provide a tool for understanding and assessing potential interactions within these complex manipulated ecosystems. Integrated bio-physical models are required in order to consider the interacting populations in the coastal marine ecosystem along with hydrodynamic influences brought about by water circulation and mixing (Duarte *et al.*, 2003; Dowd, 2005). Strong feedbacks between shellfish culture and the planktonic ecosystem, directly through the consumption of phytoplankton and excretion of ammonium, and indirectly through alterations to local nutrient cycling, imply that satisfactory estimates of carrying capacities can only be achieved by mathematical models incorporating these feedback processes (Prins *et al.*, 1998; Ross *et al.*, 1999).

7.2 MOTIVATION AND RELEVANCE TO THESIS OBJECTIVES

At the ecosystem level, ecosystem carrying capacity can be defined as "*the level to which a process or variable may be changed within a particular ecosystem, without driving the structure or function of the ecosystem over certain acceptable limits*" (Duarte *et al.*, 2003; McKindsey *et al.*, 2006). Production carrying capacity, however, can be defined as "*the stocking density of bivalves at which harvests are maximised*" (Inglis *et al.*, 2000).

Often, the ecological sustainability of bivalve culture is examined through concepts of water residence times, primary production times, and bivalve clearance times (Dame and Prins, 1998; Gibbs, 2007). The morphological nature of the Bay of Plenty, however, renders some of these traditionally applied measures of sustainability impractical. For example, water residence times and the time taken for cultured bivalves to filter a volume equal to the embayment, while often a decisive factor in enclosed embayments with limited flushing and clearly defined boundaries, are rather inappropriate concepts on the open coast.

Generally, predictive modelling has focussed on cultured bivalve productive capacity through the use of spatially simplistic 'box' models (*e.g.* Raillard and Menesguen, 1994; Bacher *et al.*, 1998; Ross *et al.*, 1999; Grant *et al.*, 2007). Chappelle *et al.* (2000) and Dowd (2005) considered ecosystem effects using the box model approach. Although useful in many different ways, box models generally fail to reproduce some important dynamic processes that may effect ecosystem functioning (Duarte *et al.*, 2003). Specific to the Bay of Plenty, these processes include non-simplified wind driven influences on currents, the inherently 3-dimensional process of coastal upwelling and density driven river dispersal, and non-simplified light and temperature regimes. Notwithstanding these shortcomings of box models, the morphology of open coastal areas such as the Bay of Plenty do not lend themselves to being split into a small number of aggregate boxes (*cf.* enclosed bays and harbours). Such coarse spatial resolution models can mask localised food depletion and tend to over-estimate environmental carrying capacities (Duarte *et al.*, 2003). A solution to these problems is fully coupled (in spatial and temporal senses) physical-biogeochemical models that simulate hydrodynamic transport phenomena along with chemical, biological, and ecological processes within a common framework.

Here, a general Nutrient-Zooplankton-Phytoplankton-Detritus (NZPD) type bio-physical model is coupled to a full 3-dimensional baroclinic hydrodynamic simulation of the shelf environment for the purposes of investigating the depletion effects of large coastal bivalve culture on its supporting ecosystem. NPZ type models are inherently complex as they attempt to replicate complex physical dynamics (Franks *et al.*, 1986; Edwards *et al.*, 2000), often leading to simplifications of hydrodynamic processes and other environmental forcings (*e.g.* temperature and light regime). Biophysical models coupled to non-simplified hydrodynamics, and

including bivalve energetics, are particularly rare in the published literature (Duarte *et al.*, 2003). Such models allow not only the effects of individual mussel farms to be considered, but the cumulative, region wide effects to also be assessed, providing a distinct advantage over more locally focussed individualistic studies.

7.2.1 CHAPTER AIMS

The primary goal of the chapter is:

- to develop and apply a general mathematical modelling framework to assess the cumulative lower trophic ecosystem level depletion impacts of marine bivalve culture.

This goal is achieved through:

- the development of a fully spatially resolved bio-physical, lower trophic level NPZD model coupled to 3-dimensional hydrodynamic predictions, as developed in chapter 5;
- the application of the model to a realistic aquaculture scenario at an optimal site (chapter 6) within the Bay of Plenty to determine the level of food available and the cumulative depletion impacts of development;
- the assessment of predicted lower trophic level changes and comparisons to other ecosystems, nationally and world-wide, where bivalve aquaculture is located in order to determine typical carrying capacity estimates; and
- an analysis of model dynamics to highlight the model's response to parameters which have less empirical basis to their selected values in order to identify areas for further research and improve predictions.

7.3 ECOLOGICAL MODEL DEVELOPMENT/DESCRIPTION

A 3-dimensional Eulerian fixed stoichiometry NPZD ecological model has been developed specifically for this study. The model (first developed within MATLAB® in one, then two dimensions was subsequently translated to FORTRAN and 3-dimensional space) solves the multiple interactive equations for the state variables in an explicit, forward time-stepping scheme over a regular grid. The model loosely follows that described by Chapelle *et al.* (2000) with simplifications in some areas and added complexity in others, influence was also gained from other similar works (*e.g.* Bowie *et al.*, 1985; Duarte *et al.*, 2003; Dowd, 2005; Grant *et al.*, 2007).

The model was run in a de-coupled arrangement with the hydrodynamic model (Chapter 5) to simulate advective and dispersive processes along with water column temperatures and salinities. Output from the hydrodynamic model is used to force the NPZD model over an identical model grid (3000 x 3000 m x 10 depth layers), with the modelled temperature and salinity fields used within several of the ecological process rate equations. Interactions within the NPZD model occur within

a finite volume of water (3000 x 3000 m x layer depth). The applied model resolution is more suited to a cumulative, regional level of interest, reflecting the thesis aims, rather than smaller farm-level or inter-farm scales. Finer resolution grids could be nested within the larger grid over targeted areas of interest, using boundary information from the larger model, to provide worthwhile insights. This would address a key weakness of the published literature which in general applies over simplified boundary conditions for this task.

The model comprises 8 (9 in mussel farm runs) state variables, phytoplankton (P), Zooplankton (Z), ammonium (NH3), nitrate+nitrite (NOx), inorganic phosphorus (PO4), detrital nitrogen (DN), detrital phosphorus (DP), dissolved oxygen (DO), mussel biodeposits (BD_M, when appropriate) and 1 diagnostic variable, cultured mussels (M), (Figure 7.1, Table 7.1). Each of the state variables are either suspended or dissolved within the water column and are subject to transport by water motion and mixing, in addition to their own characteristic transport patterns (*e.g.* sinking by phytoplankton and detritus). A population of spatially fixed mussels can be superimposed on the system, however, note that they are distinguished from the other variables in that their biomass is prescribed at a steady state value (*e.g.* Chapelle *et al.*, 2000; Dowd, 2005). Other ecosystem components are prognostic in that they interact with each other and dynamically co-evolve.

Cultured mussels interact with the system through ingestion, excretion, faecal production, and respiration. Their population dynamics is assumed to be fixed, under the control of aquaculturists and, through harvesting and restocking, assumed to have a steady state biomass.

The fixed stoichiometry scheme of the model assumes that both phytoplankton and zooplankton comprise Carbon-Nitrogen-Phosphorus in the elemental Redfield (1934; 1958) ratios of 106:16:1, a standard assumption among similar fixed stoichiometry models. In practice, however, the luxury uptake of nutrients by phytoplankton has been observed, resulting in deviations from these ratios; the present model simplifies these processes.

Processes simulated by the model include (Figure 7.1):

- phytoplankton production;
- phytoplankton sedimentation;
- non-predatory phytoplankton death;
- zooplankton grazing;
- zooplankton excretion;
- zooplankton respiration;
- non-predatory zooplankton death;
- mineralization of suspended detritus;
- sedimentation of detritus;
- mineralization of detritus and biodeposits;
- nitrification of ammonia;
- re-aeration at the air-water interface;
- cultivated mussel ingestion of phytoplankton, zooplankton, and detritus; and
- cultivated mussel excretion and respiration.

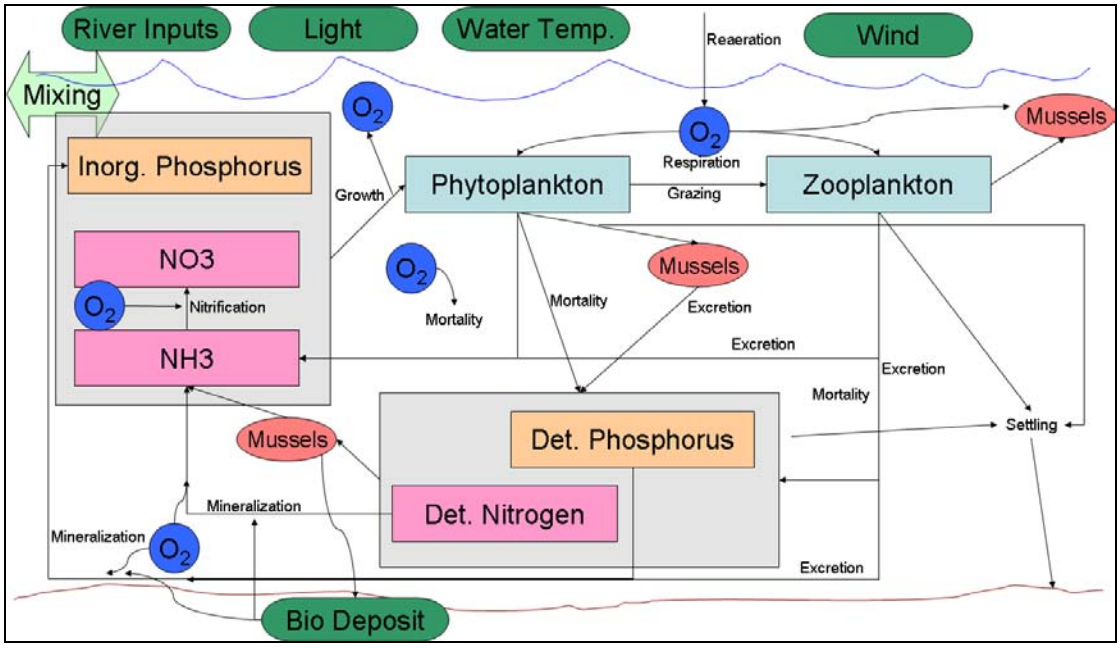

Figure 7.1 Conceptual diagram of processes and fluxes represented in the NPZD model.

Table 7.1 State variables, abbreviations and units used within the model.

State Variable	Abbreviation	Units
Phytoplankton (dry weight biomass)	P	$g.m^{-3}$
Zooplankton (dry weight biomass)	Z	$g.m^{-3}$
Nitrate + Nitrite	NOx	$g.m^{-3}$
Ammonium	NH3	$g.m^{-3}$
Detrital Nitrogen	DN	$g.m^{-3}$
Inorganic Phosphorus	PO4	$g.m^{-3}$
Detrital Phosphorus	DP	$g.m^{-3}$
Dissolved Oxygen	DO	$g.m^{-3}$
Bio-Deposits (when appropriate)	BD	$g.m^{-3}$

7.3.1 SYSTEM OF DIFFERENTIAL EQUATIONS

The numerical scheme of the model is governed by a system of interactive differential equations solving the changes in each state variable at each time step (*dt*). The equations are initially expressed in text (Table 7.2) and finally as full mathematical formulations (Table 7.3). Individual terms, variables, functions, and quantities are defined in subsequent sections. Note that mixing only acts on freely floating state variables and may act to increase or decrease concentrations. Mussels are assumed to maintain a constant biomass and participate actively in material cycling when included in model runs.

Table 7.2 System of differential equations used within the NPZD model expressed as words and processes.

$\frac{dP}{dt}$ = production(μ_P) - death(d_P) - grazing(G_{PZ}) - mussel filtering (G_{PM}) $\pm$ settling(P_{settle}) $\pm$ mixing

$\frac{dZ}{dt}$ = growth(g_Z) - death(d_z) - respiration(r_Z) - excretion(Z_{excr}) - mussel filtering(G_{ZM}) $\pm$ mixing

$\frac{d(DN, DP)}{dt}$ = generation - sedimentation - mineralization - mussel filtering $\pm$ mixing

$\frac{dNH_3}{dt}$ = generation - uptake - nitrification $\pm$ mixing

$\frac{dPO_4}{dt}$ = generation - uptake - nitrification $\pm$ mixing

$\frac{dNO_x}{dt}$ = nitrification - uptake $\pm$ mixing

$\frac{dDO}{dt}$ = production + reaeration - consumption $\pm$ mixing

$\frac{dMUSS}{dt}$ = 0 = harvest - (ingestion - excretion)

$\frac{dBD}{dt}$ = generation - mineralisation $\pm$ settling

Table 7.3 System of differential equations used within the NPZD model, see text for detailed explanation of terms.

$$\frac{dP}{dt} = \left(\mu_{P\max}.f(T).f(I).f(NO_xNH_3, PO_4) - d_{P\max}.f(T) - M_{CL}.M.E_{PM}\right)P$$
$$- \frac{\mu_Z}{E_{PZ}}.Z \pm settling \pm mixing$$

$$\frac{dZ}{dt} = \begin{pmatrix} g_{Zref}.f(T).f(Pt).E_{PZ} - r_{Zref}.f(T).\dfrac{\mu_Z}{E_{PZ}} - d_{zref}.f(T) \\ -\max(\dfrac{\mu_z}{E_{PZ}} - g_z - r_z - d_z, 0) - M_{CL}.M.E_{ZM} \end{pmatrix} Z \pm mixing$$

$$\frac{dDN}{dt} = (1-P_{\min I})d_P.RR_N.P + \left[d_Z.RR_N + (1-Z_{excr\min I}).Z_{excr}.RR_N\right]Z$$
$$-\left[MIN_{ref(N)}.f(T).f(DO) - M_{CL}.M.E_{DM}\right]DN \pm settling \pm mixing$$

$$\frac{dDP}{dt} = (1-P_{\min I})d_P.RR_P.P + \left[d_Z.RR_P + (1-Z_{excr\min I})Z_{excr}.RR_P\right]Z$$
$$-\left[MIN_{ref(P)}.f(T).f(DO) - M_{CL}.M.E_{DM}\right]DP \pm settling \pm mixing$$

$$\frac{dNH_3}{dt} = MIN_{ref(N)}.f(T).f(DO).DN + Z_{excr}.Z_{excr\min I}.RR_N.Z + \left[P_{\min I}.d_P.RR_N - \beta_{NH3}.\mu_P.RR_N\right]P$$
$$- N_R.NH_3 + M_{NH_3excrREF}.f(T).M + MIN_{BD}.RR_N.BD \pm mixing$$

$$\frac{dNO_x}{dt} = N_R.NH_3 - \left(1-\beta_{NH3}\right)\mu_P.RR_N.P \pm mixing$$

$$\frac{dPO_4}{dt} = MIN_{ref(P)}.f(T).f(DO).DP + Z_{excr}.Z_{excr\min I}.RR_P.Z + \left[P_{\min I}.d_P.RR_P - \mu_P.RR_P\right]P$$
$$+ MIN_{BD}.RR_P.BD \pm mixing$$

$$\frac{dDO}{dt} = \left[\mu_P + P_{\min I}.d_p\right]V_o.RR_C.P - \left[r_z + Z_{excr\min I}.Z_{excr}\right]V_o.RR_C.Z - MIN_{ref(N,P)}.f(T).f(DO).V_o.RR_{(C:N,P)}.D(N,P)$$
$$- 4.5714.N_R.NH_3 - M_{respref}.M + (DO_{sat} - DO)\left[\frac{(0.728W^{0.5} - 0.317W + 0.0372W^2)}{h} + 3.93\left(\frac{V^{0.5}}{h^{1.5}}\right)\right] \pm mixing$$

$$\frac{dBD}{dt} = \left[E_{PM}.P + E_{ZM}.Z + E_{DM}.\left(DP + DN\right)\right]M_{CL}.M.BD_{\%M}$$
$$- MIN_{BD}.BD \pm settling$$

7.3.2 PHYTOPLANKTON GROWTH

Phytoplankton growth (μ_p) is a function of light f(I), temperature f(T), and dissolved nutrients $f(NO_xNH_3,PO_4)$, (*e.g.* Raillard and Menesguen, 1994; Chapelle *et al.*, 2000; Duarte *et al.*, 2003; DHI, 2004):

$$\mu_P = \mu_{P\max}.f(T).f(I).f(NO_xNH_3,PO_4).P \qquad \textbf{Equation 7.1}$$

where μ_{Pmax} (day^{-1}) is the maximum daily growth rate of phytoplankton at a reference temperature (20^{o}C) under an optimal light and nutrient environment, $f(T)$, $f(I)$, and $f(NO_xNH_3,PO_4)$ are the temperature, light, and nutrient limitation functions respectively.

The temperature function $f(T)$ represents the effects of ambient temperature variations on algal growth. Elevated temperatures result in more rapid growth of phytoplankton (Eppley, 1972). The temperature function must be consistent with the reference temperature used in μ_{Pmax}. A widely used function in the literature is based on the Arrhenuis equation (Eppley, 1972).

$$f(T) = \theta^{(T-20^oC)} \qquad \textbf{Equation 7.2}$$

where θ is the temperature adjustment coefficient (with mean of 1.066, Eppley, 1972), and T is the ambient water temperature (^{o}C).

Separate growth limiting functions are computed for light and limiting nutrients (Bowie *et al.*, 1985). Each limiting factor varies between 0 and 1, with 0 resulting in the factor inhibiting all growth, and a value of 1 indicating no limitation due to the specific factor.

The light limitation factor must consider two aspects of the sub-surface light field, the effect of light on phytoplankton growth and the attenuation of light with depth.

Light attenuation with depth is modelled with Beer's Law (*e.g.* Duarte *et al.*, 2003):

$$I_{(z)} = I_o e^{-K_L z} \qquad \textbf{Equation 7.3}$$

where $I_{(z)}$ is the diurnally and seasonally varying solar radiation (W.m^{-2}) at depth z (m), I_o is the incoming solar radiation at the water surface (W.m^{-2}) and K_L is the extinction co-efficient (m^{-1}) of light within the water column. This equation is calculated over each time step and integrated over each depth layer (Raillard and Menesguen, 1994; Chapelle *et al.*, 2000; Dowd, 2005; Duarte *et al.*, 2003). The increased depth resolution of the model layers near the surface aids the schemes representation of realistic light fields.

Steele's (1965) photosynthesis-irradiance function is used to simulate the effect of light levels on phytoplankton growth (Figure 7.2). This function incorporates the photo-inhibition effect at higher than optimal light levels and is relatively widely used in the literature (Thomann and Kirkpatrick, 1982; Bowie *et al.* 1985 and references therein; Raillard and Menesguen, 1994; Chappelle *et al.*, 2000; Duarte *et al.*, 2003). The function is,

$$f(I) = \frac{I_z}{I_{opt}} e^{\left(1 - \frac{I_z}{I_{opt}}\right)}$$ **Equation 7.4**

where I_{opt} is the optimal light intensity (W m^{-2}) (prior to photo-inhibition), (Figure 7.2). Note that self-shading by phytoplankton is not considered within the model at present; the single light attenuation coefficient is used to represent a non-varying (in space and time) light decay.

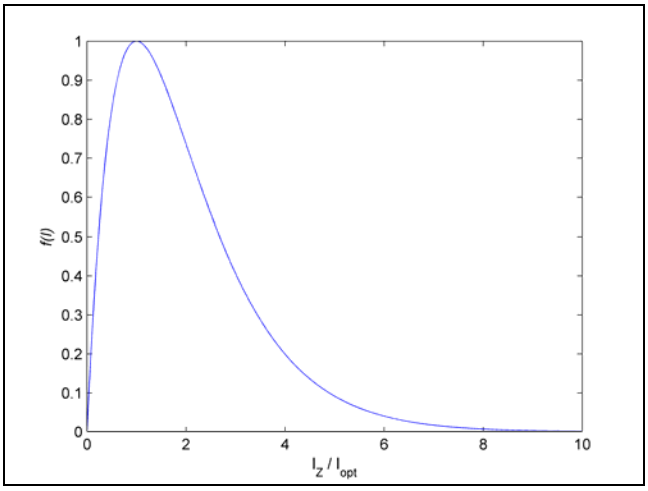

Figure 7.2 Steele's (1965) light function used in the calculation of the production of phytoplankton relative to the apparent light intensity and the optimal light intensity.

Additionally, dissolved nutrients influence phytoplankton growth. In general the limiting nutrient is nitrogen, however under certain conditions phosphorus can limit production. A Michaelis-Menten function (Figure 7.3) is used to describe the nutrient limitation effects on phytoplankton growth, $f(NO_xNH_3)$ or $f(PO_4)$, with respect to both nitrogen and phosphorus (*e.g.* Dugdale, 1967;Raillard and Menesguen, 1994; Dowd, 2005):

$$f(N) = \frac{N}{k_N + N}$$ **Equation 7.5**

where N is the nutrient concentration (g.m^{-3}) and k_N is the half saturation constant (g.m^{-3}) *i.e.* the concentration of the nutrient at which the rate of growth is half the maximum (Figure 7.3). A separate function f(N) is determined for both nitrogen (NOx + NH_3) and phosphorus (PO_4).

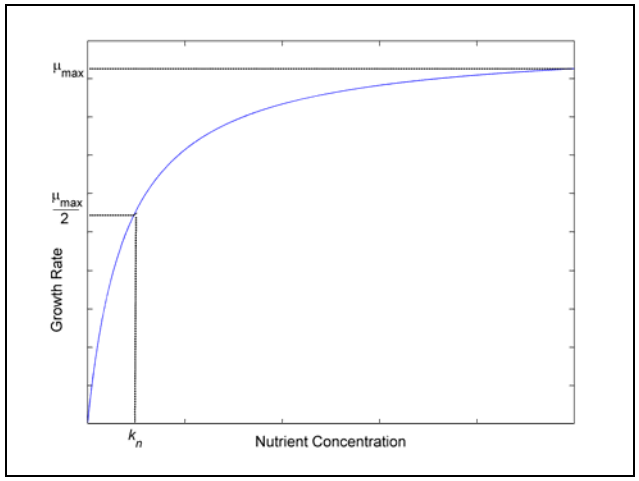

Figure 7.3 Algal growth rate and nutrient concentration modelled with the Michaelis-Menten function.

The fixed stoichiometry scheme of the model implies that nutrient uptake occurs in Redfield (1934; 1958) ratios (molar ratio of 106:16:1 for C:N:P) proportionately to phytoplankton growth, itself limited by the external pool of nutrients. Variable stoichiometry models allow for the luxury uptake of nutrients and their internal storage such that growth is limited by the internal pool of nutrients. This key difference, has led to the adoption of the harmonic mean or 'Bloomfield' formulation (*e.g.* O'Neil *et al.*, 1989; DHI, 2004) to combine the effects of both nitrogen limitation and phosphorus limitation (the light limitation function is multiplicative):

$$f(I)\,f(NO_xNH_3, PO_4) = f(I).\frac{2}{\frac{1}{f(NO_x + NH_3)} + \frac{1}{f(PO_4)}} \qquad \textbf{Equation 7.6}$$

By using the harmonic mean type approach, the influence of the luxury uptake of nutrients is simulated in a much more simplistic manner than that of a full variable stoichiometry model formulation. The harmonic mean implies that a severe shortage of one nutrient can be offset by abundant quantities of another. While this in itself is somewhat unrealistic, over short time periods, the internal pool of nutrients (not simulated in fixed stoichiometry models) can be used to overcome the external shortage. Indeed, O'Neill *et al.* (1989) in testing several multiple nutrient limitation formulations, identified the harmonic mean (along with 3 others) as performing well in fitting observed data. The formulation is not valid, however, if the shortages of required nutrients persist over long time-periods relative to the growth rate of the phytoplankton.

7.3.3 PHYTOPLANKTON SETTLING/MORTALITY

Non-predatory phytoplankton mortality is a significant process within the marine ecosystem; decaying material is partially mineralised in the water column (Jassby and Goldman, 1974). This process is modelled as a function of temperature (*e.g.* Eppley, 1972; Chapelle *et al.*, 2000; DHI, 2004):

$$d_P = d_{P\max}.f(T).P \qquad \textbf{Equation 7.7}$$

where d_P is the phytoplankton mortality rate (day^{-1}), and d_{Pmax} is the maximum non-predatory mortality rate (day^{-1}) at the reference temperature. The temperature function here has an identical form to that of phytoplankton growth (Equation 7.2).

Grazing on phytoplankton by zooplankton is back-calculated from zooplankton growth rates. This is a common method to determine zooplankton grazing rates (Bowie, 1985 and references therein):

$$G_{PZ} = \frac{\mu_Z}{E_{PZ}}.Z \qquad \textbf{Equation 7.8}$$

where G_{PZ} is the grazing on phytoplankton by zooplankton (g.day^{-1}), μ_Z is the zooplankton growth rate (day^{-1}), and E_{PZ} is the assimilation efficiency of the zooplankton, a constant percentage of grazing (Conover, 1966; Butler *et al.*, 1969).

Grazing on phytoplankton (G_{PM}), by cultured mussels (M) is reflected by (assuming a unit volume):

$$G_{PM} = M_{CL}.M.E_{PM}.P \qquad \textbf{Equation 7.9}$$

This equation is simplified somewhat in that the clearance rate is dependent on the size class of mussels (M) modelled within each cell. The details and factors influencing the mussel clearance (filtration) rate (M_{CL}, $m^3.g^{-1}.day^{-1}$) are detailed in a following mussel sub-model section.

Phytoplankton settling is simulated by incorporating a typical settling velocity for the entire phytoplankton population. The settling velocity is designated as a model constant and the effects of temperature on the density and viscosity of the water are incorporated through the use of a temperature function (Equation 7.2)

$$s = V_s \times \frac{157.5}{0.069T^2 - 5.3T + 177.6} \qquad \textbf{Equation 7.10}$$

(Tetra Tech, 1980)

where s is the temperature specific settling velocity ($m.day^{-1}$), V_s is the reference settling velocity at 20°C ($m.day^{-1}$), and T is the water temperature in °C.

7.3.4 ZOOPLANKTON GROWTH

Zooplankton growth (μ_Z) is a function of temperature, food availability, and the assimilation efficiency of the zooplankton (Dowd, 2005):

$$\mu_Z = g_{Zref}.f(T).f(Pt).E_{PZ}.Z \qquad \textbf{Equation 7.11}$$

where g_{Zref} is the reference zooplankton grazing rate at 20°C ($gP.gZ^{-1}.day^{-1}$), *f(T)* is a temperature function of similar form to Equation 7.2 (though with differing constants), and *f(Pt)* is a Michaelis-Menten limitation factor (Figure 7.3) based on food availability above the threshold value (Bowie *et al.*, 1985 and references therein; Dowd, 2005):

$$f(Pt) = \frac{P - P_T}{K_Z + P - P_T} \qquad \textbf{Equation 7.12}$$

where K_Z is the half saturation constant for zooplankton feeding and growth ($g.m^{-3}$), P is the food density (assumed to be phytoplankton) ($g.m^{-3}$), and P_T is the threshold food concentration, below which no feeding occurs ($g.m^{-3}$). The adoption of such thresholds is common practice in ecological models to prevent the complete removal of the 'food' (phytoplankton) and to represent decreased zooplankton-food interactions which take place at low food (phytoplankton) concentrations.

7.3.5 ZOOPLANKTON RESPIRATION

Zooplankton respiration is modelled as a function of both temperature and the activity of the zooplankton:

$$r_Z = r_{Zref}.f(T).\frac{\mu_Z}{E_{PZ}}.Z \qquad \textbf{Equation 7.13}$$

where r_Z is the respiration of the zooplankton (day^{-1}), r_{Zref} is the reference zooplankton respiration at 20C (day^{-1}), *f(T)* is a temperature function (Equation 7.2), and μ_Z is the zooplankton growth rate from Equation 7.11.

7.3.6 ZOOPLANKTON MORTALITY

Combined non-predatory and predatory zooplankton mortality (excluding that portion filtered by cultured mussels) is modelled as a function of temperature:

$$d_z = d_{zref} . f .(T).Z \qquad \textbf{Equation 7.14}$$

where d_{zref} is the reference zooplankton mortality at 20^oC (day^{-1}) and *f(T)* is a temperature function as in Equation 7.2.

Zooplankton are also grazed on by cultured mussels (G_{ZM}). Mussels are less effective at filtering zooplankton relative to phytoplankton (*e.g.* Zeldis *et al.*, 2004b; Lehane and Davenport, 2006). This is modelled through a reduced feeding efficacy of mussels on zooplankton (E_{ZM}) relative to that of phytoplankton. The equation is (assuming a unit volume):

$$G_{ZM} = M_{CL} .M .E_{ZM} .Z \qquad \textbf{Equation 7.15}$$

7.3.7 ZOOPLANKTON EXCRETION

Zooplankton excretion is modelled as the difference between grazing, production, and respiration, or 0 if losses are greater than growth (Goldman and Caron, 1985; Verity, 1985):

$$Z_{excr} = \max(\frac{\mu_z}{E_{PZ}} - g_z - r_z - d_z, 0).Z \qquad \textbf{Equation 7.16}$$

The excretion products enter the detritus and organic matter pools as detailed in the appropriate mass balance equations (Table 7.3).

7.3.8 DETRITUS GENERATION

Detritus is added to the water column through non-predatory phytoplankton and zooplankton mortality, and zooplankton excretion. Both DN and DP are simulated within the model. The equations for each are essentially the same, though differing constants and reference values reflect variations in the mineralisation processes.

A fraction (P_{minI}) of the non-predatory phytoplankton is immediately mineralised on death (DHI, 2004), the remainder contributes to the detritus pool according to:

$$D(N,P) \text{ from } d_P = (1 - P_{\min I}).d_P .RR_{(N,P)} .P \qquad \textbf{Equation 7.17}$$

where $RR_{(N,P)}$ is the Redfield ratio by mass of nitrogen or phosphorus in the decaying phytoplankton.

Zooplankton excretion and death also contribute to the detrital nutrient pool:

$$D(N,P) \text{ from } Z_{excr} \text{ and } d_z = \left[d_Z.RR_{(N,P)} + (1 - Z_{excr\min I}).Z_{excr}.RR_{(N,P)} \right] Z$$ **Equation 7.18**

where $Z_{excrminI}$ is the fraction of excreted zooplankton material which is mineralised immediately.

7.3.9 DETRITUS REMOVAL

Mineralisation processes convert the detrital forms of nitrogen and phosphorus *D(N,P)* into their inorganic forms as a function of the local temperature and oxygen environment (Nakanashi *et al.*, 1986; Chapelle *et al.*, 2000; DHI, 2004; Dowd, 2005):

$$D(N,P)\text{mineralisation} = MIN_{ref\,(N,P)}.f(T).f(DO).D(N,P)$$ **Equation 7.19**

where $MIN_{ref(N,P)}$ is the reference mineralization rate (day^{-1}) for nitrogen or phosphorus at 20^oC, *f(T)* is a temperature function of similar form to Equation 7.2 representing an increase in the rate of mineralization at elevated temperatures, and *f(DO)* is a dissolved oxygen function to indicate a reduction in mineralization at low oxygen concentrations:

$$f(DO) = \frac{DO^2}{DO^2 + DO_{MIN}}$$ **Equation 7.20**

where DO is the dissolved oxygen concentration of the water body ($g.m^{-3}$) and DO_{MIN} is the oxygen concentration at which reduced rates of mineralization occur due to a lack of dissolved oxygen ($g.m^{-3}$).

Detritus particles fall through the water column at a constant user defined rate.

Cultured mussels filter detrital particles from the water column (Gardner, 2002; Hatton *et al.*, 2005). The filtration of detritus from the water column by mussels is governed by the mussel clearance rate, temperature (included in M_{CL} equation), the mussel mass, and the mussel efficacy for filtering detritus particles (E_{DM}), and is represented by:

$$D(N,P) \text{ filtering by M} = M_{CL}.M.E_{DM}.D(N,P)$$ **Equation 7.21**

7.3.10 INORGANIC NUTRIENTS

7.3.10.1 AMMONIUM

Ammonium is generated through the mineralization of DN, the immediate mineralisation of fractions of phytoplankton death and zooplankton excretion (Equations 7.19, 7.7, and 7.16), by excretion from cultured mussels (Dame *et al.*, 1991; Prins *et al.*, 1998; James *et al.*, 2001; Ogivlie *et al.*, 2003), and by the mineralisation of mussel biodeposits. A fraction of dead phytoplankton and zooplankton excretion are immediately mineralised (DHI, 2004), according to:

$$NH_3(\text{and } PO_4) \text{ from } Z_{excr} = Z_{excr}.Z_{excr\min I}.RR_{(N,P)}.Z$$ **Equation 7.22**

$$NH_3 \text{ (and } PO_4) \text{ from } d_P = P_{\min I}.d_P.RR_{(N,P)}.P$$ **Equation 7.23**

Phytoplankton are able to use two forms of nitrogen (NOx and NH3) during uptake and growth, and often show a preference for NH3 (Bowie *et al.*, 1985; Collos *et al.*, 1997). To represent this, an NH3 preference factor is incorporated into the model, and the uptake equation for NH3 becomes (Bowie *et al*, 1985):

$$NH_3 uptake = \beta_{NH3}.\mu_P.RR_N.P \qquad \textbf{Equation 7.24}$$

where β_{NH3} is the NH3 preference factor, which can range from 1 (all the phytoplankton nitrogen requirements are gained from NH3) to 0 (all the phytoplankton nitrogen requirements are gained from nitrate). The value of the NH3 preference factor is a function of the relative concentrations of NH3 and NOx in the water column (Bowie, 1985; Chapelle *et al.*, 2000):

$$\beta_{NH3} = \frac{NH_3}{NH_3 + NO_x} \qquad \textbf{Equation 7.25}$$

NH3 is also consumed by nitrification processes converting NH3 to NOx. The nitrification rate (N_R) is based on a reference value and varies with temperature:

$$N_R = N_{Rref}\, f(T) \qquad \textbf{Equation 7.26}$$

where N_{Rref} is the reference nitrification rate (day^{-1}) at 20^{o}C.

Additionally, cultured mussels directly excrete NH3, which can influence nutrient levels in some regions (Dame *et al.*, 1991; Smaal and Prins, 1993; Prins *et al.*, 1998; James *et al.*, 2001; Ogilvie *et al.*, 2003). This NH3 source is detailed in the subsequent section on the mussel sub-model.

7.3.10.2 NITRATE / NITRITE

NOx is generated by the nitrification of NH3 (Equation 7.26) and removed through uptake by photosynthesisers. Oxidised nitrogen uptake is determined from the growth requirements of the phytoplankton (itself being limited by nutrient availability):

$$NO_x uptake = (1 - \beta_{NH3}).\mu_P.RR_N.P \qquad \textbf{Equation 7.27}$$

7.3.10.3 INORGANIC PHOSPHORUS

Inorganic phosphorus is generated through the mineralisation of DP, the immediate mineralisation of a fraction of zooplankton excretions and phytoplankton deaths (Equations 7.19, 7.7, and 7.16). Phytoplankton also uptake inorganic phosphorus during growth:

$$PO_4 uptake = \mu_P.RR_P.P \qquad \textbf{Equation 7.28}$$

7.3.11 DISSOLVED OXYGEN

Dissolved oxygen is modelled as the difference between both production and re-aeration and oxygen consumption. Oxygen is produced by photosynthesising

phytoplankton. A specific amount of oxygen is produced per gram of biomass growth (*e.g.* DHI, 2004):

$$\text{DO production by phytoplankton} = \mu_P.V_o.RR_C.P \qquad \textbf{Equation 7.29}$$

where V_o is the oxygen to biomass ratio at production (gO_2/g.algae). This stoichiometric O_2:C ratio can vary depending on the type of inorganic nitrogen used during phytoplankton growth (NH_3 = 106:106, NO_x = 138:106) (Morel, 1983). As a result, the mass of O_2 produced per gC can vary between 2.67 and 3.47 g, here, consistent with other modelling applications (DHI, 2004), a mean mass based O_2:C ratio is used (3.07 g.O_2/g.algae).

Oxygen is consumed through the immediate mineralisation of a fraction of dead phytoplankton and zooplankton excretions, the respiration of zooplankton, the mineralisation of DN and DP, the nitrification of NH3 to NOx, and cultured mussel respiration:

$$\text{DO consumption by phyto mortality} = P_{\min I}.d_p.V_o.RR_C.P \qquad \textbf{Equation 7.30}$$

$$\text{DO consumption by zoo excretion} = Z_{excr\,\min I}.d_Z.V_o.RR_C.Z \qquad \textbf{Equation 7.31}$$

$$\text{DO consumption by zoo respiration} = r_Z.V_o.RR_C.Z \qquad \textbf{Equation 7.32}$$

$$\text{DO consumption by mineralisation of detritus} = r_Z.V_o.RR_C.Z \qquad \textbf{Equation 7.33}$$

$$\text{DO cons. by min. detritus} = MIN_{ref\,(N,P)}.f(T).f(DO).V_o.RR_{(C:N,P)}.D(N,P) \qquad \textbf{Equation 7.34}$$

$$\text{DO cons. by nitrification} = 4.5714.N_R.NH_3 \qquad \textbf{Equation 7.35}$$

where the mass of phytoplankton and zooplankton are converted to equivalent units of carbon using Redfield ratios, and the nitrification of NH3 is governed by the equation $NH_4 + 2O_2 > NO_3 + H_2O + H$, resulting in the consumption of 4.5714 g of oxygen for every gram of N converted.

Reaeration (DO_{rear}) occurs at the water surface only (*i.e.* the top model layer), and is governed by the saturated dissolved oxygen concentration (DO_{sat}), the water temperature (T) and salinity (S), the existing dissolved oxygen concentration (DO), the wind speed (W), depth of the surface layer (h), and the surface water velocity (V) (Thomann and Kirkpatrick, 1982):

$$DO_{sat} = 14.652 - 0.0841S + T\left(0.00256S - 0.41022 + T\left[0.007991 - 0.0000374S - 0.000077774T\right]\right) \qquad \textbf{Equation 7.36}$$

$$DO_{\text{rear}} = (DO_{sat} - DO)\left[\frac{(0.728W^{0.5} - 0.317W + 0.0372W^2)}{h} + 3.93\left(\frac{V^{0.5}}{h^{1.5}}\right)\right] \qquad \textbf{Equation 7.37}$$

7.4 MUSSEL SUB-MODEL

7.4.1 MUSSEL CLEARANCE/FILTRATION RATES

Mussel filtering in many carrying capacity models assumes a constant value, sometimes varying with shellfish size or temperature (*e.g.* Raillard and Menesguen, 1994; Chapelle *et al.*, 2000; Dowd, 2005). However, several studies have identified relationships between mussel clearance rates and food concentration (Winter, 1978; Widdows *et al.*, 1979; Gardner, 2002). Specific to *Perna canaliculus*, a substantial body of literature is emerging investigating feeding behaviour and relationships (Waite, 1989; Hawkins *et al.*, 1999; Marsden and Weatherhead, 1999; James *et al.*, 2001; Gardner, 2002; Hatton *et al.*, 2005). General conclusions are that these mussels are capable of quickly adapting their feeding behaviour to compensate for changes in food supply (Hatton *et al.*, 2005).

James *et al.* (2001) observed that clearance rates of greenshell mussels vary linearly with mussel size at low Chl-a concentrations (0.27-1.09 $mg.m^{-3}$), while Hatton *et al.* (2005) identified a similar relationship at higher Chl-a concentrations (3.3-6.0 $mg.m^{-3}$), more typical of the Bay of Plenty environment. Improved correlations are obtained by including other particulate organic matter, in addition to phytoplankton, as the mussels' food source (Gardner, 2002; Hatton *et al.*, 2005). Gardner (2002) provides statistically significant ($p<0.001$) best fit linear relationships between weight standardised (mussel dry weight) clearance rates (M_{CL}, $m^3.g^{-1}.day^{-1}$) and particulate organic matter (*POM*), obtained over a '*full range of seston conditions*'. However, Widdows *et al.* (1979), Hawkins *et al.* (1999), and Ren and Ross (2005) note that at high seston concentrations clearance rates can plateau and even decrease as mussels are able to meet their nutritional requirements for less physiological effort.

Here, this limit is assumed to be represented by the upper limit of seston concentrations within Gardner's (2002) relationship (7.0 $g.m^{-3}$ Chl-a, corresponding to a clearance rate [$M_{CL}max$] of 0.1051 $m^3.g^{-1}.day^{-1}$). Following these concepts, the clearance rate of cultured mussels is modelled as a function of mussel size, seston concentration (phytoplankton + detrital particles), and ambient temperature (Duarte *et al.*, 2003; Ren and Ross, 2005). We infer *POM* to comprise phytoplankton and detrital particles (converted to biomass through Redfield ratios), providing:

$$M_{CL} = \min\left(f(T)\left[M_{CL}c + M_{CL}m\left(P + \frac{DN}{RR_N} \right) \right]\frac{24}{1000}, M_{CL}\max \right) \text{ (per } g^{-1}\text{D.W. individual mussel)}$$

Equation 7.38

where $M_{CL}c$ and $M_{CL}m$ are the coefficients from Gardner's (2002) relationship, 2.07 and 0.33 respectively. The equations on which this relationship is based are valid at an individual mussel level and vary linearly with mussel size. Therefore, clearance rates of individual mussels of various size fractions are determined based on expected stocking densities of farms and multiplied by the number of mussels of that fraction within the model cell.

Hatton *et al.* (2005) showed that mussel feeding efficacy (E_{PM}, E_{ZM}, E_{DM}) is generally constant with variability in mussel size and food supply, justifying the use of constant values within the model.

7.4.2 AMMONIA EXCRETION BY MUSSELS

Cultured mussels directly excrete NH3, which can influence nutrient levels and phytoplankton biomass in some regions (Dame *et al.*, 1991; Smaal and Prins, 1993; Prins *et al.*, 1998; James *et al.*, 2001; Ogilvie *et al.*, 2003). Direct estimates of excretion rates of greenshell mussels are limited to those of Marsden and Weatherhead (1999) and James *et al.* (2001). The rates presented in each of these papers are expected to over-estimate NH3 excretion by cultured bivalves within the Bay of Plenty as both studies measured release rates at times of high relative stress. The very low food concentrations during the study of James *et al.* (2001) and periodic desiccation of intertidal mussels during the study of Marsden and Weatherhead (1999) are likely to have resulted in some degree of body tissue break down and increased NH3 excretion (Bayne *et al.*, 1976; Hawkins *et al.*, 1999).

While the rates of James *et al.* (2001) can reliably be applied at times of low food concentration (*i.e.* Chl-a < 0.5 $mg.m^{-3}$), those at higher food concentrations must be inferred from other mussel species due to a lack of published data specific to sub-tidal moderate-high Chl-a environments. Bayne and Scullard (1977) and Smaal and Prins (1993) report excretion rates between $4x10^{-5}$ and $1x10^{-4}$ gNH_3 gDW day^{-1}, with a mean value of $7x10^{-5}$, for *Mytilus* mussel species.

Following these concepts, at Chl-a concentrations in excess of 0.5 $mg.m^{-3}$ a constant value ($M_{excrNH3REF}$) of $7x10^{-5}$ (day^{-1}) is applied, at Chl-a concentrations below 0.38 $mg.m^{-3}$, the limit of James *et al.*'s (2001) measurements, their relationship is applied, and a linear fit between these values is used during intermediary conditions:

where P > 0.5 ($mg.m^{-3}$ Chl-a)

$$M_{NH3}excretion = M_{excrNH3REF} M_{DW}$$ (Bayne and Scullard, 1977; Smaal and Prins 1994)

where 0.38 < P < 0.5 ($mg.m^{-3}$ Chl-a)
linear fit based on the local Chl-a concentration and
the excretion boundaries (see equations above and below)

where P < 0.38 ($mg.m^{-3}$ Chl-a)

$$M_{NH3}excretion = M_{excrNH3} A.M_{DW}^{M_{excrNH3}b} \times \frac{24}{10^6}$$ (James et al., 2001)

Equation 7.39

where $M_{excrNH3}A$ = 61.46 and $M_{excrNH3}b$ = 0.996 from James *et al.*'s (2001) results.

7.4.3 MUSSEL RESPIRATION

Mussel respiration is modelled as a function of individual animal size (Bayne *et al.*, 1976; James *et al.*, 2001). Using data from James *et al.* (2001), the oxygen consumption (g.day^{-1}) by individual mussels is expressed as:

$$\text{DO cons. by mussel respiration} = M_{resp}A \times M_{DW}{}^{M_{resp}b} \text{ (per g}^{-1}\text{D.W. individual mussel)}$$

Equation 7.40

where $M_{resp}A$ and $M_{resp}b$ are constants (modified for consistency with units) from data presented by James *et al.* (2001), with values of 0.0126 and 0.535.

7.4.4 BIODEPOSITS

The generation of biodeposits by cultured mussels (*e.g.* Pearson and Rosenburg, 1978; Dahlback and Gunnarsson, 1981; Prins *et al.*, 1998) is modelled as a constant percentage ($BD_{\%M}$) of mussel feeding (*e.g.* Chapelle *et al.*, 2000), itself a function of the seston concentration and temperature, and is calculated individually, multiplied by the number of mussels of each size class, and summed with other classes over each model cell:

$$BDgeneration = BD_{\%M} M_{CL}.M.E_{(P,Z,DN,DP:M)}(P,Z,DN,DP)$$

Equation 7.41

The mineralisation of mussel biodeposits (*BD*) on the sea bed, and as they fall through the water column, is simulated as a constant rate process and generates both NH3 and DRP:

$$BD\text{mineralisation} = MIN_{BD}.RR_{(N,P)}.BD \qquad \textbf{Equation 7.42}$$

where MIN_{BD} is the reference mineralisation rate of biodeposits (day^{-1}), taken to be 0.05 (Jorgensen *et al.*, 1991; Smaal and Prins, 1993).

7.5 MODEL LIMITATIONS

The present NPZD model is a simplification of the ecosystem it attempts to represent. Whilst simplification is an inherent property of all models, a discussion of limitations resulting from these simplifications is judicious.

The grid resolution of the present model (3000 m) while necessary as a result of the area under consideration, the 3-dimensional model scheme, and computational limitations, is adequate for identifying farm-scale and larger regional-scale changes. The resolution, however, provides no indication of intra-farm impacts or influences. Such impacts may include the regeneration of phytoplankton between mussel culture 'backbone' lines and the effects of mussel farm structures on flow velocities and mixing at farm-scales or lower. Investigating these effects could be performed by nesting a finer scale grid within the larger model, providing much improved boundary condition information than that generally found within the scientific literature.

The fixed stoichiometry scheme of the model fails to simulate the luxury uptake of nutrients and internal reserves of key nutrients. Individual cell stoichiometry can vary with age, size, physiological, or environmental condition (Bowie *et al.*, 1985). Variably stoichiometry models require many more (~2-3 times) model coefficients for each size class of phytoplankton modelled. For the present case, with no reliable data sources on which to base estimates of these values, the added complexity is likely to be less than useful. The use of a harmonic mean formulation for phytoplankton nutrient limitation (Equation 7.6) implies that large quantities of one nutrient can offset severe limitations in another. However, this approach combats the negative aspects of a fixed stoichiometry scheme in a simplistic manner. The harmonic mean formulation allows growth to continue (although slows it considerably) during a relative shortage of a single nutrient in a similar way to allowing the use of an 'internal nutrient pool' in a variable stoichiometry model. Further, O'Neil *et al.* (1989) identified this multiple nutrient limitation formulation as representing observed data well.

As previously discussed (Section 7.10.2), the simulation of a single size class of phytoplankton prevents any insights into potential changes in phytoplankton community structure as a result of mussel feeding. The addition of further size classes increases complexity, computational effort, and the need for calibration data and relatively unknown model constants and parameters. Single size class models are common amongst similar applications (*e.g.* Raillard and Menesguen, 1994; Duarte *et al.*, 2003; Dowd, 2005; Grant *et al.*, 2007), additionally, the present model like these examples does not consider turbidity effects or self shading by phytoplankton or zooplankton in the light attenuation model.

The model does not consider the general process of benthic nutrient mineralisation. While the mineralisation of detritus and bio-deposits continues once they settle to the seabed, the rate of these processes continues at those determined by the ambient water conditions rather than those within the sediment. Several studies have identified that between ~10 and ~15 % of nutrients used for production on continental shelves are remineralised locally through sediments (Rowe *et al.*, 1975; Lohse *et al.*, 1998; Jahnke *et al.*, 2005). There is an argument that the contribution of remineralised nutrient supply to the Bay of Plenty shelf may be at the lower end as a result of the strong upwelling dynamics.

Calibration data and their restricted spatial and temporal density, an inherent function of the types of data required and the cost and effort required to sample them, limit most ecological model studies. The present study is no different. While spatially dense time-series measurements of all the models state variables would be ideal, practical considerations restrict the number of measurements, the time-frequency of surveys, and the spatial extent of survey sites.

A lack of zooplankton concentration data have been a major setback during these modelling efforts. Additionally, the general lack of literature and knowledge surrounding the significance of aquaculture induced zooplankton mortality with respect to the recruitment of other water-borne marine organisms and potential impacts of mussel spat colonization at new locations outside the marine farms (resulting in decreased marine biodiversity and/or community change) have restricted conclusive abilities.

While the model simulates an entire year (2003-2004), it must be highlighted that the results and predictions serve only as a guide for resource management options. Climatological and inter-annual variability may induce changes in nutrient delivery and environmental forcings which cannot be simulated by a single year of modeling.

Despite these limitations the present model represents an advancement over most aquaculture modelling studies in several key aspects. The application of the model over a full 3-dimensional regular model grid has several benefits over the often applied box model concept (e.g. Raillard and Menesguen, 1994; Bacher *et al.*, 1998; Chapelle *et al.*, 2000; Grant *et al.*, 2007). Box models greatly simplify hydrodynamic processes through their lack of spatial resolution, and hence have no predictive or conclusive abilities at scales finer than the boxes themselves (often 4-5 per region). In addition, the oversimplification of environmental forcings such as winds, light levels, and temperatures into seasonal functions is characteristic of the literature (Raillard and Menesguen, 1994; Chapelle *et al.*, 2000; Dowd, 2005; Grant *et al.*, 2007); the present model utilises non-simplified measured or inferred (QuikSCAT) wind and light levels, and calibrated modelled temperatures (Figure 5.19). Further, despite their importance, some models fail to consider several important feedback processes between significant quantities of bivalve filter feeders (*i.e.* aquaculture development) and ecosystem functioning, for example the excretion of ammonia and pseudo-faeces and localised alterations to nutrient cycling (Prins *et al.*, 1998); the present model replicates these processes.

7.6 APPLICATION TO THE BAY OF PLENTY SHELF

7.6.1 INITIAL CONDITIONS (HOTSTART)

Initial conditions must be specified for each state variable at the beginning of the model run over the entire 3-dimensional grid. This represents a significant challenge. The effort, time, and cost required to sample these parameters generally results in limited temporal and spatial datasets. Data which are available include analysed water samples collected concurrently with the CTD casts (Chapter 4), remotely sensed chlorophyll biomass estimates at 3-daily intervals (Chapter 4), and 3rd party sources such as the WOD (Boyer *et al.*, 2006). Recognising the inherent difficulties in assigning these values, a strategy of timing the modelling period such that the model starts at a time of low biologic productivity and complexity (1-August, mid-late winter) was implemented. The selection of this period allows for

some flexibility in the setting of these initial conditions relative to other times *e.g.* the growth or decay of the spring bloom.

Initial estimates of phytoplankton biomass are inferred from SeaWiFs data corresponding to 6 August, 2003 (Figure 7.4). These data represent the nearest cloud free day for which data were available over the region. Chlorophyll data were converted to carbon biomass at an assumed ratio of 2% (Bowie *et al.*, 1985; Jorgensen *et al.*, 1991; Grant *et al.*, 1998; Duarte *et al.*, 2003; Dowd, 2005). While not ideal, these conversions are required to convert modelled biomass and the more easily and frequently measured Chl-a data (Chapelle *et al.*, 2000; Duarte *et al.*, 2003; Cugier *et al.*, 2005; Dowd, 2005). Though there are known issues with this dataset (Section 4.4.6), these data represent the best (and only) available data on which to base initial estimates of phytoplankton concentration. A vertical profile was inferred from these surface values with concentrations increasing linearly to a depth of 20 m (biomass 2x surface values) and then decreasing exponentially to a fixed value of 0.1 gm^{-3} (Chl-a) at depths of 200 m, consistent with CTD measurements. With no data on which to base initial zooplankton concentrations a ratio of zooplankton to phytoplankton biomass of 0.75:1 was employed. This ratio was developed from stability tests with the model in one-dimensional form, and is consistent with ratios inferred from other similar modelling applications (*e.g.* Chapelle *et al.*, 2000; Dowd, 2005).

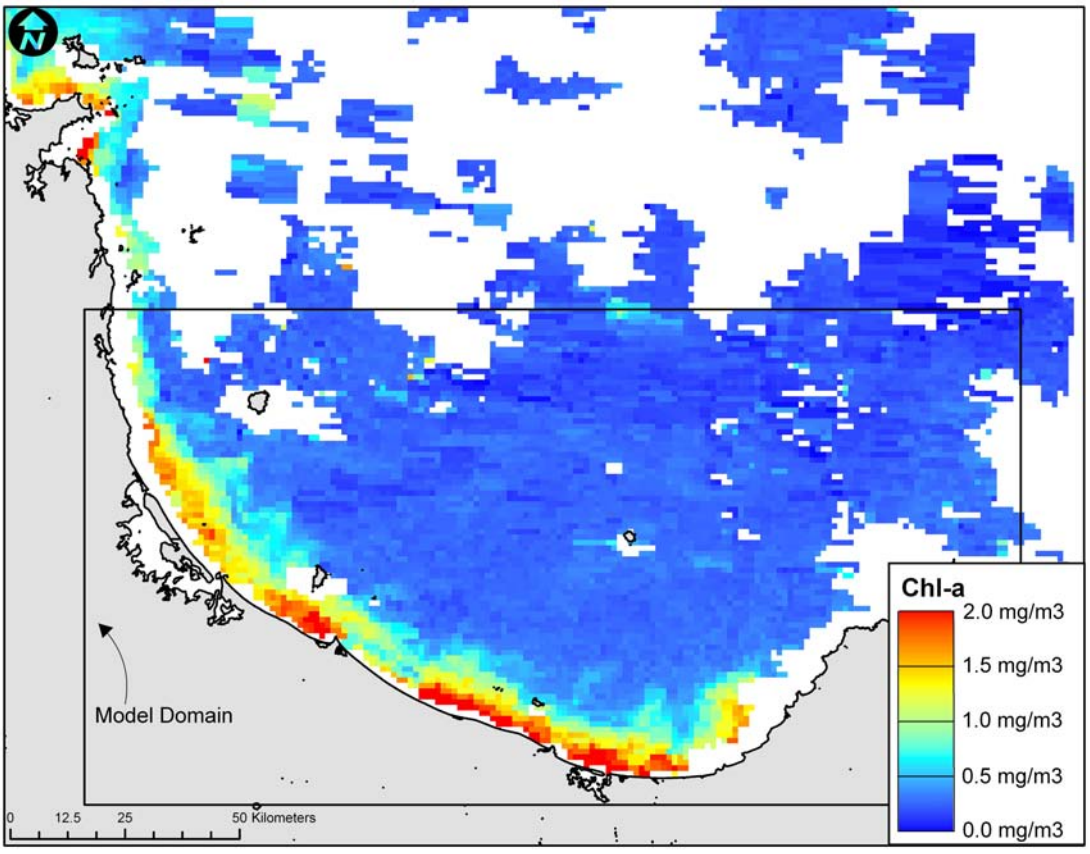

Figure 7.4 SeaWiFS 3-day mean CHL-a data from 6-August-2007. These data were spatially smoothed to fill in cloud gaps and used to determine the initial phytoplankton concentrations for the model.

Profiles of nitrate and phosphorus within 200 km of the model boundaries were obtained from the WOD (Boyer *et al.*, 2006). A total of 19 profiles, obtained between 6/3/1991 and 2/9/1992, contain nutrient (nitrate and phosphorus) data (Figure 7.5a,b). Near-shore sample data obtained from water samples during the CTD surveys (Chapter 4) complement the dataset providing coverage of both nearshore regions. The data display strong linear relationships (R = 0.98 and 0.97) with temperature (Figure 7.5c,d). On the basis of these relationships nitrate and phosphorus concentrations were inferred from the initial temperatures as described for the hydrodynamic model (see Section 5.6.1.6 and subsequent sections for a description).

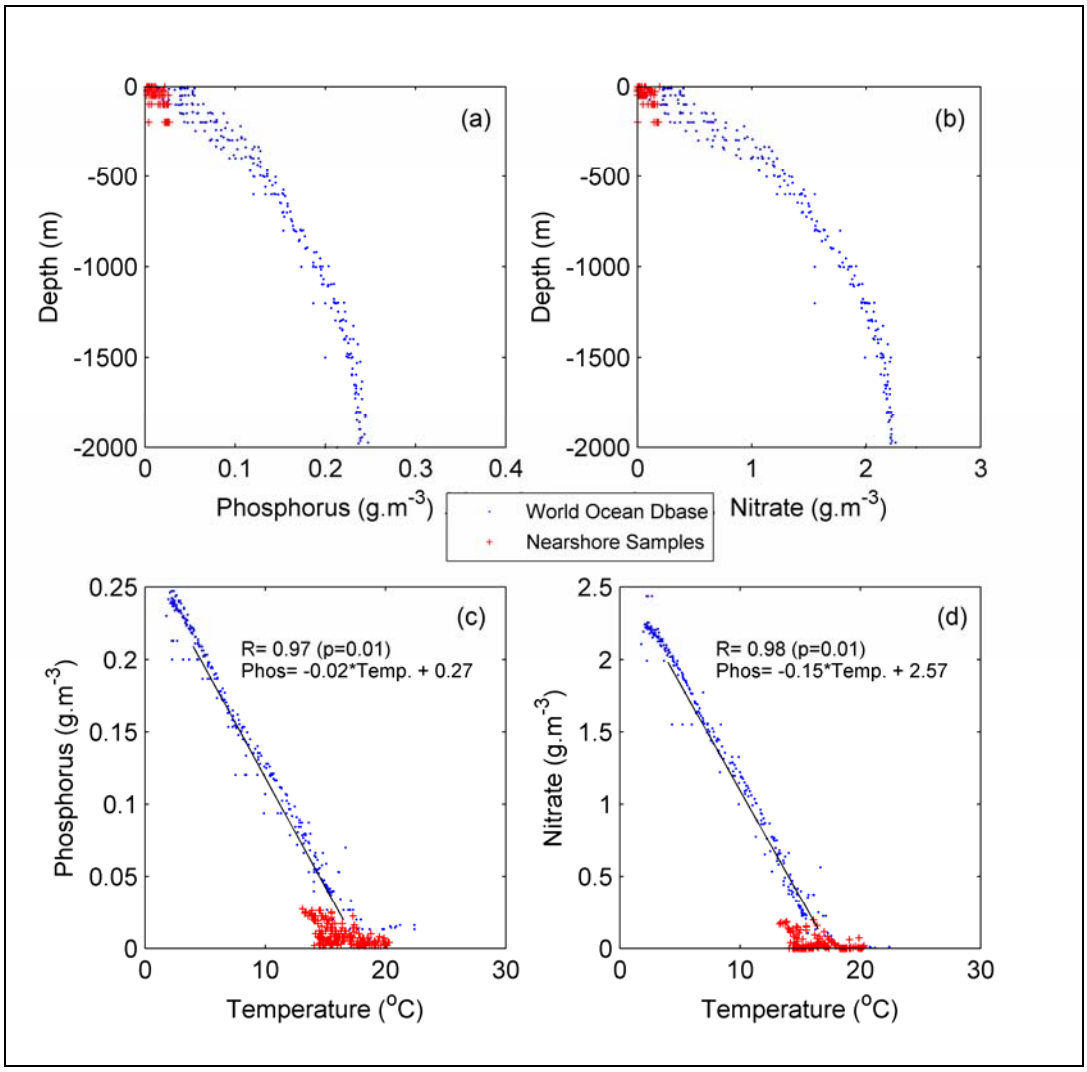

Figure 7.5 Phosphorus (a) and nitrate (b) profiles with depth from both the World Ocean Database (Boyer *et al.*, 2006), (blue dots), and from the Bay of Plenty shelf (red crosses, see Chapter 4). Phosphorus (c) and nitrate (d) relationships with temperature are strongly linear, the derived relationship is used to infer phosphorus and nitrate concentrations throughout the model domain for the hot-start, and also for the boundary conditions.

Initial values of DN, DP, and NH3 were set to constant values across the grid, based on nearshore water samples, 0.15 0.015, and 0.01 $g.m^{-3}$ respectively. DO concentrations were assigned saturation values based on the ambient temperature and salinity conditions at the initialisation of the hydrodynamic model. The model is

expected to quickly simulate any areas of oxygen demand as a result of the dynamic processes operating.

7.6.2 BOUNDARY CONDITIONS

Time-series boundary conditions were generated for each state variable at the two open boundaries (North and East) and for each of the 10 rivers modelled in the hydrodynamics. Open boundaries were specified in an identical fashion to the initial conditions; phytoplankton concentrations being inferred from 3-day composites of SeaWiFS data and a depth profile consistent with observations and initial conditions assigned. Zooplankton biomass was inferred as 75% of the total phytoplankton biomass. Concentrations of inorganic nitrogen and phosphorus were inferred from temperature boundary conditions employed within the hydrodynamic model and the observed nutrient–temperature relationships (Figure 7.5c,d). Where temperature boundary data were elevated beyond the range of the observations (*e.g.* > ~19^{o}C, Figure 7.5c,d), minimal values of 0.005 and 0.05 g.m^{-3} were applied for PO4 and NOx respectively. Concentrations of DN, DP, and NH3 were assigned constant values consistent with the initial conditions. DO was assumed to be at saturated levels, dependent on the ambient temperature and salinity conditions.

Rivers along the Bay of Plenty coastline can act as a significant source for both inorganic and organic nitrogen and phosphorus (*e.g.* Taylor and Park, 2001). Ten rivers were modelled along the Bay of Plenty coastline (Section 5.6.1.3 and Figure 5.9), their impacts on flow conditions determined by the hydrodynamic model. The regional council (EBOP) have been monitoring the concentrations of inorganic and organic nitrogen and phosphorus in these rivers since 1989 (Taylor and Park, 2001). Data from these surveys were used to calculate mean concentrations of NOx, DRP, NH3, DN, DP, and DO for each modelled river. These concentrations were multiplied by the observed time series of flow rates for each river to determine a time series of mass for each variable which is diluted within the model domain from the appropriate river cell.

7.6.3 MODEL PARAMETERS

Table 7.4 List of parameters, definitions, values and sources used within the model

Parameter	Definition	Value	Reference
Phytoplankton			
μ_{Pmax}	Phytoplankton maximum daily growth rate (@20C)	1.0 day^{-1}	Calibrated
I_{opt}	Optimal light intensity for phytoplankton growth	70 $W.m^{-2}$	Raillard and Menesguen (1994)
k_{NOxNH3}	Half saturation constant for nitrogen limitation	0.025 $g.m^{-3}$	Eppley *et al.* (1969), Raillard and Menesguen (1994), Chapelle *et al.* (2000), Grant *et al.* (2007)
k_{PO4}	Half saturation constant for phosphorus limitation	0.01 $g.m^{-3}$	Bowie *et al.* (1985) and references therein.
d_{Pmax}	Maximal non-predatory phytoplankton mortality rate (@20C)	0.05 day^{-1}	Jorgensen *et al.* (1991), Raillard and Menesguen (1994), Duarte *et al.* (2003), Grant *et al.* (2000)
V_S	Phytoplankton settling velocity (@20C)	0.3 $m.day^{-1}$	Calibrated
P_{minI}	Fraction of non-predatory phytoplankton death mineralised immediately	0.05	Calibrated
Zooplankton			
g_{Zref}	Reference zooplankton grazing rate (@20C)	0.4 day^{-1}	Hall *et al.* (2006)
E_{PZ}	Assimilation efficiency of zooplankton on phytoplankton	0.6	Connover (1966), Raillard and Menesguen (1994), Chapelle *et al.* (2000), Cugier *et al.* (2005)
P_T	Threshold food concentration	0.04 $g.m^{-3}$	Calibrated
K_Z	Half saturation constant for zooplankton feeding	0.2 $g.m^{-3}$	Bowie *et al.* (1985), Dowd (2005)
r_{Zref}	Reference zooplankton respiration rate (@20C)	0.035 day^{-1}	Jorgensen *et al.* (1991)
d_{Zref}	Reference zooplankton mortality (@20C)	0.05 day^{-1}	Duarte *et al.* (2003), Grant *et al.* (2007)
$Z_{excrminI}$	Fraction of zooplankton excretions mineralised immediately	0.05	Calibrated
Nutrients			
MIN_{refN}	Reference mineralisation rate for $DN>NH_3$ (@20C)	0.001 day^{-1}	Bowie *et al.* (1985) and references therein.
MIN_{refP}	Reference mineralisation rate for $DP>PO_4$ (@20C)	0.02 day^{-1}	Bowie *et al.* (1985) and references therein.
N_{Rref}	Reference nitrification rate (@20C)	0.035 day^{-1}	Calibrated
MIN_{BD}	Reference mineralisation rate of biodeposits	0.05 day^{-1}	Jorgensen *et al.*, (1991), Smaal and Prins (1993)
DO_{MIN}	Half saturation constant (dissolved oxygen) for mineralisation	7 gm^{-3}	Calibrated
V_D	Settling velocity of detritus	1.0 $mday^{-1}$	Raillard and Menesguen (1994)
Mussels			
Θ_M	Mussel filtration temperature coefficient	1.066	
E_{PM}	Filtering efficacy of mussels on phytoplankton	1	Chapelle *et al.* (2000)
E_{ZM}	Filtering efficacy of mussels on zooplankton	0.8	Chapelle *et al.* (2000)
E_{DM}	Filtering efficacy of mussels on detritus	1	Chapelle *et al.* (2000)
$M_{excrNH4}$	Mussel ammonia excretion constant (Chl-a > 0.5 $mg.m^{-3}$)	$7x10^{-5}$ day^{-1}	Bayne and Scullard (1977), Smaal and Prins (1993)
$M_{excrNH3}A$	Mussel ammonia excretion coefficient (Chl-a < 0.38 $mg.m^{-3}$)	61.46	James *et al.* (2001)
$M_{excrNH3}b$	Mussel ammonia excretion coefficient (Chl-a < 0.38 $mg.m^{-3}$)	0.996	James *et al.* (2001)
$BD_{\%M}$	Fraction of mussel feeding egested as biodeposits	0.2	Bayne (1993), Hatton *et al.* (2005)
V_{BD}	Settling velocity of mussel biodeposits	50 $m.day^{-1}$	
$M_{resp}A$	Oxygen respiration coefficient A ($y=Ax^b$)	0.0126	James *et al.* (2001)
$M_{resp}b$	Oxygen respiration exponent b ($y=Ax^b$)	0.535	James *et al.* (2001)
$M_{CL}m$	Clearance coefficient M (y=Mx+C)	0.33	Gardner (2002)
$M_{CL}c$	Clearance coefficient C (y=Mx+C)	2.07	Gardner (2002)
$M_{CL}max$	Clearance maximal value	0.1051 $m^3.g^{-1}.day^{-1}$	Gardner (2002)
General			
θ	Temperature adjustment coefficient	1.066	Eppley (1972)
K_L	PAR light extinction coefficient	0.06 m^{-1}	1-d heat model and observed data.
V_o	Oxygen to carbon ratio at production	3.07	Stoichiometric relation
RR_N	Mass of nitrogen per combined CNP mass	0.14	Redfield (1934, 1958)
RR_P	Mass of phosphorus per combined CNP mass	0.02	Redfield (1934, 1958)
RR_C	Mass of carbon per combined CNP mass	0.84	Redfield (1934, 1958)
	Phytoplankton chlorophyll:carbon ratio	0.02	Jorgensen *et al.*, (1991), Duarte *et al.*, (2003), Dowd, 2005.
	Albedo	0.08	
	Horizontal eddy diffusivity	10 m^2s^{-1}	HD model calibration
	Vertical eddy diffusivity	0.0001 m^2s^{-1}	HD model calibration
dt	Model time step	10 s	N/A

*Most values were averaged from the ranges provided by stated authors.

7.7 MODEL-DATA COMPARISONS

The model was initially run 'without mussels' to ensure that measured data were replicated effectively during calibration tests. Model values were calibrated using a 'trial and error' approach to determine calibration parameter values (Table 7.4) enabling the model to best replicate observed measurements.

Field data used to calibrate the ecological model (CTD and water sample data) were collected between October 2003 and May 2004 during five (CTD) and four (water samples) transect surveys (Figure 4.1 and 4.2). These data are capable of resolving seasonal patterns in Bay of Plenty shelf water structure and properties over 5-10 km spatial scales. This is suitable for the model being applied within this chapter. More spatially and temporally dense data would be required if farm scale models were to be nested within the larger model. There is some level of uncertainty in these measured data as a result of instrument calibration, sample handling, and laboratory procedures and detection limits. This is most noticeable in the analysed water sample data where some spurious measurements are apparent (e.g. observed ammonia, Figure 7.10a,c). Quality assurance measures by way of blind replicates or sample blanks being sent to the laboratory may have been able to quantify the level of accuracy of these measurements.

Modelled concentrations and distributions of state variables were compared to measured data from CTD casts (Chl-a, DO), discrete water samples (Chl-a, NO_x, NH_3, PO_4), and to remotely sensed data (Chl-a). Sections 4.4, 4.4.1, and 4.4.2 detail the sampling program and processing methodology for these parameters (CTD casts, water samples, SeaWiFs data retrievals).

An accurate calibration of a NPZD model coupled to a non-simplified fully spatially resolving hydrodynamic model requires that physical dynamics, NPZD initial and boundary conditions, and ecological processes are replicated effectively. Accurate replication of physical dynamics is essential for the simulation of nutrient delivery through advective and dispersive processes. Physical processes such as the upwelling observed within the Bay of Plenty (Chapter 4) must be adequately simulated or the replication of phytoplankton biomass will suffer from a lack of nutrients to sustain growth. Additionally, ecological processes such as phytoplankton-zooplankton and phytoplankton-nutrient interactions must be adequately simulated for the model to replicate observed measurements. Any inaccuracies in the simulation of any of these processes will lead to inaccuracy in the model solution. Significant inaccuracies in process discretisation will, over short time scales, lead to significant errors in the model solution. Lesser inaccuracies can be expected to result in more minor errors in model solution over longer time frames.

7.7.1 DEPTH-TIME COMPARISONS: SHORE-NORMAL TRANSECTS (CTD AND WATER SAMPLES)

7.7.1.1 CHLOROPHYLL-A DISTRIBUTIONS

Modelled Chl-a (used as a proxy for phytoplankton concentration) depth profiles exhibit similar characteristics to observed values across three shore-normal near-shore transects (Figures 7.6 and 7.7). Modelled values at the time of the October survey (Figure 7.7a,e,i) slightly under predict the magnitude and offshore extent of the observed Chl-a mass (Figure 7.6a,e,i). The depth of the Chl-a maxima (~ 20-30 m) is correctly modelled when the feature is present in the measurements (October, December). The model replicates the very low observed concentrations of Chl-a below 50 m depth throughout the year. The location and magnitude of the modelled Chl-a mass in December is very similar to observations (Figures 7.6 and 7.7b,f,j). High observed Chl-a concentrations apparent in the Whakatane transect observations during December (Figure 7.6f) are limited in vertical extent, the result of only a few fluorometer measurements, reducing the reliability of comparisons to these high (~15 $mg.m^{-3}$) measurements. The model accurately reflects the relative lack of Chl-a observed during the March and May surveys across all three transects (Figures 7.6 and 7.7 d,h,l).

7.7.1.2 OXIDISED NITROGEN DISTRIBUTIONS

Modelled NOx concentrations from October and March reflect similar patterns to those observed from discrete water sample analysis (Figures 7.8 and 7.9a,c,e,g,i,k). No measurements were taken during December as a result of technical and weather issues during field sampling excercises. NOx profiles indicative of upwelling are both observed and modelled during both October and March. At these times, modelled NOx concentrations are in the range of 0-20 $mg.m^{-3}$ at the surface, consistent with observations, and ~140 $mg.m^{-3}$ at depth, a slight increase over observed values of 120-140 $mg.m^{-3}$. Modelled NOx values during late May (Figure 7.9d,h,l) generally overestimate observed concentrations by ~50-100% (Figure 7.8d,h,l), although it should be noted that the observations are limited to the nearshore and shallower depths *cf.* those during October and March. In all cases (Figures 7.6-7.15) the reader is reminded that the model predictions, as plotted, span a greater distance offshore and depth range than the observations and, though the scale of all plots are consistent, results in modelled data being plotted in areas where no observational data can be. It is important for the reader to compare 'like with like' and only compare those areas where observed data exists.

7.7.1.3 AMMONIUM-NITROGEN DISTRIBUTIONS

Observed NH3 profiles exhibit no consistent pattern and a variety of distribution patterns often obviously influenced by one or two potentially spurious measurements; in general observed concentrations are below 10 $mg.m^{-3}$ (Figure 7.10a-l). Modelled concentrations reflect this general observation with

concentrations typically showing no consistent patterns and being below 10 $mg.m^{-3}$ (Figure 7.11a-l). Immediately offshore from Pukehina the combined influence of the relatively high nitrogen loads from the Kaituna River, Pongakawa Stream, and the Waitahanui Stream (Taylor and Park, 2001) is apparent in the model predictions during October and December (Figure 7.11i,j). There is some evidence of this feature in the observations (Figure 7.10j).

7.7.1.4 DISSOLVED REACTIVE PHOSPHORUS DISTRIBUTIONS

DRP profiles (Figure 7.12) exhibit similar characteristic upwelling profiles in a similar manner to those of NOx (Figure 7.8). Upwelling profiles of DRP with surface concentrations ~ 4 $mg.m^{-3}$ (note that the detection limit for DRP in the analysis is 4 $mg.m^{-3}$, Table 4.3) and concentrations at depth of 16-20 $mg.m^{-3}$ are apparent from the water samples during October, December, and March (Figure 7.12). Observations during May are less conclusive due to their restricted offshore and depth-wise extent, though generally indicate enhanced near-surface concentrations (8-10 $mg.m^{-3}$). Modelled DRP concentrations during October, December, and March exhibit similar upwelling profiles with surface concentrations < 4 $mg.m^{-3}$ (detection limit for observations) (Figure 7.13). Modelled concentrations of DRP in upwelled water are consistent with observations along both Whakatane and Pukehina transects (Figures 7.12 and 7.13 e,f,g,i,j,k), slightly underestimated along the Opotiki transect during October and December (Figures 7.12 and 7.13a,b), and slightly overestimated during March (Figures 7.12 and 7.13c). Notably the influence of a local peak in DRP concentrations in surface waters, thought to be the result of a river plume, observed offshore from Pukehina (Figure 7.12j) is accurately replicated by the model (Figure 7.13j).

The model generally over predicts DRP concentrations during May, though similar to NOx the observations are limited in offshore and depth-wise extent. The observations indicate a general increase in near-surface DRP concentrations at this time of year, though not to the extent of that predicted by the model (Figures 7.12 and 7.13 d,h). Notably, however, along the Whakatane transect the concentrations and pattern of DRP during May are similar given the limitations of the observed dataset (Figure 7.12 and 7.13h).

7.7.1.5 DISSOLVED OXYGEN DISTRIBUTIONS

Observed DO profiles indicate a near surface (< 15 m depth) decrease in concentrations occurring initially in December and being more pronounced during March (< 50 m depth); below 100 m the observations indicate little seasonal change (Figure 7.14). Modelled concentrations replicate these patterns in terms of their magnitude, timing, and location (Figure 7.15). Consistent with the near surface observations, model predictions are depressed initially in December, and more prominently in March. Modelled concentrations below 100 m show little seasonal variation (Figure 7.15), again consistent with observations.

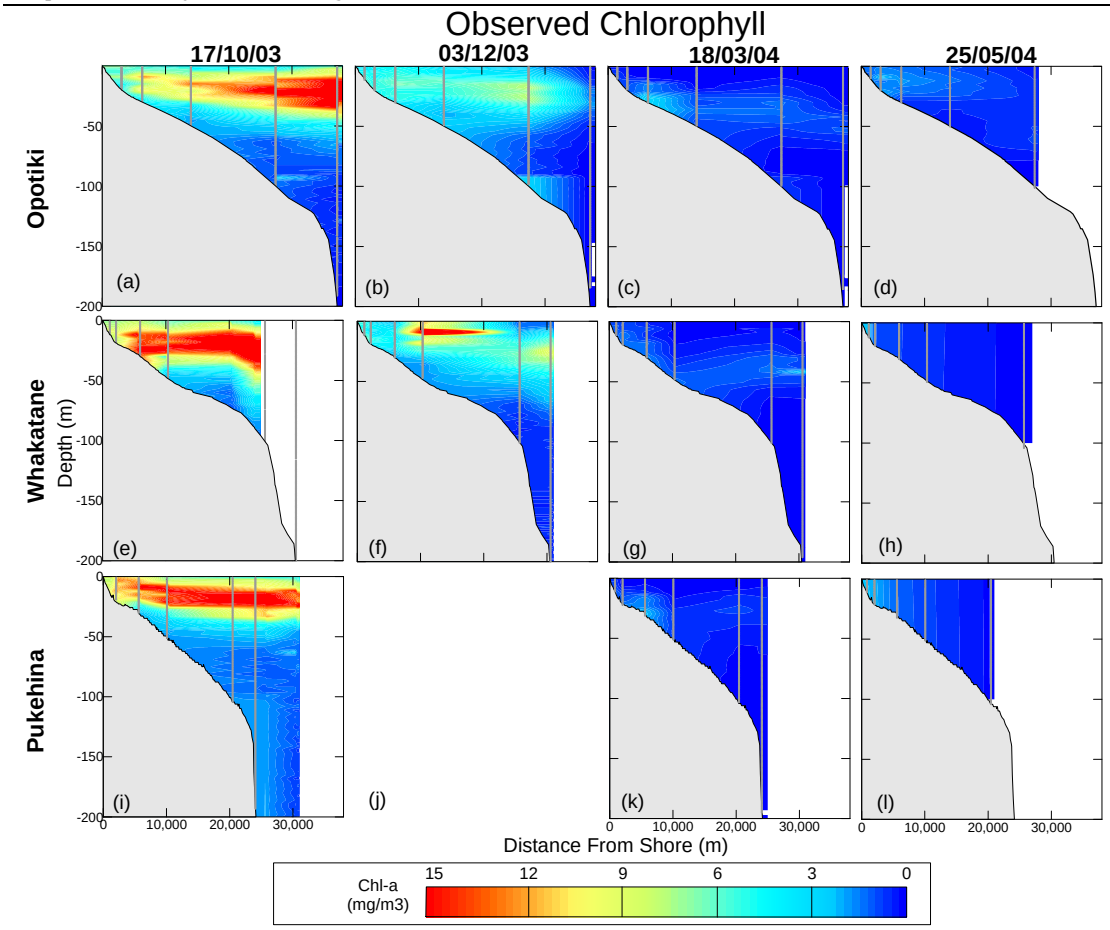

Figure 7.6 Observed chlorophyll-a concentrations along three shore-normal transects from a calibrated fluorometer attached to a CTD. Data interpolated over a 300 x 3 m grid with measurement positions indicated by grey dots.

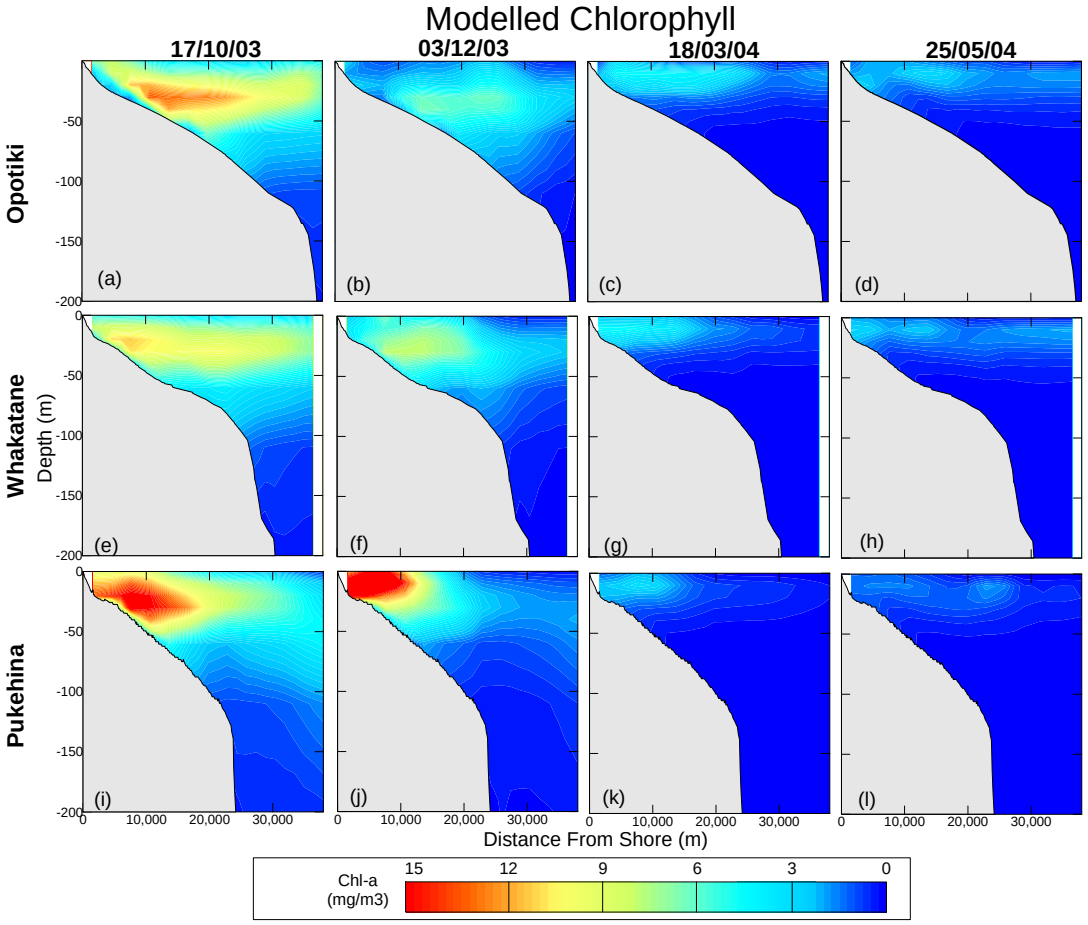

Figure 7.7 Modelled chlorophyll-a concentrations from the NPZD numerical model. Model results smoothed over a 1500 m x 15 m grid and presented on an identical colour scale to observations.

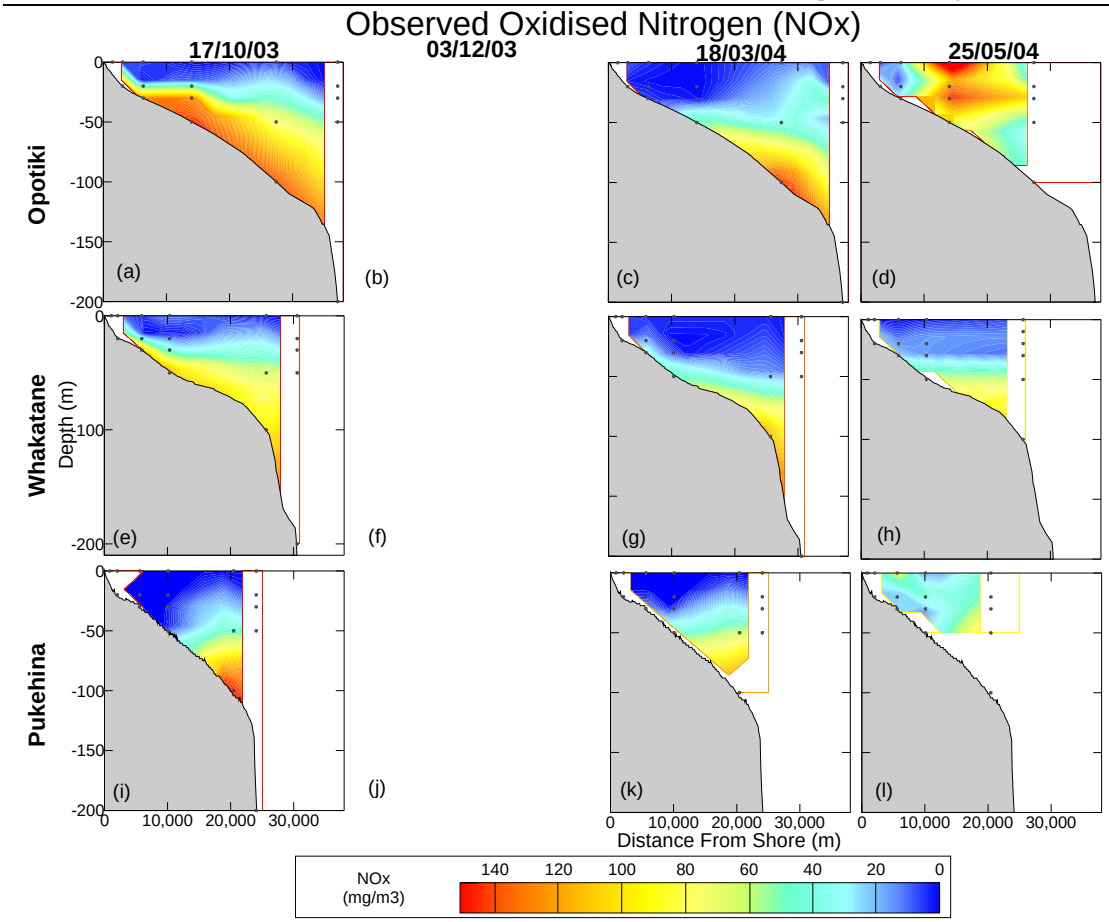

Figure 7.8 Observed nitrate-nitrite concentrations along three shore-normal transects from discrete water samples. Data interpolated over a 3000 x 15 m grid with measurement positions indicated by grey dots. Measurements have a detection limit of 1 mg.m^{-3}.

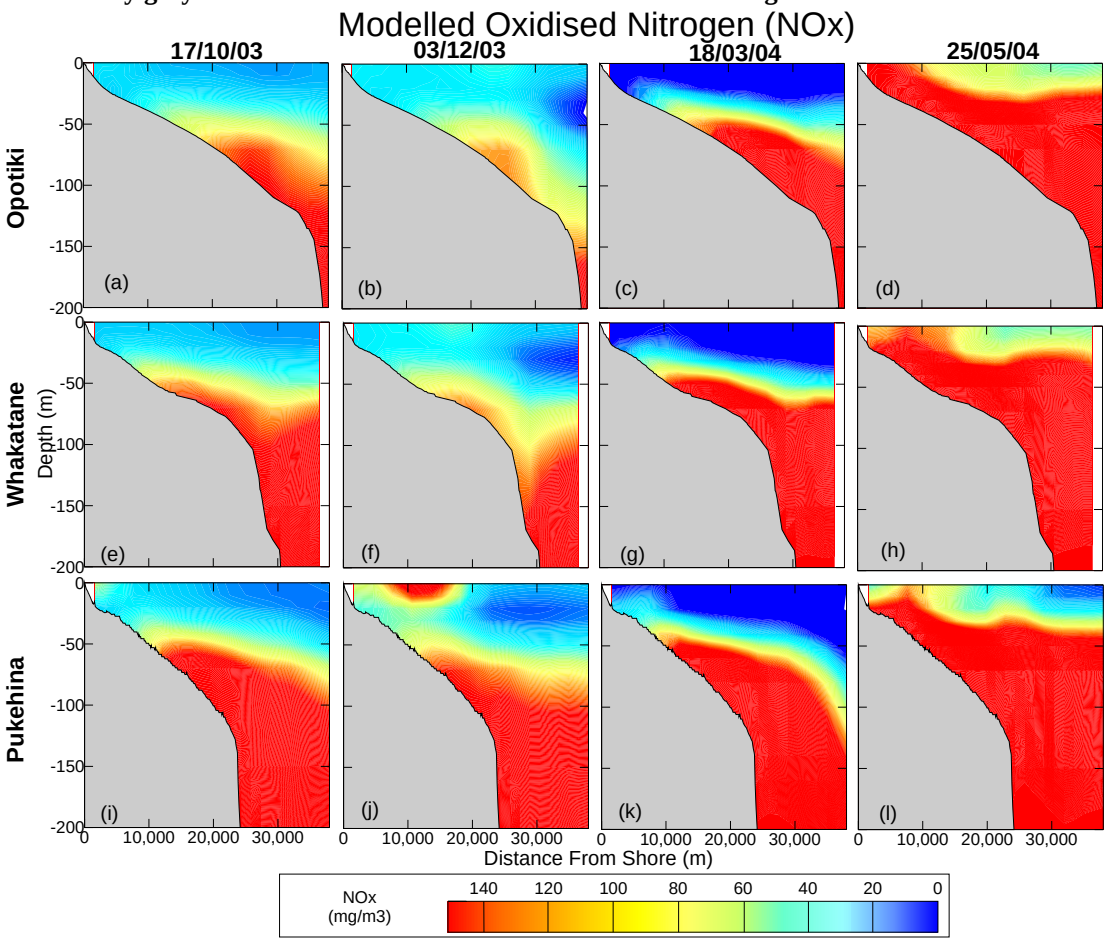

Figure 7.9 Modelled nitrate-nitrite concentrations from the NPZD numerical model. Model results smoothed over a 1500 m x 15 m grid and presented on an identical colour scale to observations.

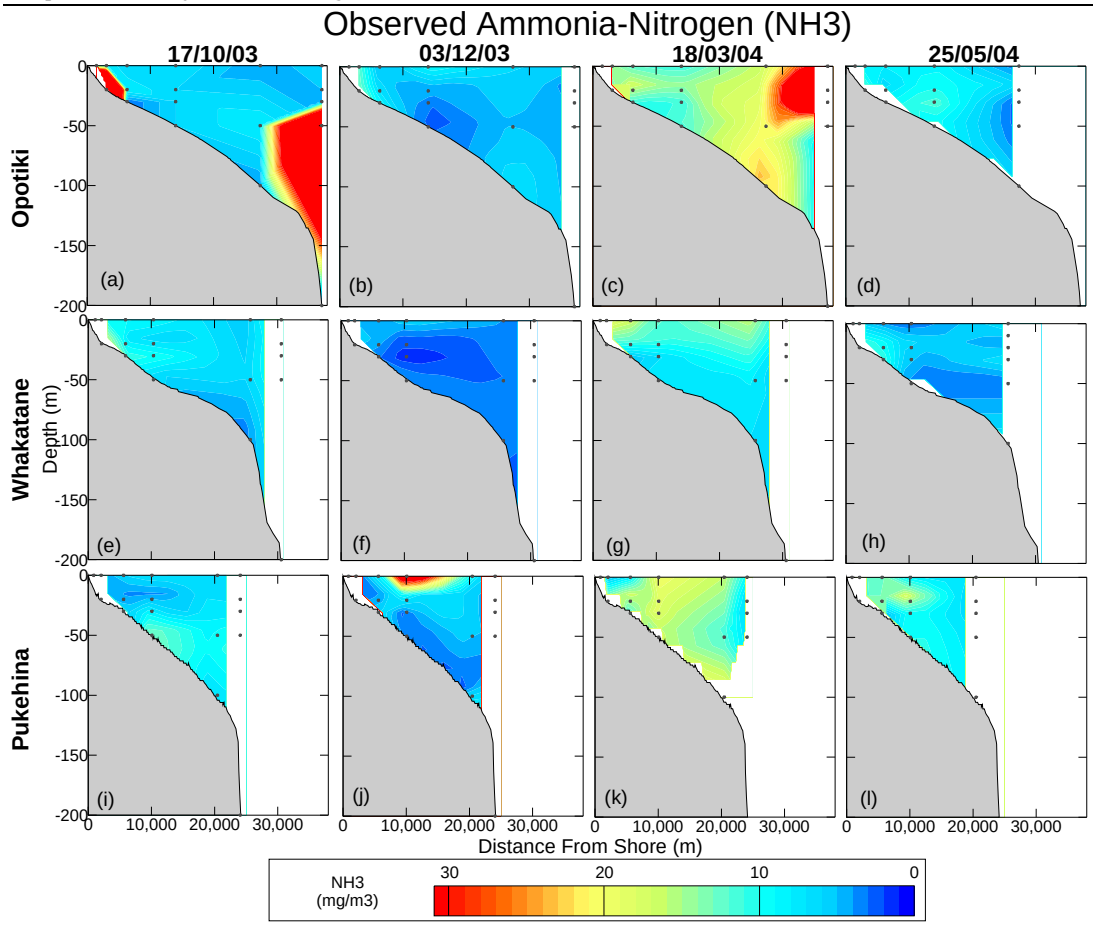

Figure 7.10 Observed ammonium concentrations along three shore-normal transects from discrete water samples. Data interpolated over a 3000 x 15 m grid with measurement positions indicated by grey dots. Measurements have a detection limit of 1 mg.m^{-3}.

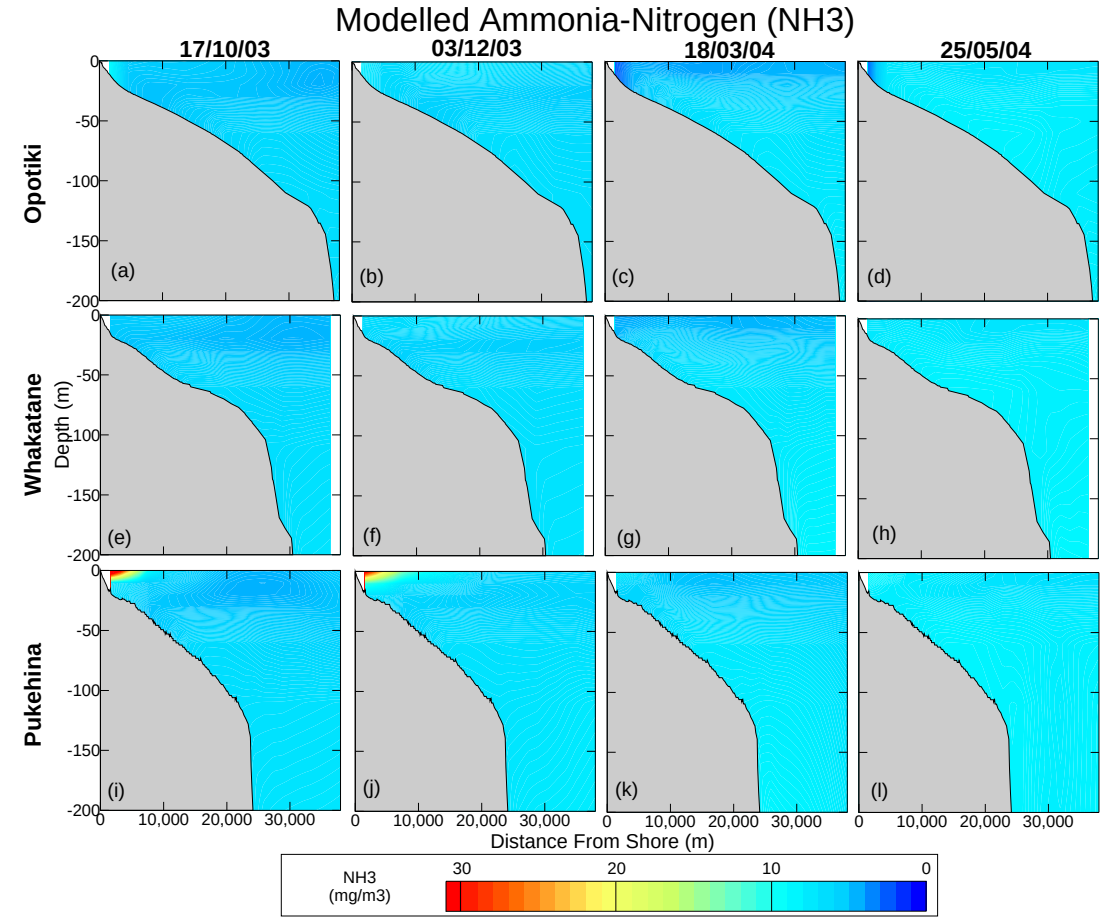

Figure 7.11 Modelled ammonium concentrations from the NPZD numerical model. Model results smoothed over a 1500 m x 15 m grid and presented on an identical colour scale to observations.

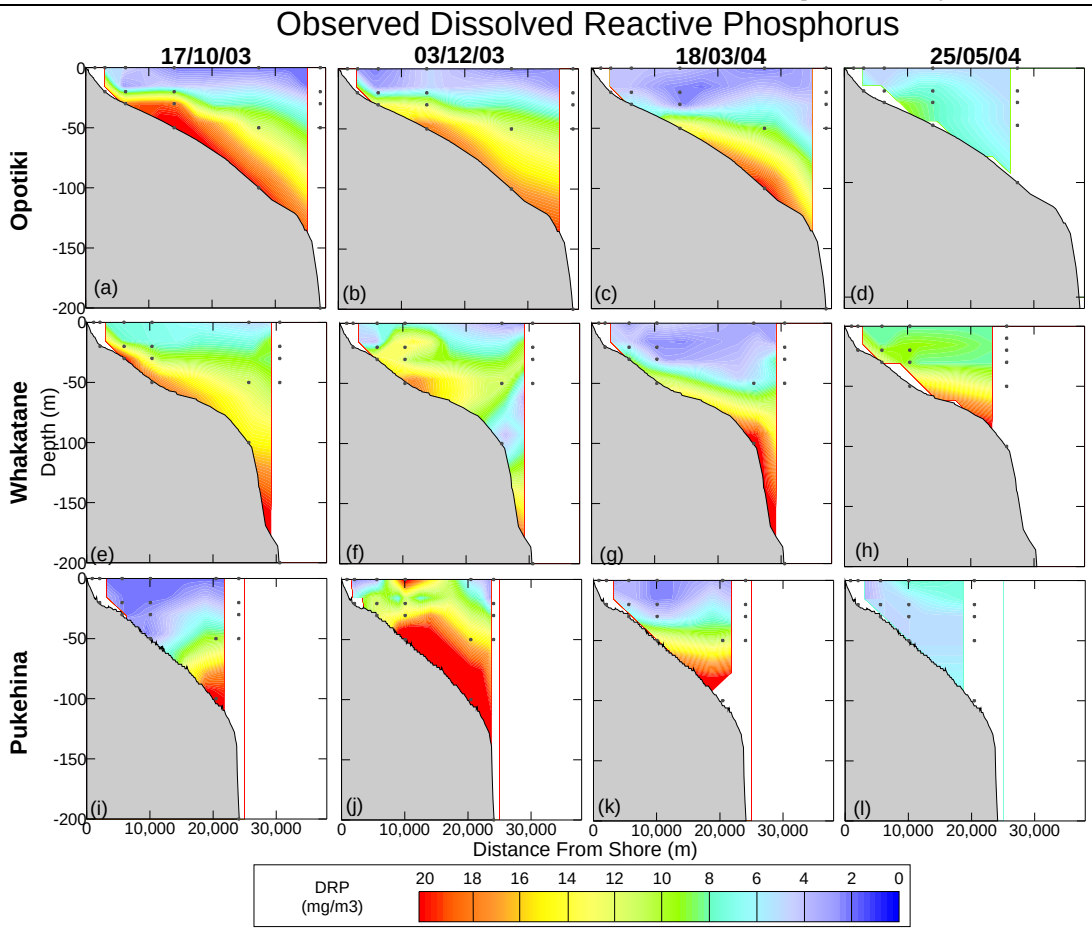

Figure 7.12 Observed dissolved reactive phosphorus concentrations along three shore-normal transects from discrete water samples. Data interpolated over a 3000 x 15 m grid with measurement positions indicated by grey dots. Measurements have a detection limit of 4 mg.m^{-3}.

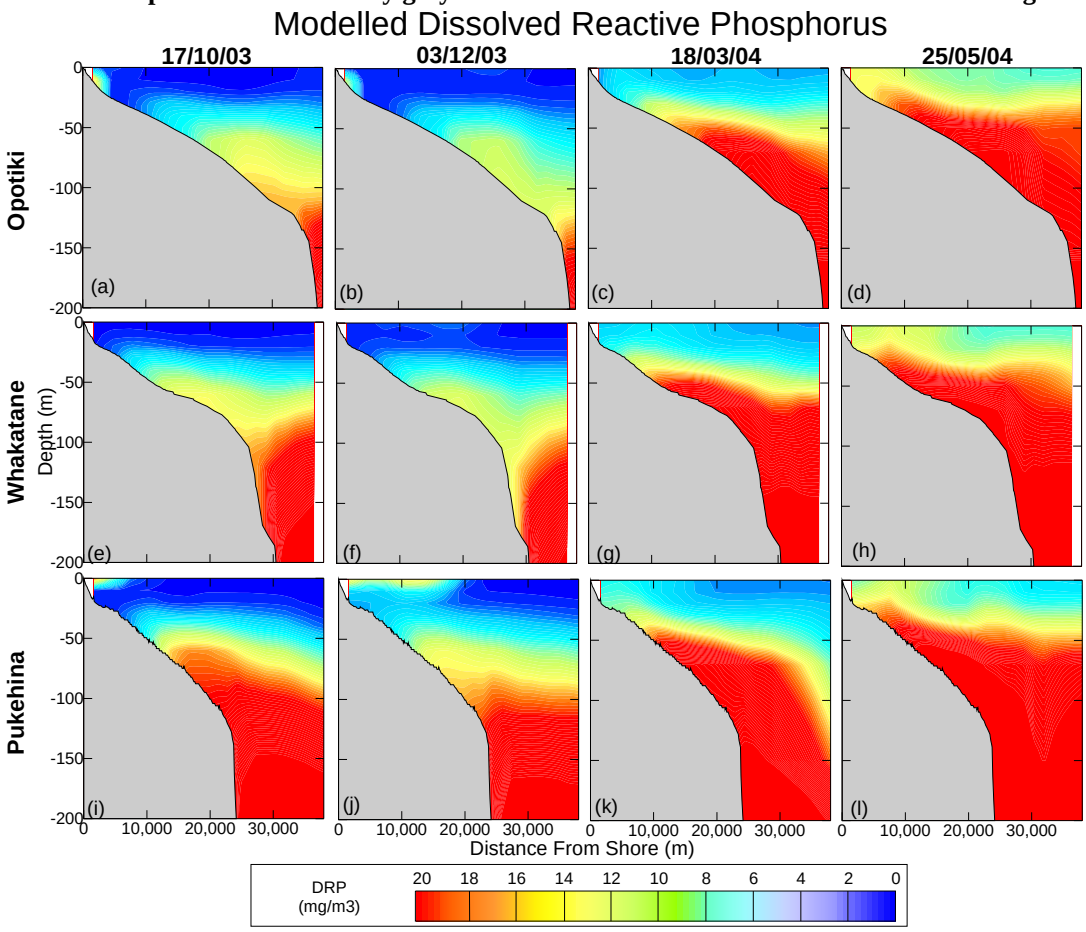

Figure 7.13 Modelled dissolved reactive phosphorus concentrations from the NPZD numerical model. Model results smoothed over a 1500 m x 15 m grid and presented on an identical colour scale to observations

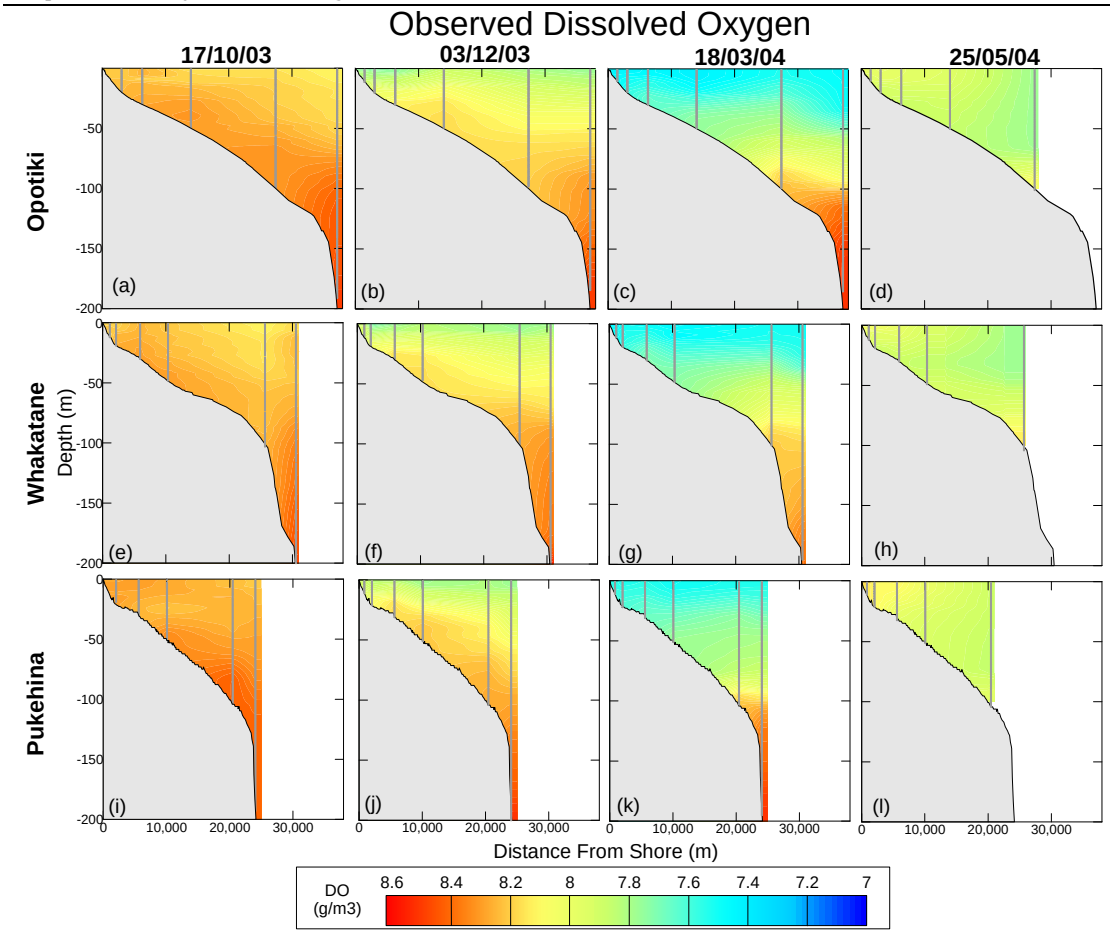

Figure 7.14 Observed dissolved oxygen concentrations along three shore-normal transects from CTD casts. Data interpolated over a 300 x 3 m grid with measurement positions indicated by grey dots.

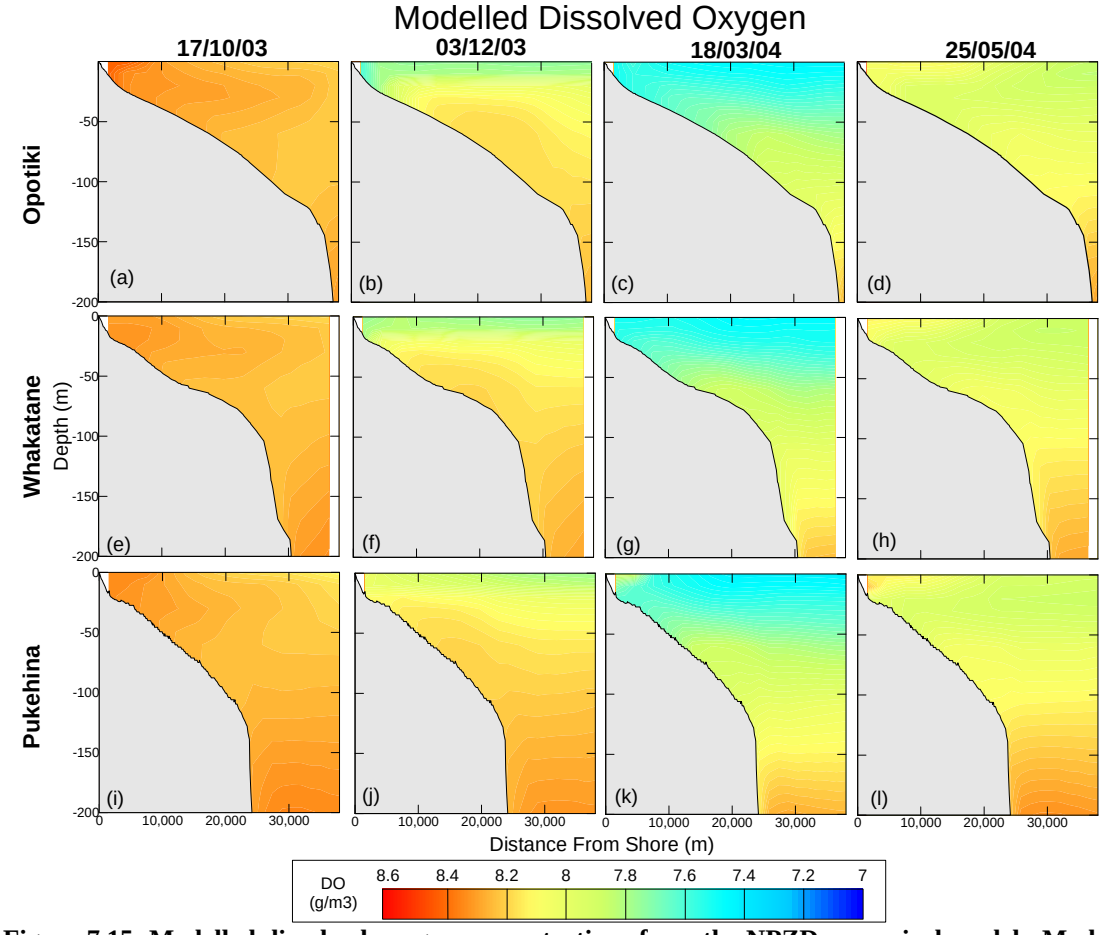

Figure 7.15 Modelled dissolved oxygen concentrations from the NPZD numerical model. Model results smoothed over a 1500 m x 15 m grid and presented on an identical colour scale to observations.

7.7.2 SURFACE CHL-A DISTRIBUTION COMPARISONS (SEAWIFS CHL-A)

Selected relatively cloud-free satellite remote sensed three day composites of sea surface Chl-a data at 1 km resolution from the SeaWiFS sensor (see Section 4.4.6 for a summary) were compared to surface layer (0-5 m depth) model output. Though there are weaknesses in these remotely sensed data (inherent errors of ±35% plus local calibration errors, Section 4.4.6) they represent the best available, spatially dense indication of surface layer Chl-a distributions within the Bay of Plenty. Cloud coverage greatly limited the number of time periods suitable for comparison to model output.

Remotely sensed Chl-a distributions centred on 19-November 2003 (110 days after model initialisation and during the 'spring-bloom') indicate high Chl-a concentrations (~8 $mg.m^{-3}$) in nearshore zones between Pukehina and Whakatane with lower concentrations off Opotiki and very low concentrations through the rest of the Bay of Plenty (Figure 7.16a). Modelled distributions at the same time indicate a similar pattern in both magnitude and offshore/alongshore extents (Figure 7.16b). The model predicts elevated concentrations of Chl-a (~2-4 $mg.m^{-3}$) off Te Kaha in the eastern Bay of Plenty which are not present in the satellite data.

During summer, peak remotely sensed surface Chl-a concentrations were typically lower than those during the spring-bloom (Figure 7.17a, peak of 6 $mg.m^{-3}$). The SeaWiFS data of 19 December, 2003 (140 days after model initialisation) indicates the greatest concentration of Chl-a to be located immediately offshore from Pukehina, extending ~12.5 km in both directions and offshore to Motiti Island; concentrations are < 1.5 $mg.m^{-3}$ throughout the rest of the Bay of Plenty (Figure 7.17a). The model replicates these patterns, observed magnitudes, and the extent of the peak Chl-a mass remarkably well (Figure 7.17b).

Both observed and modelled peak surface Chl-a concentrations decrease further during the late-summer period (Figure 7.18a,b). The observed distribution, while centered immediately to the west of Pukehina, and extending almost to Motiti Island, is more spread in the along-shore dimension than that during summer (Figure 7.17a). Consistent with the observations, the modelled peak Chl-a mass occurs between Matakana Island (to the west of Tauranga) and Whakatane in the east. SeaWiFS data indicates slightly elevated Chl-a concentrations nearshore in the eastern Bay of Plenty (1-1.5 $mg.m^{-3}$) which are not replicated within the model. Consistent with observations, modelled Chl-a concentrations in the oceanic regions of the Bay of Plenty are < 1.0 $mg.m^{-3}$.

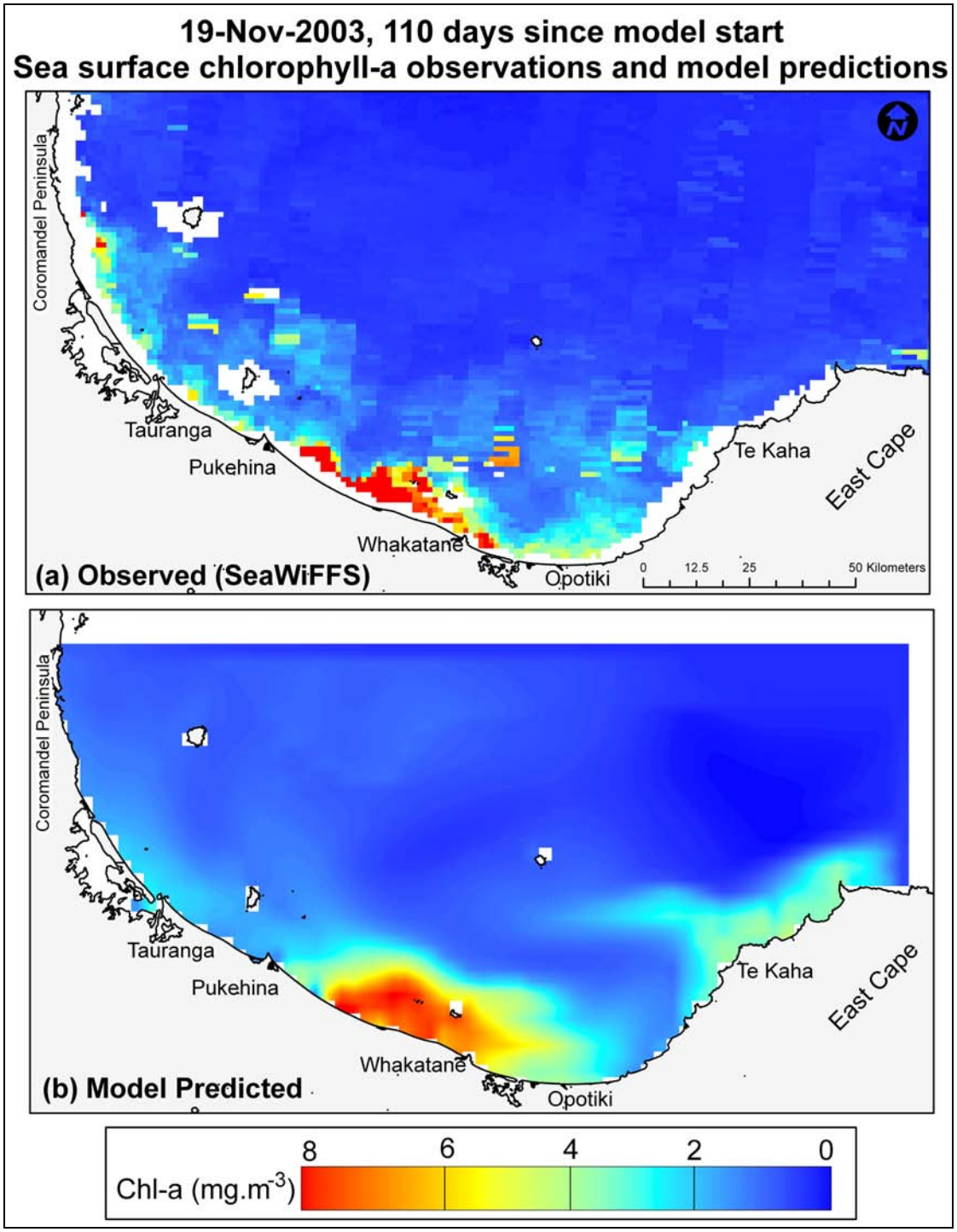

Figure 7.16 Observed (a) and model predicted (b) surface chlorophyll-a concentrations on 19 November 2003, 110 days after model initialisation. Observed chlorophyll from SeaWiFS satellite sensor with data partially obscured by cloud cover. Model predictions smoothed over a 250 m grid and plotted over an identical colour scale.

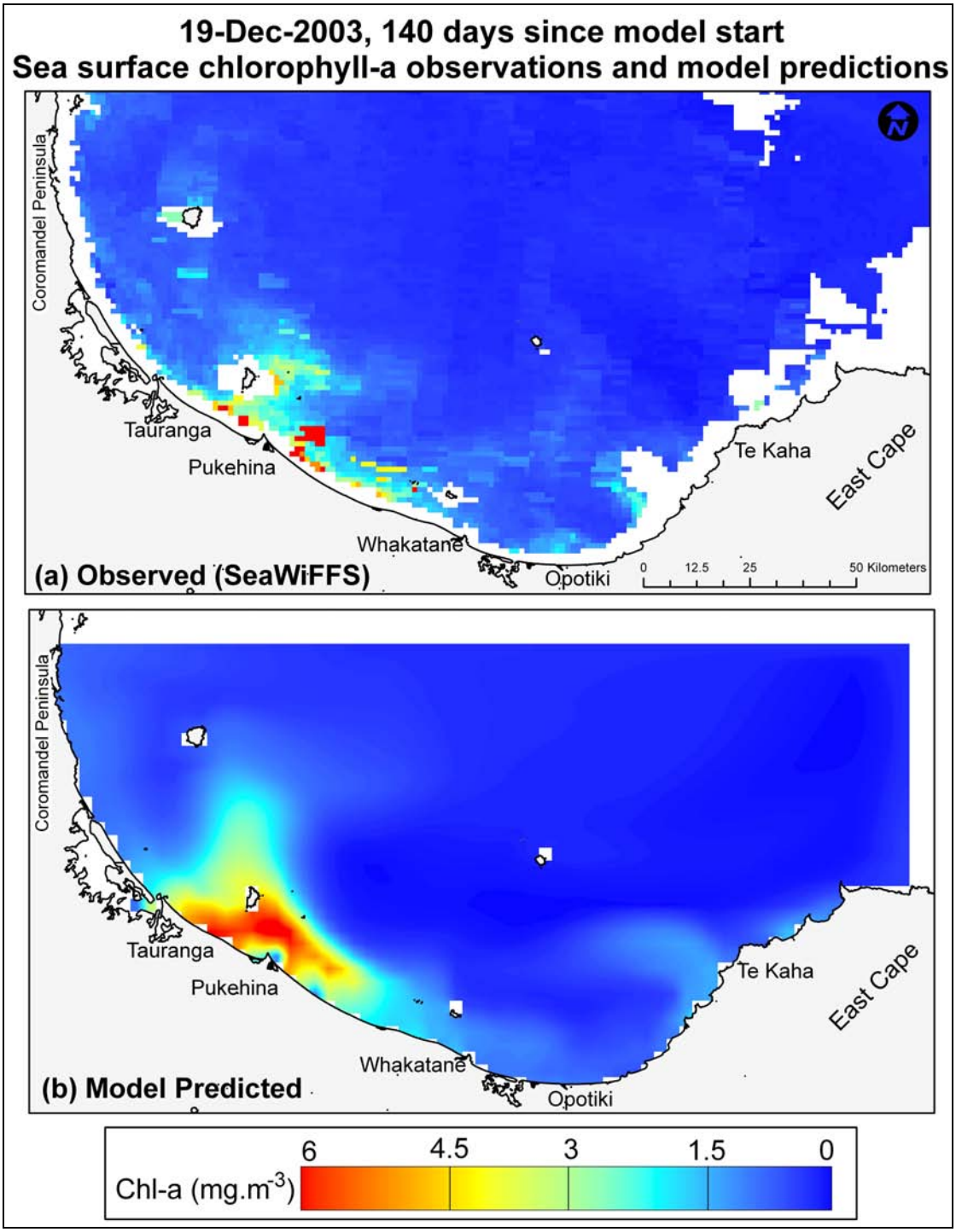

Figure 7.17 Observed (a) and model predicted (b) surface chlorophyll-a concentrations on 19 December 2003, 140 days after model initialisation. Observed chlorophyll from SeaWiFS satellite sensor with data partially obscured by cloud cover. Model predictions smoothed over a 250 m grid and plotted over an identical colour scale.

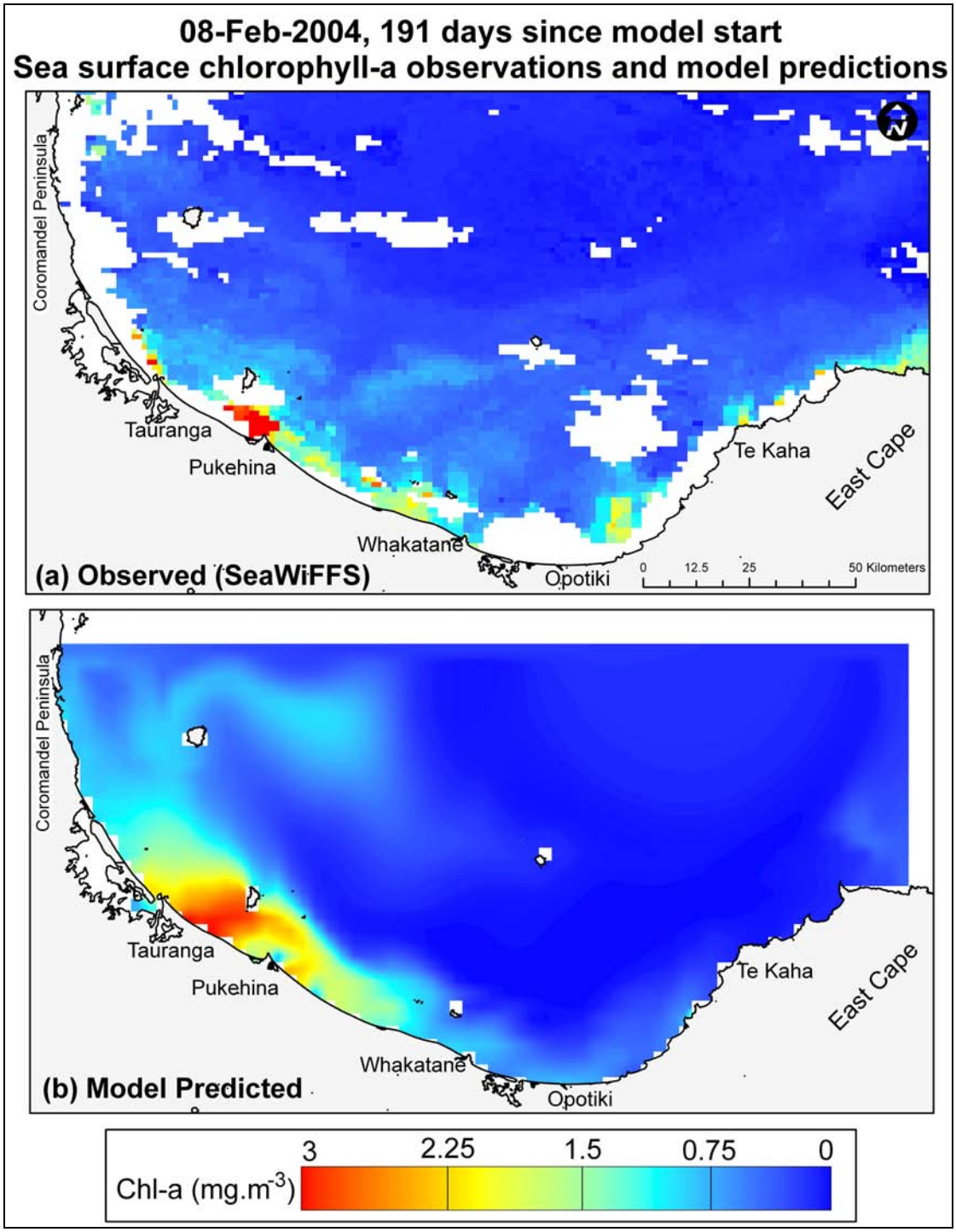

Figure 7.18 Observed (a) and model predicted (b) surface chlorophyll-a concentrations on 08 February 2004, 191 days after model initialisation. Observed chlorophyll from SeaWiFS satellite sensor with data partially obscured by cloud cover. Model predictions smoothed over a 250 m grid and plotted over an identical colour scale.

7.7.3 TIME-SERIES – DEPTH LAYER COMPARISONS (CTD AND WATER SAMPLES)

Time series of modelled Chl-a over depths between 0-70 m at both the Pukehina 200m site (Figure 7.19) and the Whakatane 100m site (Figure 7.20) show the timing of the modelled spring phytoplankton bloom and its similarity to observed measurements both temporally and with depth through the water column. Model results indicate that near-surface Chl-a is more responsive to short-term events than concentrations at depth, indicated by the modelled short-term variability in near surface Chl-a concentrations. Observations of Chl-a at both sites in autumn/winter indicate low relative (to the spring-bloom) concentrations, a feature replicated by the model.

Nutrient concentrations (NOx and DRP) increase with depth in both observations and model output (Figures 7.19 and 7.20). The model over-predicts both NOx and DRP concentrations at these sites toward the end of the model run by a factor of 50-150%. This could be the result of either slight inaccuracies in the modelling of physical dynamics (*i.e.* too much upwelling at this time of year) or the transmission through the model domain of potentially overestimated boundary information at this time of year; no detailed observations of the temporal variability of nutrient concentrations at the boundaries are available. Inaccuracy in the modelling of mineralisation processes could potentially also lead to the over-prediction, however, this can be largely discounted as there is no large mass of source material (*i.e.* phytoplankton, zooplankton) in the months immediately before the over-prediction.

NH3 concentrations are generally stable throughout the year, a feature of both observations and model output, with the model replicating observed concentrations well at both sites.

DO concentrations exhibit seasonal variation, with largest changes occuring in the near-surface layers (Figures 7.19 and 7.20). The model replicates this seasonal variation accurately and also indicates the potential for some shorter term (and lower magnitude) variability which, along with other model parameters, could not be captured in the observed data with discrete water samples of CTD casts.

Modelled temperatures are taken directly from the baroclinic hydrodynamic model output and have already been shown to effectively predict observations (Figure 5.19), at these sites this replication is further shown to be accurate (Figures 7.19 and 7.20).

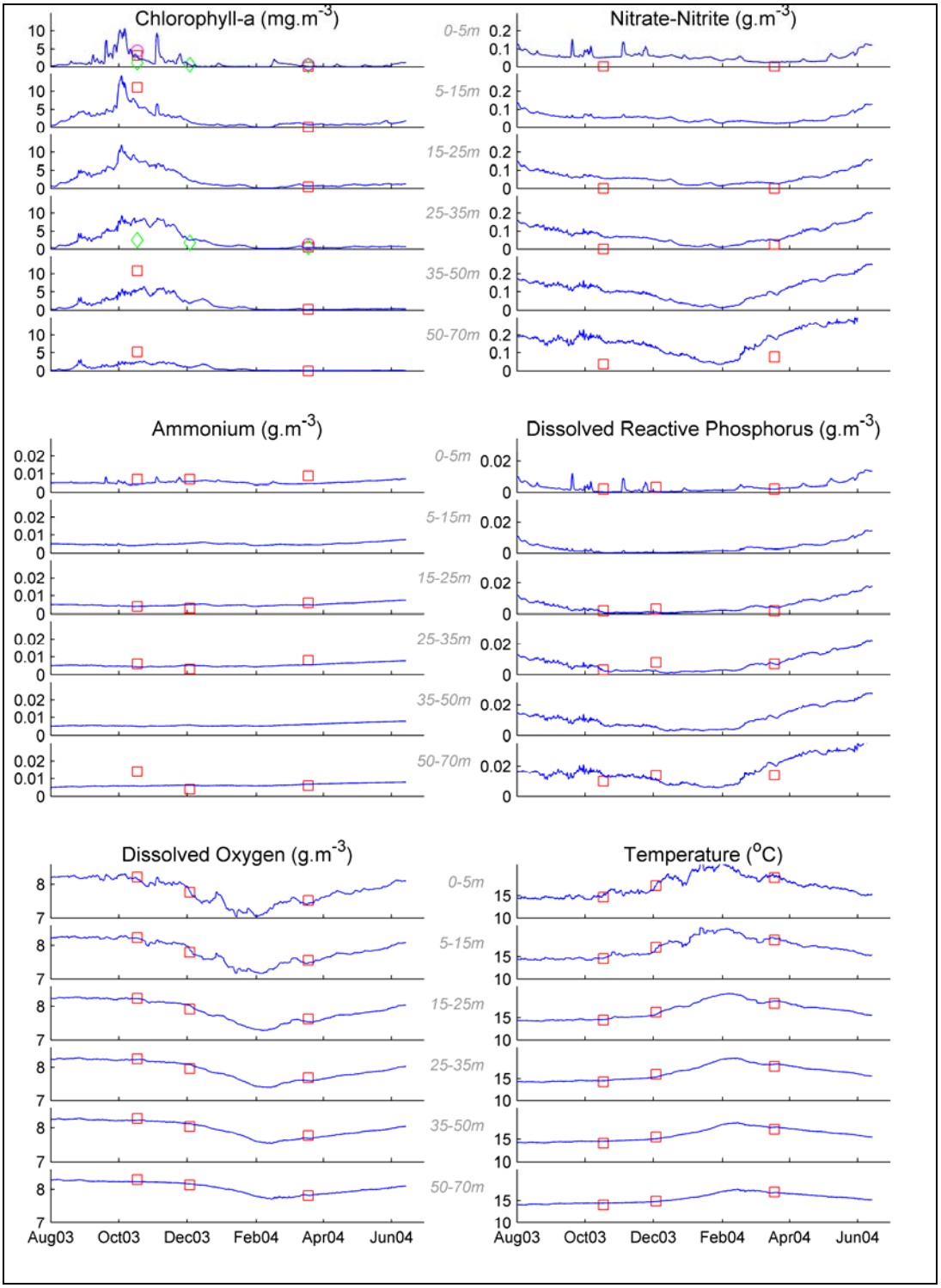

Figure 7.19 Time-series of observed (red squares) and modelled (blue line) variables with depth layers at the 200m depth contour offshore from Pukehina. Chlorophyll-a data also contains measurements obtained from filtered water samples (green diamonds) and a laboratory fluorometer (pink circles).

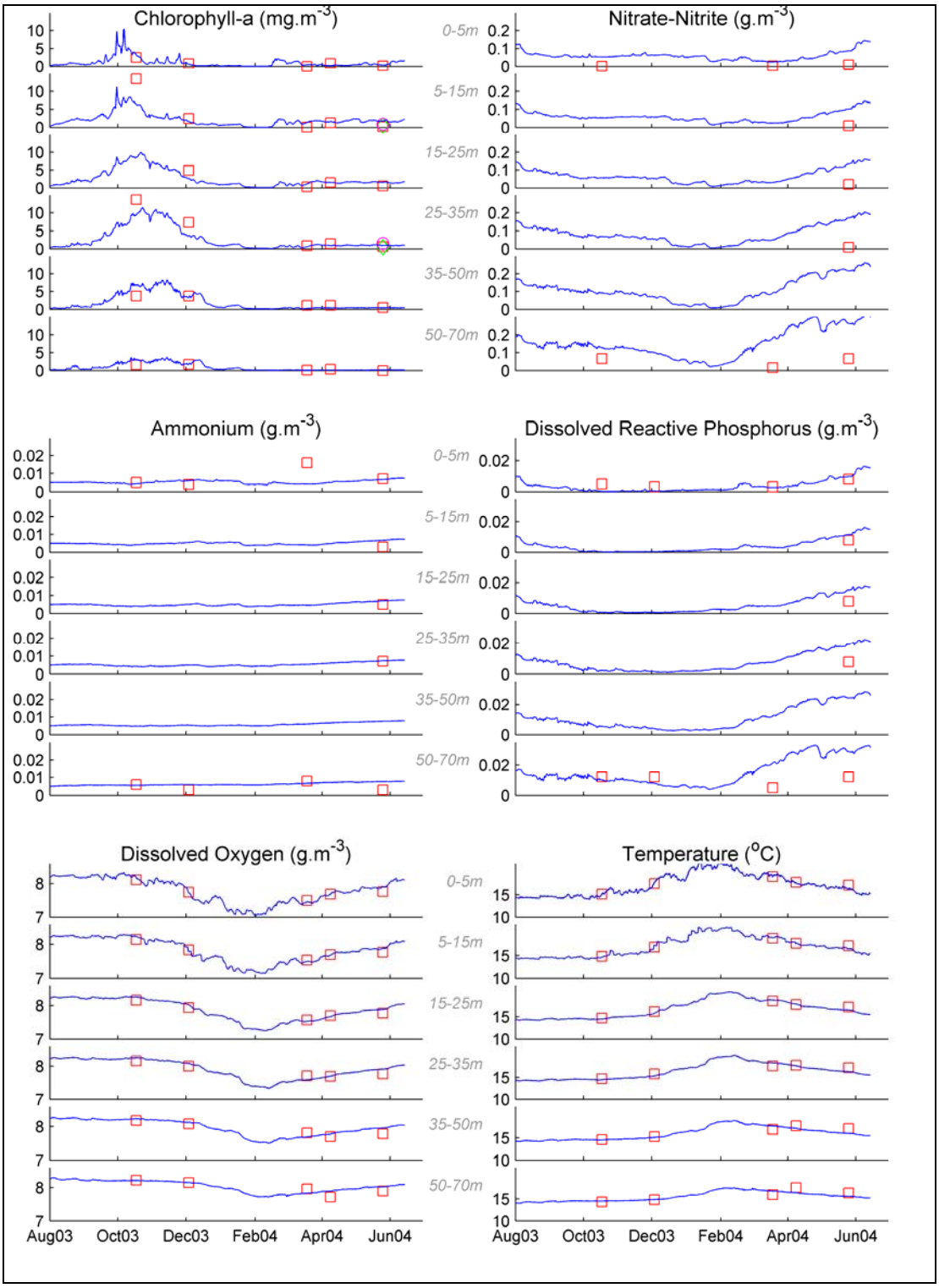

Figure 7.20 Time-series of observed (red squares) and modelled (blue line) variables with depth layers at the 100m depth contour offshore from Whakatane. Chlorophyll-a data also contains measurements obtained from filtered water samples (green diamonds) and a laboratory fluorometer (pink circles).

7.7.4 GENERAL COMMENTS ON MODEL-DATA COMPARISONS

Given that available comparison data are limited, the main objective for model calibration was to replicate measurements within the range of observed values while maintaining an accurate reflection of seasonal dynamics. Reasonable model comparison was achieved. In general the model effectively replicates observed concentration profiles and distributions of model parameters through time.

The timing and depth of the sub-surface spring Chl-a bloom are modelled in similar locations to those observed. However, the model does underestimate the offshore extent of the sub-surface bloom at this time. Phytoplankton growth is a function of the temperature and light environments, reference growth rates, and local nutrient concentrations (Equation 7.1). Given that the light regimes of nearshore and offshore waters will be identical (spatially uniform light decay constants), and that the temperature is more favourable offshore (Figures 4.5, 4.8, and 5.19) these can be discounted as a likely cause of the offshore underestimation. Nutrient limitation or enhanced grazing by zooplankton remain as potential causes for the modelled pattern. Nutrient delivery mechanisms to euphotic offshore waters are typically horizontal advection processes or the vertical mixing or diffusion (assuming no localised eddy upwelling). Enhancing vertical (and/or horizontal) mixing within the model would act to increase near-surface nutrient concentrations here, however, this also a degrading effect on the calibration of several other parameters (*e.g.* temperature, salinity).

The upwelling of NOx and DRP, a key nutrient delivery mechanism within the Bay of Plenty, is simulated by the model and visible through the profiles of these nutrients with depth. In addition to the depth profiles of Chl-a, nutrients, and DO the NPZD model is able to accurately predict the spatial distribution of near-surface Chl-a concentrations (the only data for which comprehensive spatial distributions are available).

The model indicates the potential for some short term variability in near-surface Chl-a and DO concentrations which are unable to be verified due to the data sampling regime; intensive time-series measurements would be required. This modelled variability decreases with depth and is not an unrealistic estimation of potential time-series patterns with depth.

Time-series of modelled Chl-a is consistent with observations throughout the year, and the model successfully predicts the initialisation, extent of, and subsequent depletion and decay of the spring phytoplankton bloom. Nutrient concentrations (NOx and DRP), however, are over predicted toward the end of the model run, during winter, though it is noted that there is also a relative lack of field data at this time.

Comparison of model calibration plots to similar figures in the published literature (*e.g.* Chapelle *et al.*, 2000; Duarte *et al.*, 2003; Dowd, 2005) indicates that, given the

limitations of the available data, the fit of model predictions to these data within the Bay of Plenty is arguably more effective than similar studies.

7.8 YEARLY MEAN PHYTOPLANKTON (CHLOROPHYLL-A) ABUNDANCES

Predicted phytoplankton abundances were averaged throughout the year (1-Aug-2003 to 31-Jul-2004) to provide an estimate of yearly mean Chl-a abundance (Figures 7.21 and 7.22). Surface layer concentrations are highest in the nearshore zone (< 20 km offshore) between Tauranga and Whakatane (Figure 7.21a and 7.22) with concentrations between 2-3 $mg.m^{-3}$. Nearshore surface layer concentrations in the eastern Bay of Plenty (near Te Kaha) are remarkably depressed (~ 1.0 $mg.m^{-3}$) relative to those in more eastern areas, with the transitional area occurring near Opotiki.

Though the predictions represent a single year (August 2003 – August 2004), multi year remotely sensed surface layer Chl-a composites (Figure 6.2) exhibit patterns similar to the predictions. These Chl-a anomalies, indicating regions of above or below 'normal' Chl-a concentration, indicate neritic waters between Tauranga and Whakatane to be most productive, and those of the eastern Bay of Plenty to be the least, a pattern also evident in the single year predictions (Figure 7.21a).

Despite the existence of two major rivers within the Eastern Bay of Plenty (Ruakokere and Motu Rivers, Figure 5.9), the nearshore zone in this region is relatively less productive than more central and western regions (Figures 7.21 and 7.22). The nutrient loads of these rivers are typically 50-75% less than that of rivers within the Bay of Plenty (Taylor and Park, 2001), a result potentially from the relative lack of pasture land in the catchments of the Ruakokere and Motu Rivers (predominantly native and exotic forest). The reduced nutrient load from both riverine and upwelling sources in this region are the likely cause of the lower modelled mean Chl-a concentrations.

Mean concentrations typically increase with depth, indicative of a mean sub-surface Chl-a maxima, often observed as a result of photo-inhibition within the surface layers (light conditions above optimal levels); the peak is located between 10-25 m depth (Figure 7.22). Similar to the surface layer, sub-surface Chl-a concentrations are highest in the nearshore zone. Nutrients to support phytoplankton growth are provided to the euphotic zone through the upwelling of nutrient-rich deep water near the coast and through river borne nutrient loads. The modelled year long pattern of Chl-a concentrations is consistent with wind driven upwelling resulting from wind stress from the northwest over a shelf/coastline with variable orientation (Chapter 4). Notably, while ADP data indicated a strong wind driven upwelling relationship on the shelf offshore from Pukehina; no similar response was observed at Opotiki (Chapter 4). Modelled mean year long Chl-a abundances are consistent with these findings,

with high mean concentrations offshore from Pukehina (~ 3-3.5 mg.m^{-3}) and lower mean concentrations offshore from Opotiki (~1.5-2.5 mg.m^{-3}).

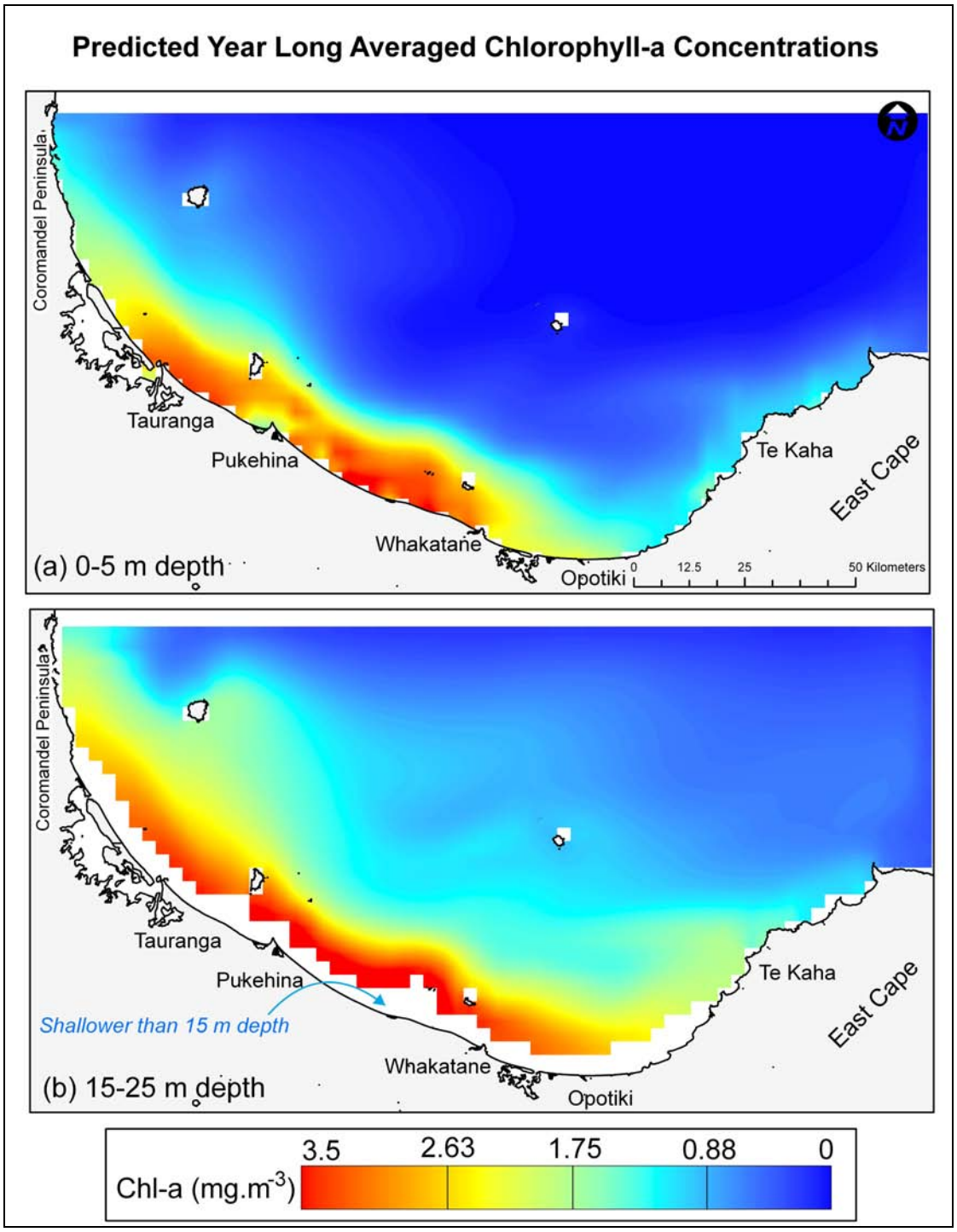

Figure 7.21 Yearly averaged modelled chlorophyll-a concentrations at 0-5 m depth (a) and 15-20 m depths (b).

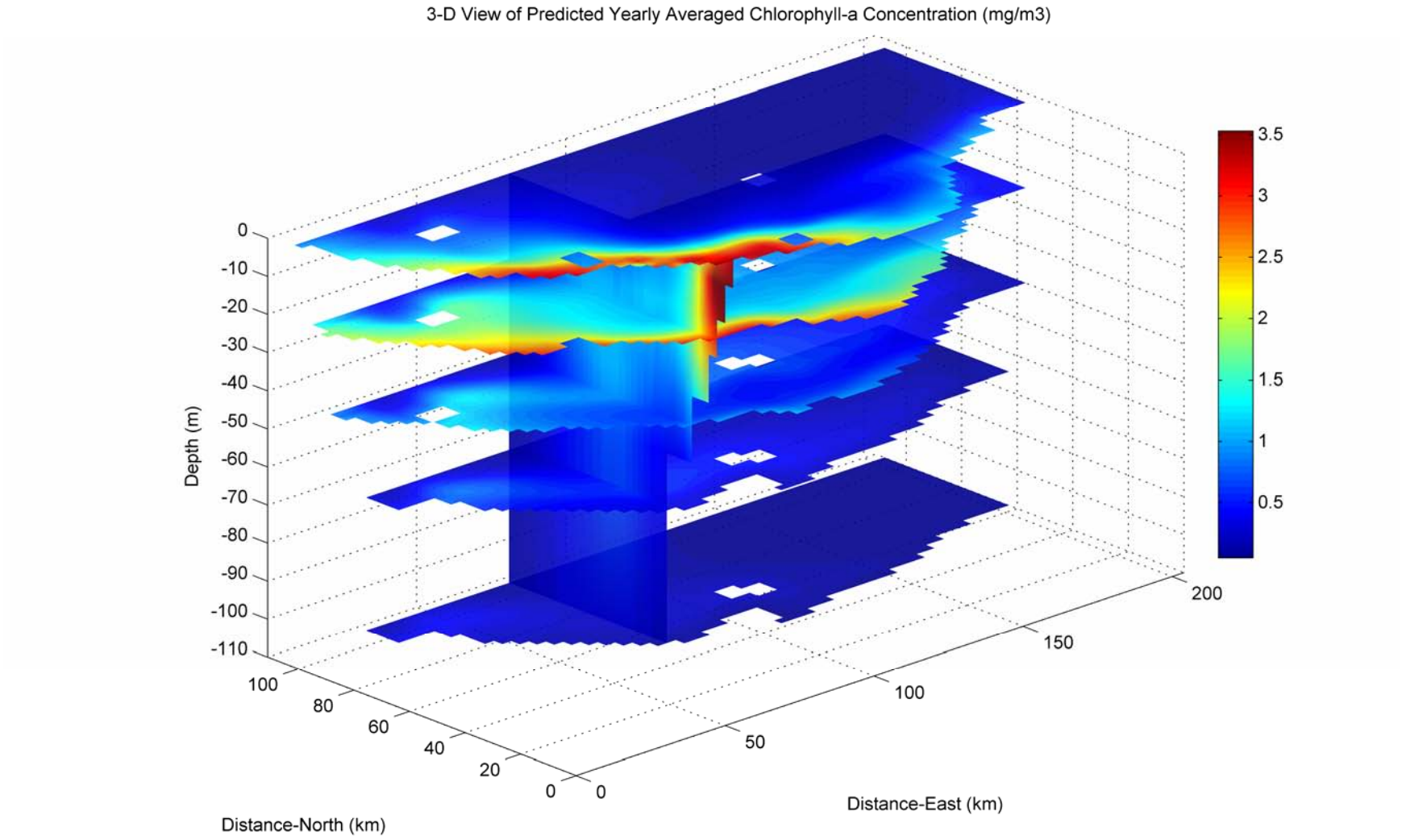

Figure 7.22 Three-dimensional slice view of yearly averaged modelled chlorophyll-a concentrations. Distances north and south are relative to model origin (2761000, 6339000 NZMG49). Horizontal slices are located at 2.5, 25, 50, 75, and 110 m depths, and one vertical slice (oriented N-S) along 2839000 NZMG offshore from Pukehina.

7.9 INCORPORATING CULTURED BIVALVE SPECIES

Two large offshore mussel farms are proposed within the Bay of Plenty (pers. comm. EBOP), offshore from Pukehina and Opotiki (Figure 7.23). The farms are expected to consist of numerous 200 m backbones, each with 3100 m of culture rope (droppers); backbones and droppers are arranged such that mussels grow within the range of 15-25 m (pers. comm. Eastern Seafarms). The proposed farm off Opotiki (Figure 7.23) consists 1312 backbones over an area of 3800 Ha (pers. comm. Eastern Seafarms), corresponding to 4067.2 km of culture rope. At identical stocking densities the farm offshore from Pukehina would consist of 4290.1 km of culture rope.

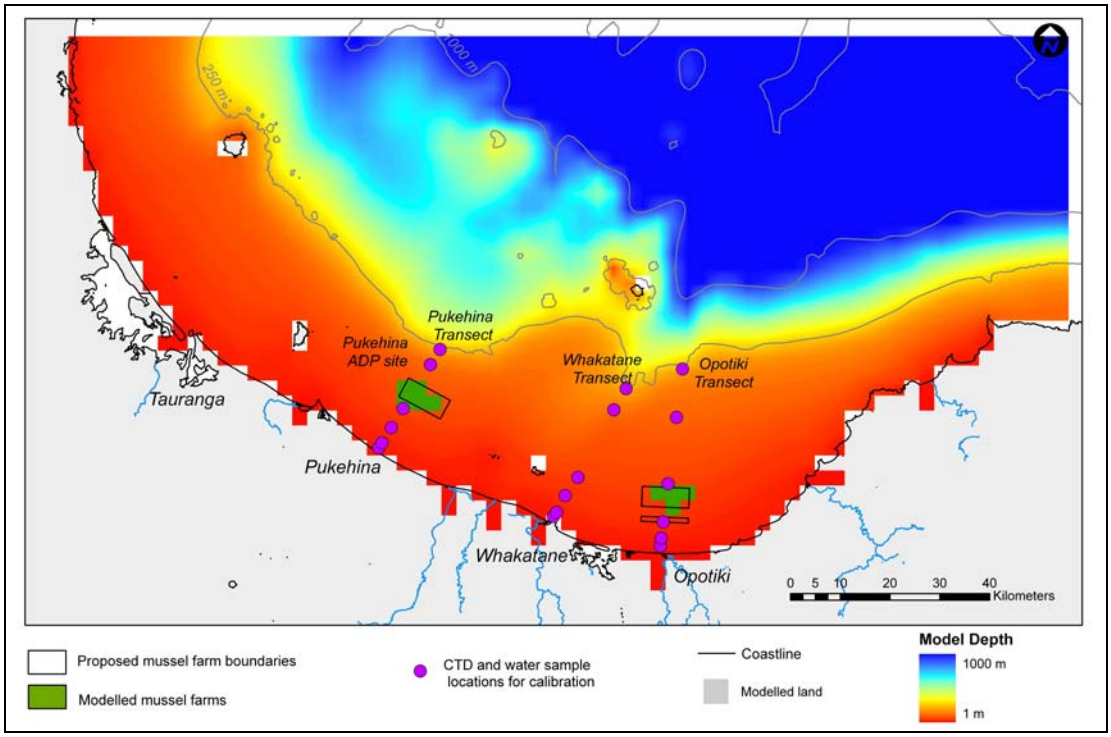

Figure 7.23 Proposed and modelled mussel farm boundaries within the Bay of Plenty. Calibration points for both CTD (fluorometer) and water samples (nutrients) bisect both proposed locations, ensuring that model is locally accurate (as calibrated) surrounding these areas. Proposed mussel farm boundary extents courtesy of EBOP.

Typical suspended offshore mussel farm lines contain, at any one time, 35 mm mussels over 28% of lines, 75 mm mussels over an additional 28% of lines, and a further 28% with 95 mm mussels, the remaining lines being empty or used for spat catching (pers. comm. Eastern Seafarms). Lines are generally seeded at 180 mussels per meter. Greenshell mussel shell length (M_{SL}, mm), for animals not subject to periodic desiccation, can be converted to dry tissue weight (M_{DW}, g), (Marsden and Weatherhead, 1999) by (R^2=0.921):

$$M_{DW} = M_{DW}A.M_{SL}^{M_{DW}b} \qquad \textbf{Equation 7.43}$$

where $M_{DW}A$ = 1.84 x10^{-6} and $M_{DW}b$ = 3.08 from Marsden and Weatherhead's (1999) data. This gives individual mussel dry weights of 0.1048, 1.0965, and 2.2709 for 35, 75, and 95 mm shell lengths respectively. An average meter of mussel farm line will contain 50.4 of each size class of mussels.

Culture rope is assumed to be evenly distributed throughout the farms and, with a model cell size of 900 Ha (3km x 3km), farm sizes are approximated to 4 and 5 model cells (3600 Ha and 4500 Ha) for the Opotiki and Pukehina farms respectively. The density of culture ropes is adjusted slightly to maintain a 'consistent-with-reality' number of mussels being farmed (Table 7.5).

Table 7.5 Actual and modelled details of mussel farm size, lengths of culture rope, and number of mussels farmed.

Farm details	Pukehina Farm	Opotiki Farm
Actual size (Ha)	4009	3800
Modelled size (Ha)	4500	3600
Model cells (900 Ha each)	5	4
Actual culture rope (km)	4290.1	4067.2
Modelled culture rope (km)	4290.1	4067.2
Actual culture rope density ($m.m^{-2}$)	0.107	0.107
Modelled culture rope density ($m.m^{-2}$)	0.0953	0.113
Actual depth of cultivation (m)	15-25	15-25
Modelled depth of cultivation (m)	15-25	15-25
Actual number of mussels farmed	648663120	614960640
Modelled number of mussels farmed	648663120	614960640
Actual dry tissue weight of farmed mussels (kg)	750763	711755
Modelled dry tissue weight of farmed mussels (kg)	750763	711755
Number of 35 mm mussels per model farm cell	43244208	51246720
Number of 75 mm mussels per model farm cell	43244208	51246720
Number of 95 mm mussels per model farm cell	43244208	51246720
Number of 35 mm mussels per m^{-3}	0.4805	0.5694
Number of 75 mm mussels per m^{-3}	0.4805	0.5694
Number of 95 mm mussels per m^{-3}	0.4805	0.5694

During the 'mussel-farming' model runs the location, stocking density and mussel size for each of the 3 mussel size classes was specified and corresponding clearance rates, NH3 excretion, oxygen consumption, and bio-deposit generation determined based on internal model dynamics, local temperature, and on the concentration of seston. The model, inclusive of mussel farms, was run for an entire year and both seasonal and year-long differences to the 'no mussel farm' model predictions determined.

7.10 'MUSSEL-FARMING' RESULTS

Year-long averaged mean absolute changes in Chl-a as a result of the mussel farms are of the order of 0.2 $mg.m^{-3}$ in the immediate vicinity of the mussel farms (Figure 7.24) and decrease rapidly with vertical scales of ~15 m and horizontal (long-shore) scales of ~50 km (relative to the farm size of 10 m vertical and ~10 km horizontally). Expressed as a percentage of the 'no mussel farm' simulations, peak year-long mean depletion estimates are in the range of 6-8 % in the immediate vicinity of the mussel farms. Percentage wise depletion halos (Figure 7.25) extend a much greater distance along East Cape relative to other locations within the Bay of Plenty as a result of low natural phytoplankton concentrations predicted there (Figures 7.21 and 7.22). The low natural concentrations result in a greater percentage wise reduction (for a given absolute depletion amount, *e.g.* 0.1 $mg.m^{-3}$), whilst also restricting the potential for rapid recovery through the reduced biomass. Zooplankton depletion estimates are of similar magnitude (percentage-wise) to that of Chl-a in the immediate vicinity of the farms, yet exhibit far greater spatial extents of depletion (Figure 7.26). A likely cause of this is the much slower growth rates (and hence recovery rates) of zooplankton relative to phytoplankton. In addition, low ambient concentrations of zooplankton in the oceanic regions of the Bay of Plenty require only a small decrease in absolute terms to return a percentage based decrease of ~0.5-1%.

Additional mussel farm induced changes occur to DO concentrations (Figure 7.27). Mussels directly consume oxygen through respiration and indirectly decrease concentrations through the addition of NH3 (which can be subsequently converted to oxidised nitrogen, consuming oxygen) and by filtering phytoplankton which are capable of photosynthesising and producing oxygen. Additionally, they may indirectly increase oxygen concentrations through the stimulatory addition of NH3 increasing phytoplankton concentrations (as observed during summer, Figure 7.30), and by filtering detrital particles which may otherwise be mineralised and consume oxygen during this process. Predicted year-long mean changes to DO concentrations within the Bay of Plenty resulting from farmed mussels are insignificant (-0.006% - +0.001%).

Cultured mussels influence NH3 concentrations directly through the excretion of NH3 products and indirectly through the filtering of detrital particles leading to reduced potential mineralisation of these particles to NH3 by-products. Additionally, impacts on phytoplankton and zooplankton communities through filtering reduce the potential detritus pool for mineralisation. Modelled year-long averaged impacts of cultured mussels on the NH3 environment within the Bay of Plenty include a localised increase (~ 2-3%) in the immediate vicinity of the farms and a more wide spread decrease of much lower magnitude (~0.2%) in the upper 25 m throughout the Bay of Plenty (Figure 7.28).

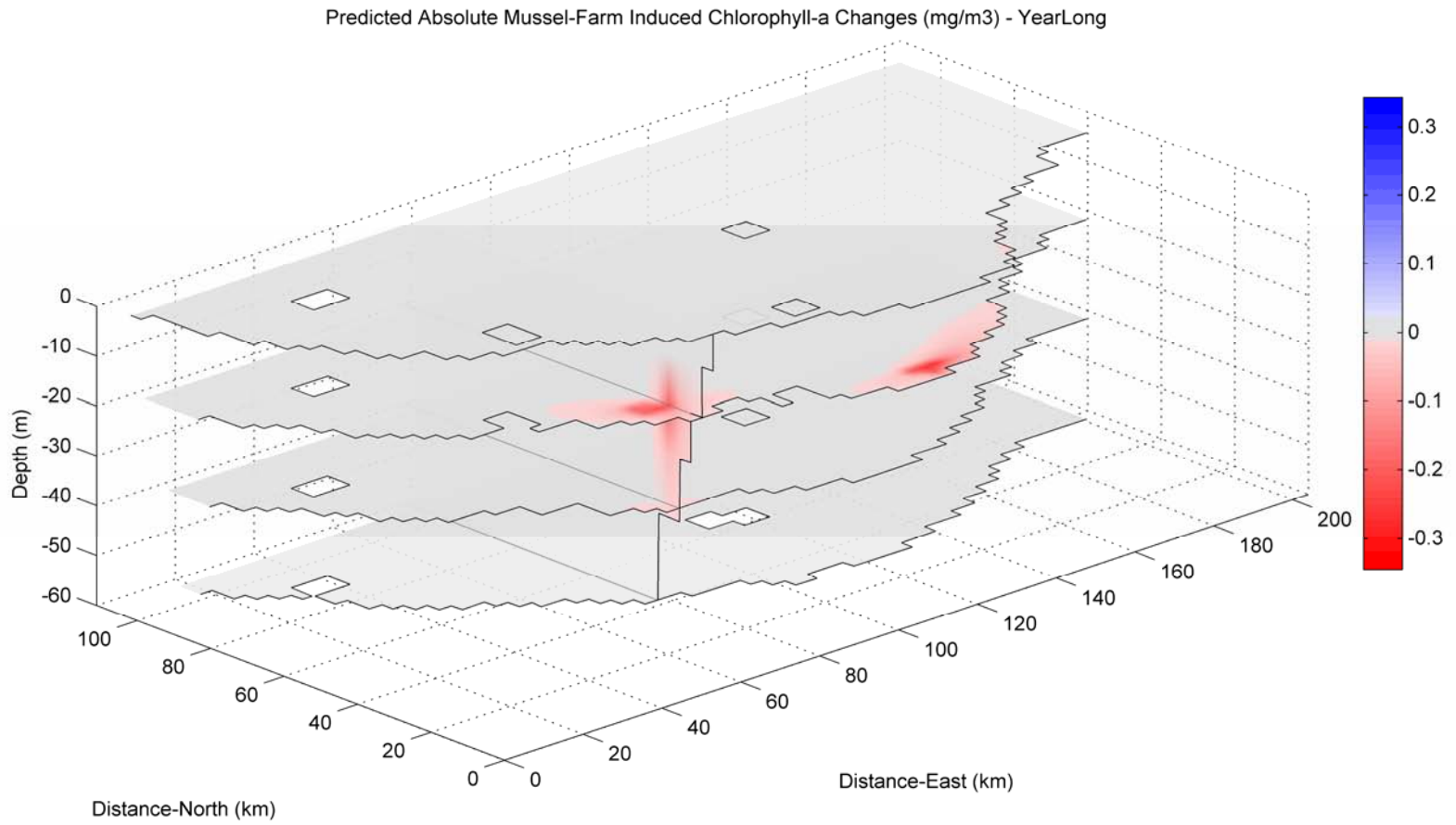

Figure 7.24 Modelled absolute change in chlorophyll-a concentration averaged throughout the year as a result of two mussel farms. Image location is relative to the model origin (2761000 mE, 6339000 mN NZMG1949) and represents horizontal surfaces at -2.5, -20, -40, and -60 m depths, with a vertical section (N-S) through 2839000 mE NZMG1949.

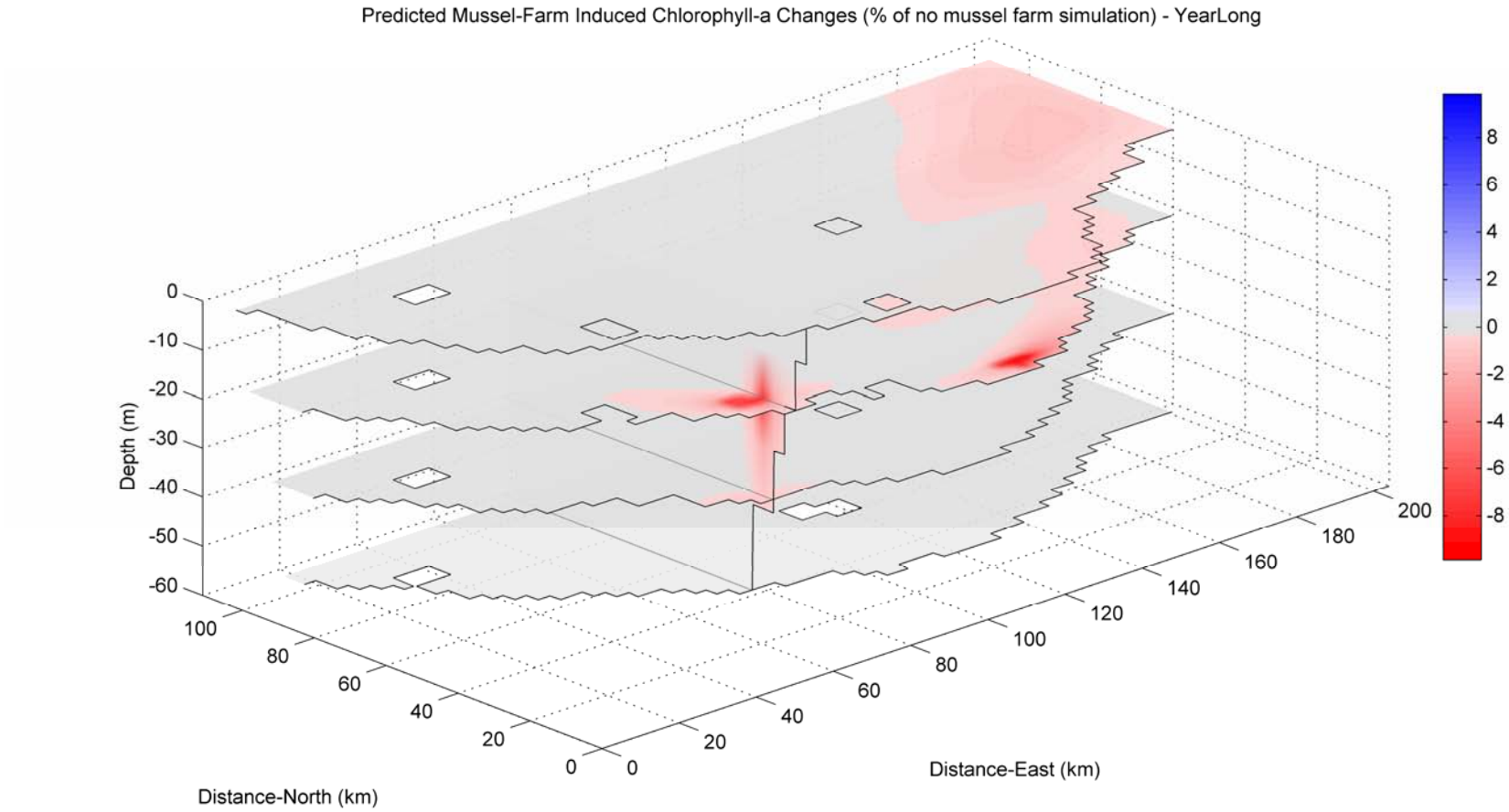

Figure 7.25 Modelled changes in chlorophyll-a concentration resulting from two mussel farms (% change from no mussel farm scenario). Image location is relative to the model origin (2761000 mE, 6339000 mN NZMG1949) and represents horizontal surfaces at -2.5, -20, -40, and -60 m depths, with a vertical section (N-S) through 2839000 mE NZMG1949.

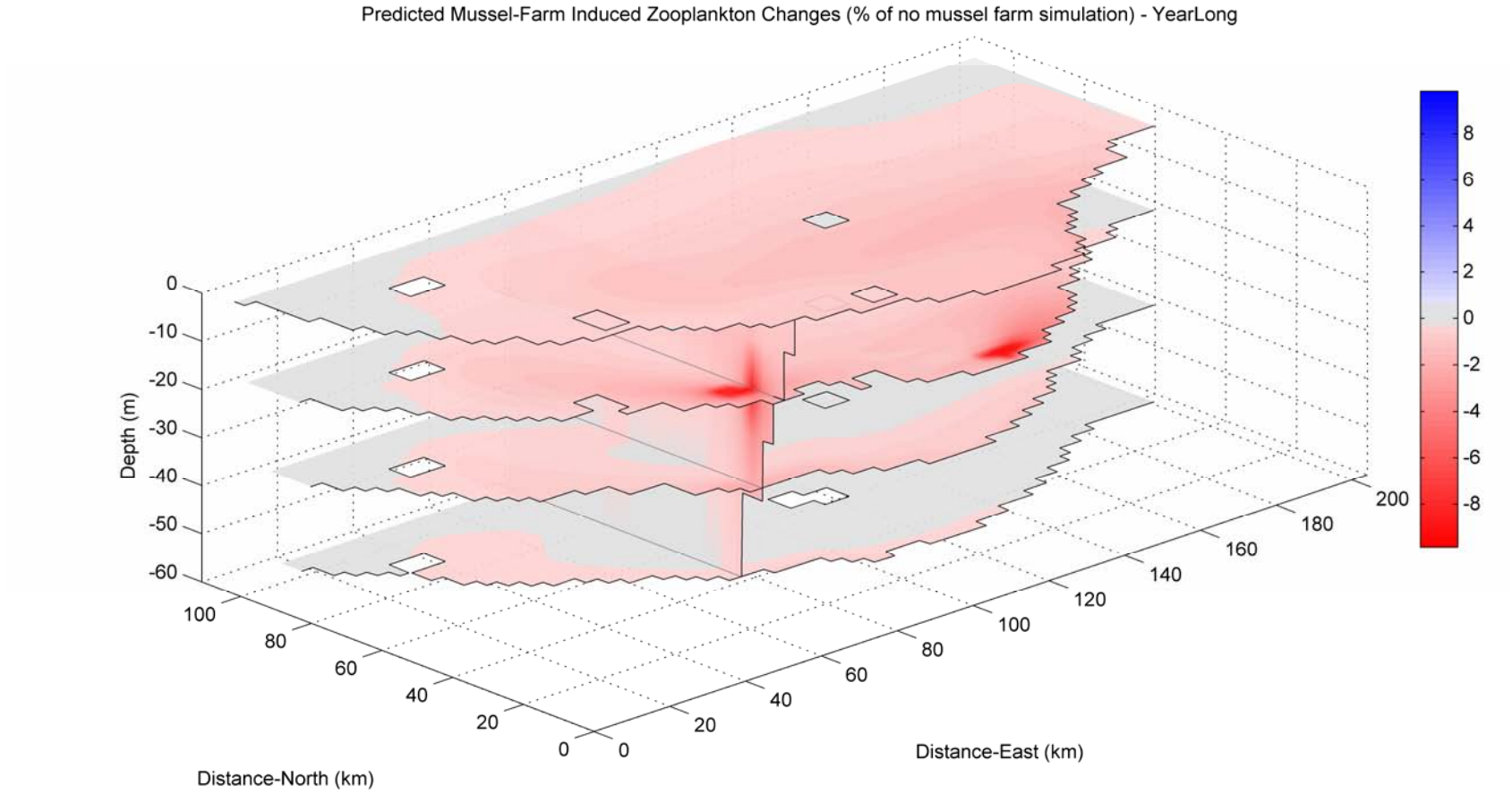

Figure 7.26 Modelled changes in zooplankton biomass resulting from two mussel farms (% change from no mussel farm scenario). Image location is relative to the model origin (2761000 mE, 6339000 mN NZMG1949) and represents horizontal surfaces at -2.5, -20, -40, and -60 m depths, with a vertical section (N-S) through 2839000 mE NZMG1949.

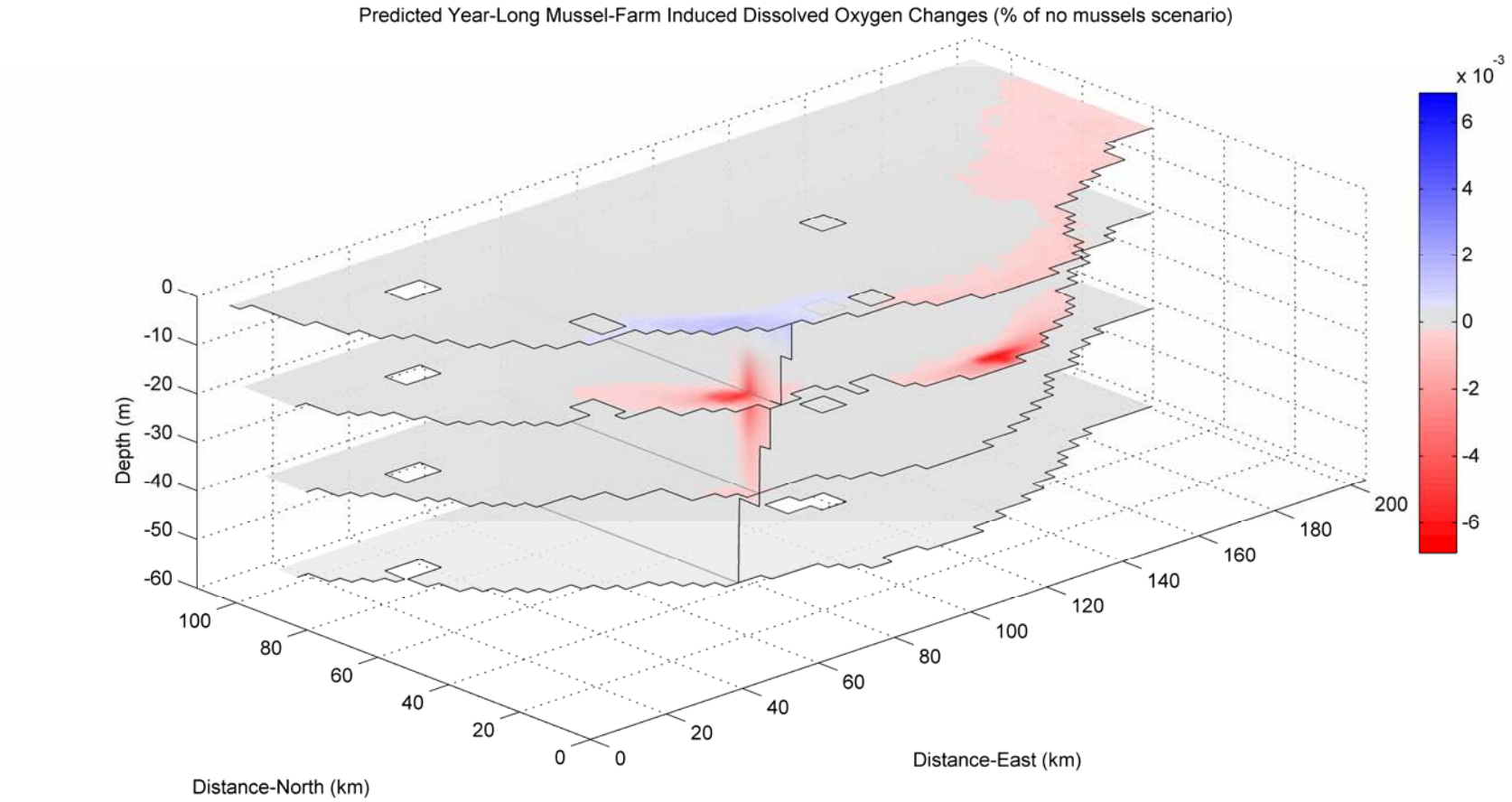

Figure 7.27 Modelled changes in dissolved oxygen concentration resulting from two mussel farms (% change from no mussel farm scenario). Image location is relative to the model origin (2761000 mE, 6339000 mN NZMG1949) and represents horizontal surfaces at -2.5, -20, -40, and -60 m depths, with a vertical section (N-S) through 2839000 mE NZMG1949.

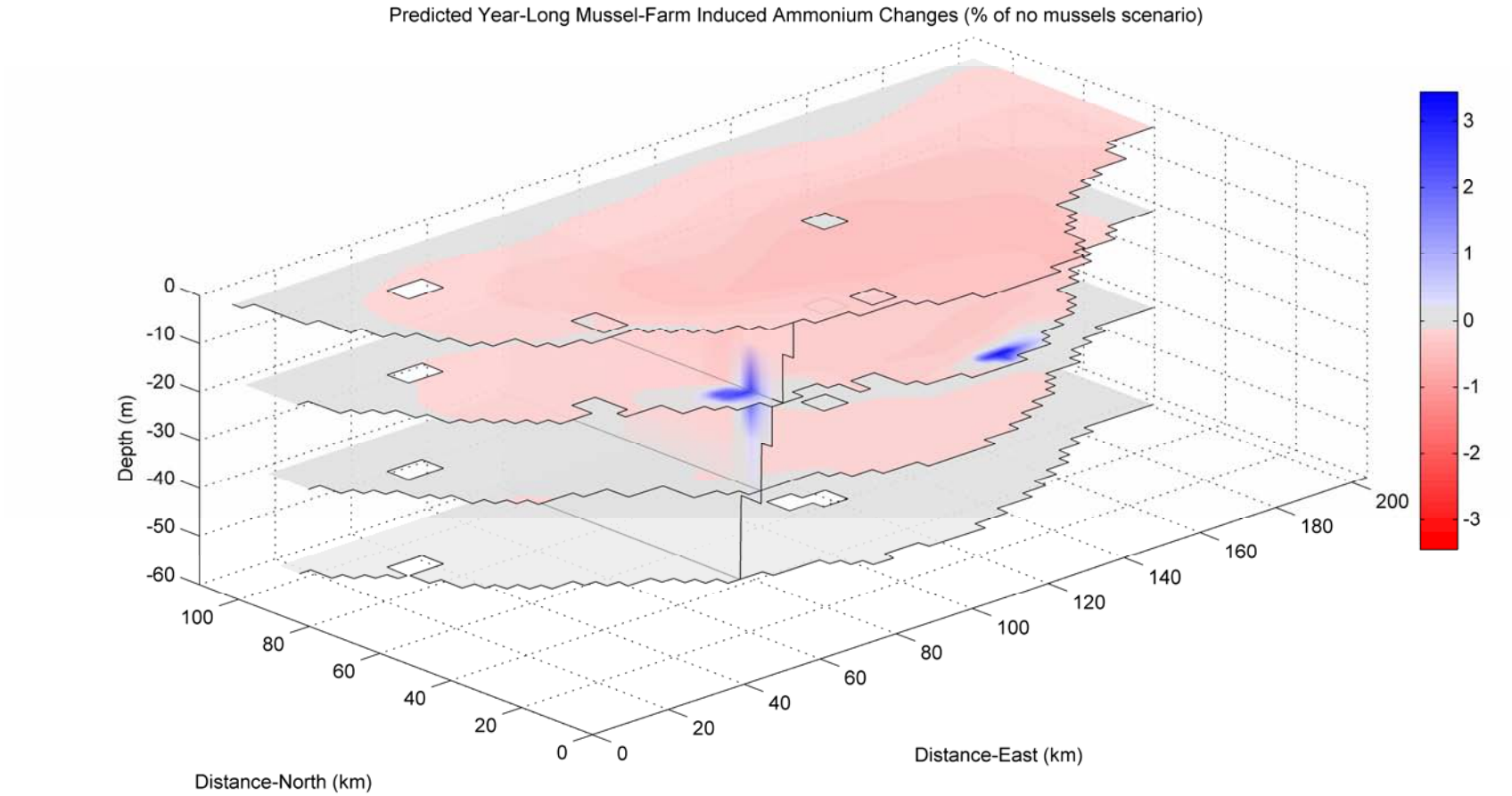

Figure 7.28 Modelled changes in ammonium concentration resulting from two mussel farms (% change from no mussel farm scenario). Image location is relative to the model origin (2761000 mE, 6339000 mN NZMG1949) and represents horizontal surfaces at -2.5, -20, -40, and -60 m depths, with a vertical section (N-S) through 2839000 mE NZMG1949.

As the concentration of Chl-a (and hence phytoplankton) has been observed to vary significantly over seasonal time-scales (Figures 7.19 and 7.20), the depletion effects of a large mass of filtering bivalves can equally be expected to vary over similar time-scales. Additionally, as the model is less effective at replicating the observed nutrient concentrations from March to August 2004 a seasonally based analysis of model results is appropriate. To investigate this proposition, model outputs are considered over periods corresponding to Spring (Sep-Oct-Nov, Figure 7.29), Summer (Dec-Jan-Feb, Figure 7.30), Autumn (Mar-Apr-May, Figure 7.31), and Winter (Jun-Jul-Aug, Figure 7.32). Seasonal ambient Chl-a concentrations, mussel induced changes and the extent of depletion halos are tabulated in Table 7.6. Variation of predicted depletion levels over shorter time scales (daily-weekly) was relatively weak meaning seasonal time frames are the most appropriate scales on which to consider depletion predictions.

Predicted changes are of greatest magnitude and small horizontal/vertical extents during spring, when localised depletion estimates are ~0.3 $mg.m^{-3}$ (Figure 7.29). During summer the magnitude of depletion is lower (~ 0.1 $mg.m^{-3}$), and the extent of the depletion halo is similar to that during spring (Figure 7.30). Notably, near the Pukehina farm there is evidence of some stimulatory increase in phytoplankton biomass (Figure 7.30), likely to be a result of the excretion of NH3 from the mussels at a time when ambient light and temperature conditions are suitable for phytoplankton growth and ambient nutrient concentrations are depressed following the spring bloom (*e.g.* Smaal *et al.* 2001). During autumn, localised depletion is weaker at the Pukehina farm *cf.* the Opotiki farm (Figure 7.31). The extent of the depletion halo during autumn is remarkably larger than that during either spring or summer, potentially a result of slower phytoplankton growth rates in the reduced light and temperature environment. The depletion halo extends from the mussel farms along the coast toward East Cape. Consistent with spring and summer, the greatest magnitude and depletion halo extent is found between 15-25 m depths, the same depths at which the modelled mussels are cultivated. Depletion estimates during winter (low ambient Chl-a) follow a pattern of reduced localised depletion (absolute reductions < 0.1 $mg.m^{-3}$) and greater horizontal and vertical depletion halo extents (Figure 7.32).

At both farm sites, and throughout all individual seasons, farm induced Chl-a depletion is greatest between 15-25 m depth (Table 7.6), the same depth at which the mussels are cultivated. While the absolute change in Chl-a concentration is greatest during spring time (Figures 7.29-7.32), on a 'percent-of-original' scale the changes are greatest during autumn at both Opotiki and Pukehina farms (Table 7.6). Highest estimates of depletion are ~17% at the Opotiki site (where ambient Chl-a concentrations are typically lower than at Pukehina, Figures 7.21 and 7.22) between 15-25m depth during autumn. Also at this time, both 1 and 5% depletion halos are at their maximal extents (Table 7.6).

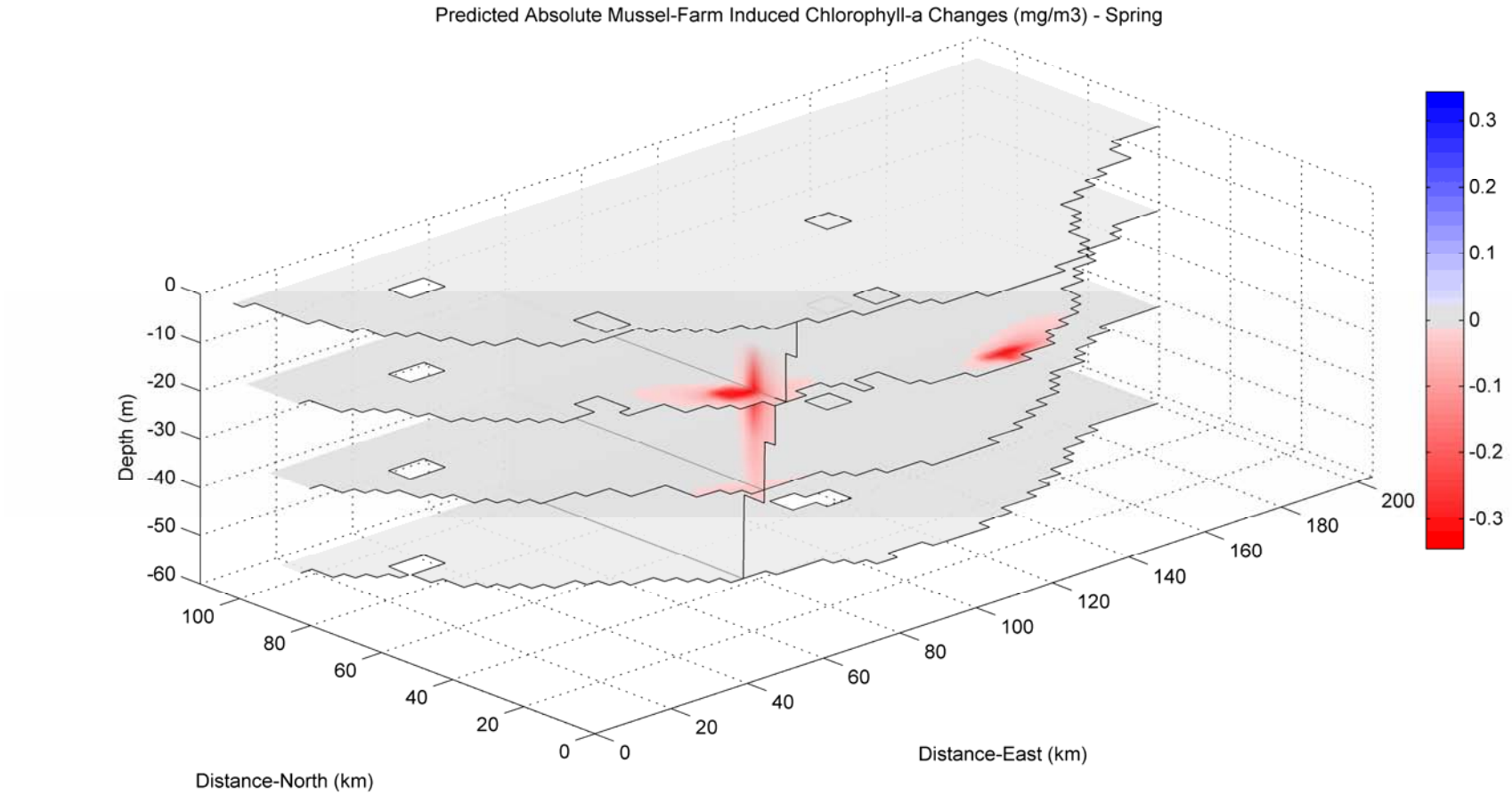

Figure 7.29 Modelled absolute change in chlorophyll-a concentration averaged through spring (Sep-Oct-Nov) as a result of two mussel farms. Image location is relative to the model origin (2761000 mE, 6339000 mN NZMG1949) and represents horizontal surfaces at -2.5, -20, -40, and -60 m depths, with a vertical section (N-S) through 2839000 mE NZMG1949.

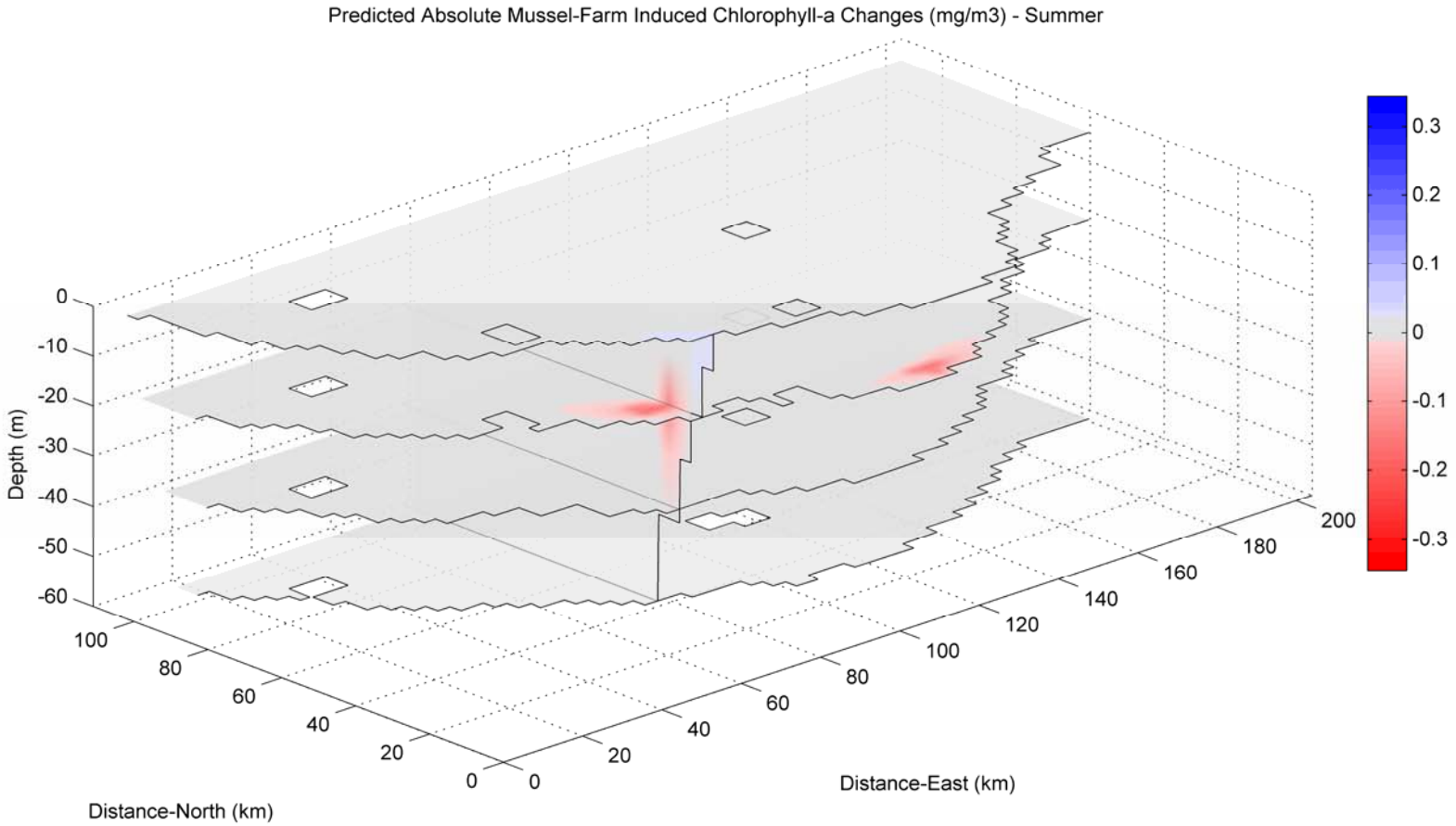

Figure 7.30 Modelled absolute change in chlorophyll-a concentration averaged through summer (Dec-Jan-Feb) as a result of two mussel farms. Image location is relative to the model origin (2761000 mE, 6339000 mN NZMG1949) and represents horizontal surfaces at -2.5, -20, -40, and -60 m depths, with a vertical section (N-S) through 2839000 mE NZMG1949.

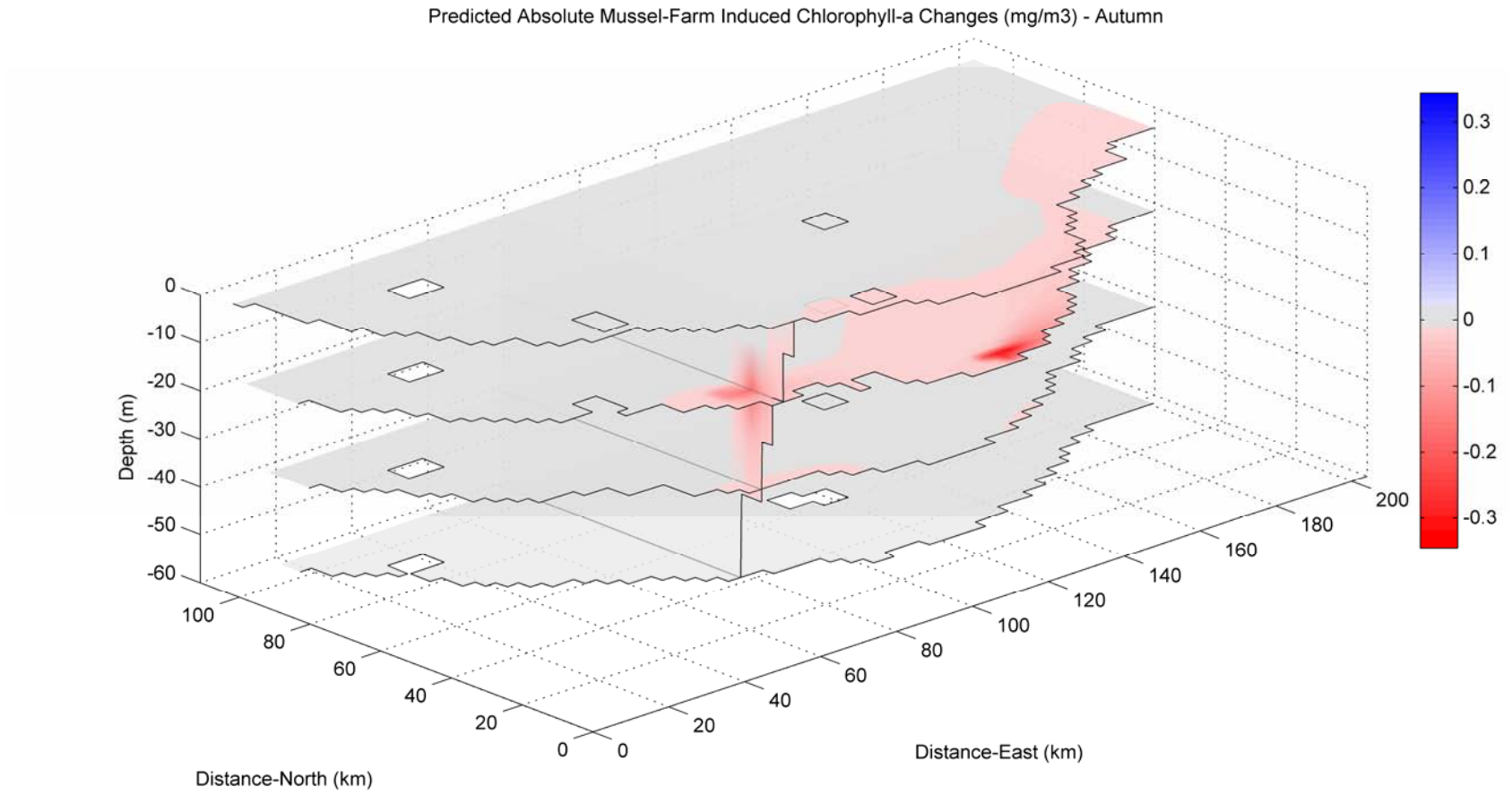

Figure 7.31 Modelled absolute change in chlorophyll-a concentration averaged through autumn (Mar-Apr-May) as a result of two mussel farms. Image location is relative to the model origin (2761000 mE, 6339000 mN NZMG1949) and represents horizontal surfaces at -2.5, -20, -40, and -60 m depths, with a vertical section (N-S) through 2839000 mE NZMG1949.

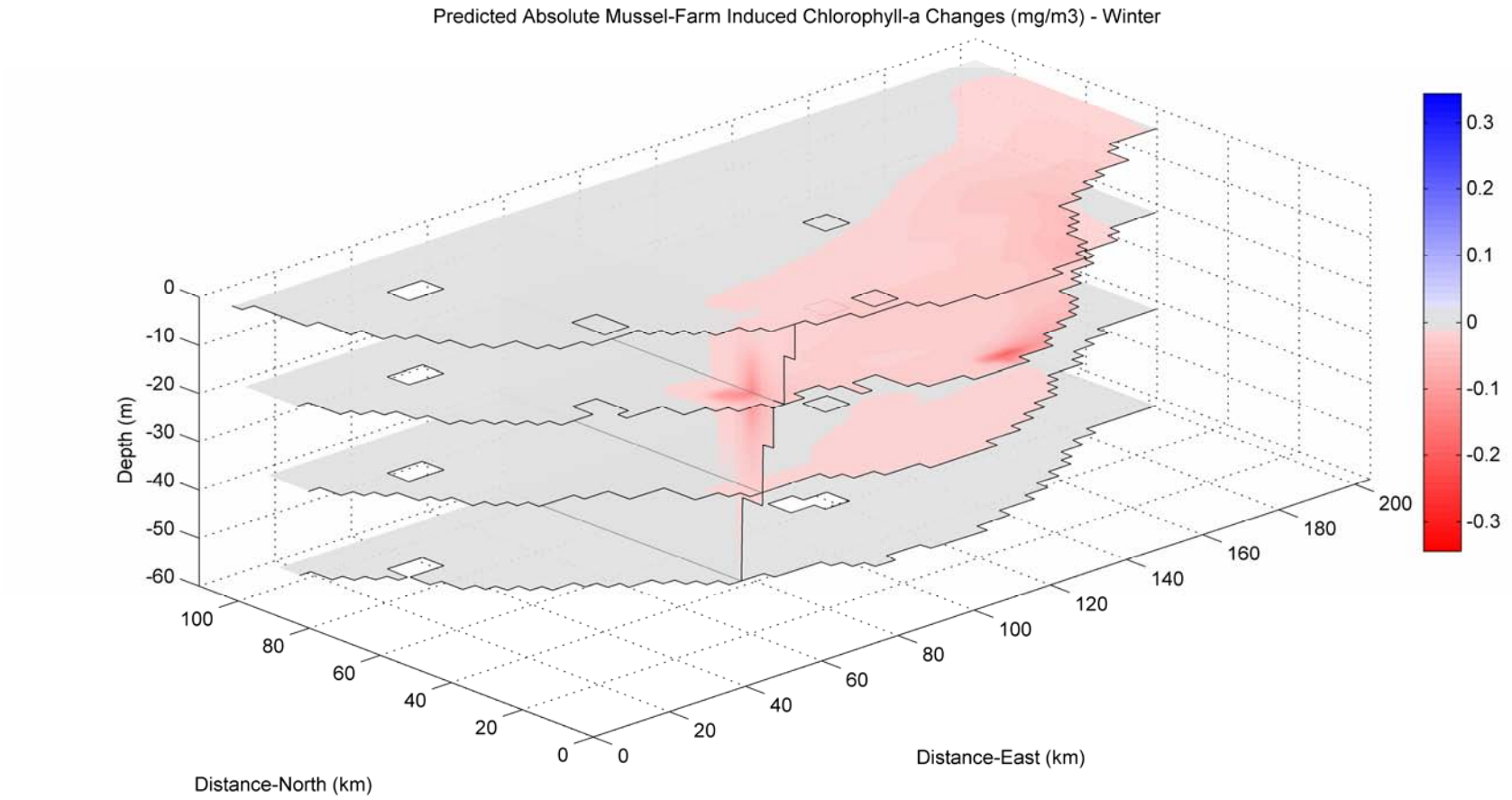

Figure 7.32 Modelled absolute change in chlorophyll-a concentration averaged through winter (Jun-Jul-Aug) as a result of two mussel farms. Image location is relative to the model origin (2761000 mE, 6339000 mN NZMG1949) and represents horizontal surfaces at -2.5, -20, -40, and -60 m depths, with a vertical section (N-S) through 2839000 mE NZMG1949.

Table 7.6 Modelled mean chlorophyll-a concentrations at farm sites (in the absence of aquaculture), potential mussel farm induced change, and horizontal extents of the 1 and 5 % Chl-a depletion halos through depth and season.

	Individual Farm Scale (avg. across entire farm)				Cumulative Regional scale	
	Pukehina		Opotiki			
0-5 m depth	**Mean Chl-a without mussels ($mg.m^{-3}$)**	**Mussel induced change (%)**	**Mean Chl-a without mussel ($mg.m^{-3}$)**	**Mussel induced change (%)**	**Extent of 1% depletion halo (km^2) [size relative to farmed area]**	**Extent of 5 % depletion halo (km^2) [size relative to farmed area]**
Spring	4.12	+0.2	2.77	+0.3	0	0
Summer	1.55	+0.4	0.82	+0.1	234 [2.9]	0
Autumn	0.87	-0.4	1.22	-1.1	3456 [42.7]	0
Winter	0.93	-1.0	1.33	-2.0	7821 [96.6]	0
Year-Long	2.14	+ 0.1	1.61	-0.2	927 [11.4]	0
5-15 m depth						
Spring	4.89	-0.2	3.74	-0.3	0	0
Summer	1.90	+0.3	1.14	-0.2	0	0
Autumn	1.31	-0.5	2.16	-1.4	3780 [46.7]	0
Winter	1.19	-1.8	1.68	-2.8	6741 [83.2]	0
Year-Long	2.73	-0.2	2.43	-0.7	0	0
15-25 m depth						
Spring	4.97	-6.4	4.69	-6.7	270 [3.3]	81 [1.0]
Summer	1.79	-8.3	1.31	-11.7	405 [5.0]	90 [1.1]
Autumn	1.81	-11.1	1.82	-16.8	4527 [55.9]	243 [3.0]
Winter	1.07	-9.7	1.47	-11.6	6084 [75.1]	198 [2.4]
Year-Long	2.68	-7.1	2.68	-9.6	567 [7]	90 [1.1]
25-35 m depth						
Spring	4.97	-1.5	5.28	-0.7	45 [0.6]	0
Summer	1.77	-1.5	1.59	-0.7	45 [0.6]	0
Autumn	0.90	-4.1	1.11	-4.4	4104 [50.7]	81 [1.0]
Winter	0.77	-4.7	1.03	-4.2	5040 [62.2]	0
Year-Long	2.54	-1.7	2.66	-1.5	189 [2.3]	0
35-50 m depth						
Spring	3.79	-0.6	4.68	-0.1	0	0
Summer	1.50	no change	1.67	+0.6	0	0
Autumn	0.52	-1.8	0.61	-2.4	3411 [42.1]	0
Winter	0.44	2.7	0.69	-3.0	4167 [51.4]	0
Year-Long	1.93	-0.6	2.30	-0.4	0	0

7.11 MODEL SENSITIVITY

As there are no data available to calibrate the mussel sub-model component of the numerical model, a sensitivity analysis was conducted to determine the model response to parameter manipulation. Following the Plackett-Burman (1946) sensitivity analysis procedure, each parameter within the mussel sub-model was varied in isolation by ±10% and the change in the extent of the year-long averaged 1% depletion halo at 15-25 m depth determined. Using this approach the direction of parameter sensitivity reflects the relationship of the parameter to the given outcome. For example $M_{DW}b$ (Equation 7.43) has a positive relationship with the extent of the depletion halo (Figure 7.33), indicating that an increase in the parameter (reflecting an increase in mussel dry weight size per shell length) results in an increase in the depletion halo extent. By contrast, E_{ZM} (Equation 7.15) has a negative relationship with depletion halo extent, an increased efficacy of mussel feeding on zooplankton results in increased removal of zooplankton from the water column and a smaller phytoplankton depletion halo as there a fewer zooplankton to prey on remaining phytoplankton.

The model is generally insensitive to mussel sub-model parameters with the exception of $M_{DW}b$ (Equation 7.43), the exponent in Marsden and Weatherhead's (1999) equation relating mussel shell length to the animal's dry weight, and θ_M, the mussel filtration temperature coefficient (Equations 7.2 and 7.38, Figure 7.33). Further investigative work to improve the reliability of these values would provide additional confidence in model results. Each of these factors indirectly influences the modelled filtration rate of the simulated mussel farms as a whole, indicating depletion halo extent is sensitive to farm level filtration and clearance rates. Additionally, $M_{DW}b$ (Equation 7.43) being an exponent in the equation to determine mussel dry weight body mass has a significant influence on the mussel mass for a given shell length size. Mussel clearance rates, NH3 excretion rates, and respiration rates are all a function of individual mussel dry weight body mass, meaning that changes to this factor ($M_{DW}b$) induce relatively wide ranging variation within the model dynamics.

The extents of modelled depletion halos are insensitive to changes in parameters directly influencing mussel respiration, mussel clearance rates, mussel NH3 excretion, and the mussel filtration efficacy on zooplankton and detritus (Figure 7.33).

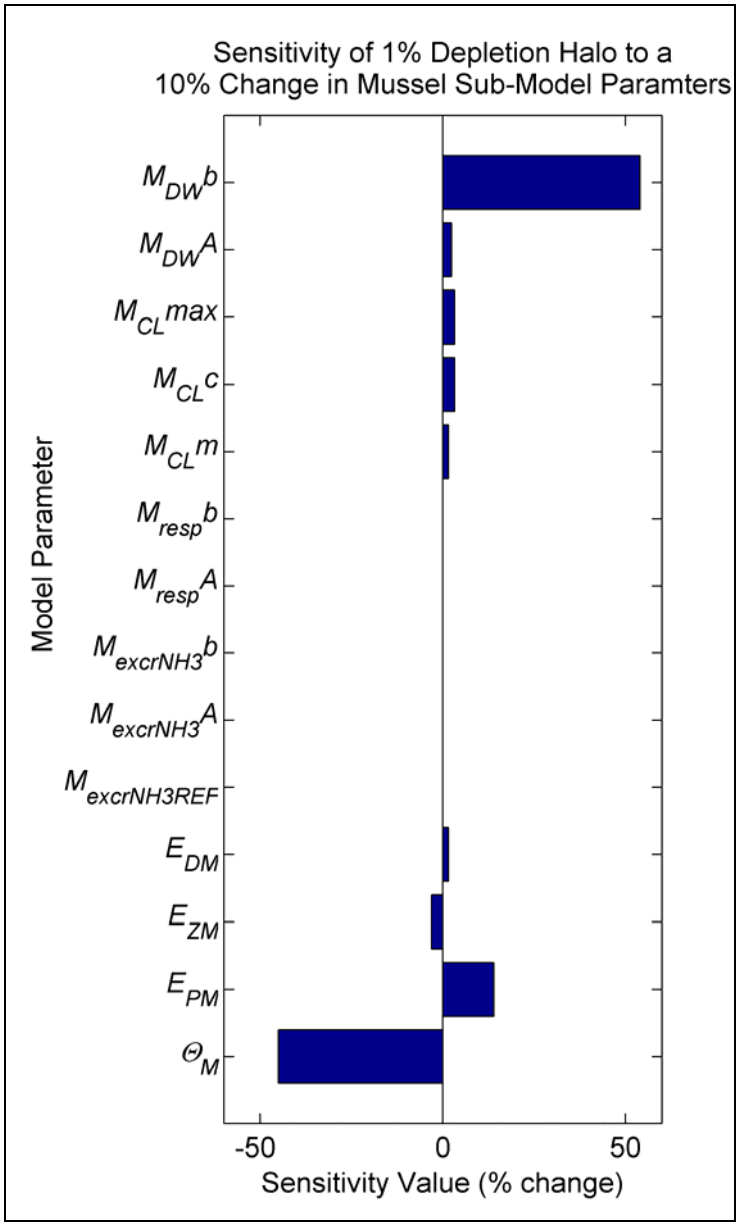

Figure 7.33 Sensitivity of modelled 1% depletion halo (15-25 m depth) to a 10% manipulation in mussel sub-model parameters. The sensitivity value represents the percent change in the depletion halo for a 10% change in model parameter. A large value indicates the model outcome exhibits a large response from the 10% change in parameter. A positive sensitivity value indicates a positive relationship between the model outcome and parameter, while a negative value indicates a negative relationship.

7.12 DISCUSSION/IMPLICATIONS OF DEPLETION ESTIMATES

Numerical simulations within the Bay of Plenty indicate that Chl-a (as a proxy for phytoplankton) is typically higher in the nearshore areas (< 10-15 km from shore) than offshore (> 25 km from shore) regions and highest between Tauranga and Whakatane (Figures 7.21 and 7.22). Predicted Chl-a is generally 2-3 times higher at the Pukehina farm site than the Opotiki site (Figures 7.12 and 7.22, Table 7.6), and throughout the Bay of Plenty is highest during spring (October – December) and lowest during autumn and winter both at the surface and at 15-25m depths (Figures 7.6, 7.7, 7.19, 7.20).

Simulated mussel farms located at both Pukehina and Opotiki induce temporally and spatially variable impacts on ecosystem components, including (but not limited to) phytoplankton, zooplankton, ammonium, and dissolved oxygen (Figures 7.24-7.30).

Maximal Chl-a depletion (≥ 5%) is restricted vertically to the depths at which the mussels are farmed (15-25 m) and horizontally to scales of similar dimensions to those of the farms themselves; greatest depletion effects are predicted during autumn and winter (Table 7.6).

Greatest absolute reductions of Chl-a occur during the spring bloom period (Figure 7.29), however, when viewed as a percentage of the 'original' concentration, greatest reductions occur during autumn, when ambient Chl-a concentrations are lower by a factor of 3-4 *cf.* spring (Table 7.6). Poor ambient conditions for phytoplankton production during autumn and winter (reduced light and temperature environments) result in slow phytoplankton growth rates and restrict the ability of the phytoplankton community to 'recover' from the localised depletion at these times. During spring, more favourable conditions (nutrients, light and temperatures) result in more rapid growth rates and a faster 'recovery'. A consequence of this is that the horizontal and vertical extents of phytoplankton depletion halos are greatest during autumn and winter (Figures 7.31 and 7.32, Table 7.6). The potential for mussel farms to positively contribute to the phytoplankton biomass indirectly through the excretion of NH3, as observed by Dame *et al.* (1991) and Smaal *et al.* (2001) is predicted to a limited degree near the surface during spring and to a greater degree during summer (Table 7.6). The effect is thought to be greatest during summer as phytoplankton are typically nutrient limited at this time as opposed to autumn and winter where the ambient light and temperature conditions additionally restrict growth. Notably, a modelling study by Chapelle *et al.* (2000) identified a similar stimulatory response of the phytoplankton during summer to grazing pressure and excretion of NH3 by bivalves in their study of the Thau Lagoon.

Predicted zooplankton depletion halos extend over much larger spatial extents than those for phytoplankton. This occurs due to the slower growth potential of zooplankton relative to phytoplankton. However, the magnitude and spatial scale of

zooplankton depletion is directly related to the mussel feeding efficacy on zooplankton, a figure for which there is little empirical data on which to base model assumptions (Zeldis *et al.*, 2004b)

Jiang and Gibbs (2005) defined the production carrying capacity to be when cultured bivalves essentially replace zooplankton as the 'top' consumers of phytoplankton, creating a nutrient-phytoplankton-bivalve-detritus system, a situation very unlikely within the Bay of Plenty, given the low level of modelled zooplankton depletion (Figure 7.26). The ecological carrying capacity was deemed to be that level of culture which does not significantly alter the major energy fluxes or structure of the food web (Jiang and Gibbs, 2005). Using a linear food web model, they found that the ecological carrying capacity of Tasman and Golden Bays in New Zealand was ~80% lower than the production carrying capacity.

Predicted depletion extents are most sensitive to factors which influence dry weight size. The inference from this is that should the cultured mussels vary considerably in their dry weight tissue mass to shell length ratio from that described by Marsden and Weatherhead (1999), then model predictions are less valid. A potential scenario is that the industry breeds a 'more efficient' mussel which has higher tissue mass for a given shell length; in this case revised predictions would be required.

With respect to production potential and the production carrying capacity for mussel farms at the two sites, Waite (1989), Hawkins *et al.* (1999), Ross *et al.* (1999), and Inglis *et al.* (2000) identified Chl-a concentrations below ~1.0 $mg.m^{-3}$ to be poor for mussel growth. At the depths at which mussels are likely to be cultured (15-25 m) Chl-a concentrations are consistently above this level at both potential farm sites (~ 2.7 $mg.m^{-3}$, Table 7.6); a value similar to mean annual concentrations at highly productive bivalve aquaculture sites worldwide (Dame and Prins, 1998; Duarte *et al.*, 2003).

7.12.1 IMPACTS ON ECOLOGICAL CARRYING CAPACITY

At the ecosystem level, ecosystem carrying capacity can be defined as "*the level to which a process or variable may be changed within a particular ecosystem, without driving the structure or function of the ecosystem over certain acceptable limits*" (Duarte *et al.*, 2003; McKindsey *et al.*, 2006).

Currently there are few studies which have focussed on regional level ecological carrying capacity with respect to aquaculture, *i.e.* percentage wise changes in ecosystem parameters which may invoke subsequent changes to other ecosystem compartments. Most studies which have been undertaken have focussed on restricted embayments (*e.g.* Rodhouse and Roden, 1987; Grant *et al.*, 1998; Ross *et al.*, 1999; Chapelle *et al.*, 2000; Dowd, 2005; Telfor and Robinson, 2005; Grant *et al.*, 2007), as opposed to large coastal areas such as the Bay of Plenty. Such sites potentially reach

carrying capacity at an earlier stage as a result of their inherently poor (*cf.* open coastal areas) flushing characteristics, nutrient delivery mechanisms, and current speeds.

Often the ecological sustainability of bivalve culture is examined through concepts of water residence times, primary production times, and bivalve clearance times (Dame and Prins, 1998; McKindsey *et al.*, 2006; Gibbs, 2007). The morphological nature of the Bay of Plenty, however, renders some of these 'traditionally' applied (and non-spatially explicit) measures of aquaculture sustainability impractical. For example water residence and bivalve clearance times, while often a decisive factor in enclosed embayments with limited flushing and clearly definable boundaries, are rather inappropriate concepts on open coastlines with limited definable boundaries at their offshore extents. Applying these concepts at open coast locations could lead to either overestimates or underestimates of carrying capacity depending on where boundaries are located.

Sustainability Indicator Curves

Phytoplankton depletion is commonly used as an indicator of ecosystem health with respect to aquaculture development. A general observation from other studies is that authors often conclude that ecological carrying capacity is reached at depletions greater than ~50% at scales ranging from 'farm size' to 'box size' (~ $^{1}/_{16}$ - ¼ embayment size) (Table 7.7). Incze *et al.* (1981), Rodhouse and Roden (1987), and Duarte *et al.* (2003) predicted that when 50% of the available primary production (in restricted embayments) was diverted through cultured mussels, significant modifications of the environment may occur. However, Inglis *et al.* (2005) suggest that there is minimal empirical basis for this 50% figure as natural rates of primary production are extremely variable in space and time.

Presently, using phytoplankton depletion estimates as an indicator of ecosystem change is limited as there are no guidelines detailing depletion levels at which some aspect of ecosystem health is compromised. One promising methodology is that of depletion limits. The methodology requires that consideration be given to both the magnitude of depletion and the spatial extent over which it occurs (Figure 7.34). Specific definitions, and the application of, 'acceptable depletion limits' or 'trigger levels' is difficult and is presently only in the initial stages of implementation with respect to aquaculture globally, with New Zealand at the leading edge. Zeldis *et al.* (2006) and Gibbs (2007) introduced the concept and general shape of sustainable depletion curves, although only limited indications were provided as to their specific shape and depletion magnitude-extent combinations which were (un)sustainable.

Table 7.7 Examples of phytoplankton depletion at various sites of bivalve culture.

Location	Phytoplankton/Chl-a Depletion	Production Capacity	Ecological Capacity	Reference Scale	Notes	Source
Lagune de la Grande-Entrée, Québec, Canada	5% spring 25% autumn	well below	under capacity	box	'does not alter natural biophysical processes'; converted from carbon units; large spatial area relative to the BOP model	Grant *et al.* (2007)
Carlingford Lough, Ireland	4%	below capacity	under capacity	box	enhanced depletion sustainable due to strong water flows and exchange	Bacher *et al.* (1998)
Beatrix Bay, New Zealand	10-25% over 10% of bay 0-10% over 50% of bay	below capacity	at capacity	various		Ogilvie *et al.*, 2000; Gibbs, 2007
Sungo Bay, China	50% annual mean	below capacity	close to / over capacity	not specified, potentially farm	Ecological carrying capacity reached at well before 50% reduction in Chl-a	Duarte *et al.* (2003)
Saldanha Bay , South Africa	7.5%	below capacity		bay wide		Grant *et al.* (1998)
Saldanha Bay, South Africa	88%	not specified	at capacity	within farm	'significant grazing pressure at local scales'	Heasman *et al.* (1998)
Marennes-Oleron Bay, France	30%	over capacity	at capacity	box		Bacher *et al.* (1998)
Killaroy Harbour, Ireland	50 - 60%	over capacity	over capacity	bay wide	'significant modifications'	Rodhouse *et al.*, (1985); Rodhouse and Roden (1987)

In the absence of published guidelines for sustainable depletion magnitude-extent combinations, the findings of studies detailing bivalve culture induced phytoplankton depletion (observed and modelled) are compiled (Table 7.7) and compared to those predicted within the Bay of Plenty (Figure 7.34). A sustainability indicator curve is inferred, with its basic shape taken from Gibbs (2007), and detailed depletion magnitude-extent combinations based on various studies and the authors' assessment of ecological carrying capacities (Figure 7.34, Table 7.7).

Of sites deemed to be operating at or below an 'ecological carrying capacity' (Table 7.7, Figure 7.34), depletion estimates are in the range of 5-25% (seasonal differences and over 'box-scales'; Grant *et al.*, 2007), 10-25% (over 10% of embayment; Gibbs, 2007), 0-10% (over 50% of embayment; Gibbs, 2007), and up to 88% within farms themselves (Heasman *et al.*, 1998).

Within the Bay of Plenty, in the immediate vicinity of the modelled farms, predicted seasonally averaged Chl-a depletion reaches a maximal value of 17% during Autumn (15-25 m water depth, Table 7.6). The predicted extent of the 5% depletion halo reaches a maximal value of 243 km^2 during Autumn in 15-25 m water depths, while the 1 % depletion halo reaches a maximal value of 7821 km^2 during Winter (Table 7.6). Converting the extent of these depletion halos to a percentage based value (required for depletion magnitude-extent values, Figure 7.34) presents a problem on open coast sites as a 'total area' must be defined in a location with no definitive boundaries. Suitable boundaries within the Bay of Plenty are the continental shelf (extending to 200 m water depth) and the regional council marine area (Figure 2.3). The use of both areas results in multiple potential depletion magnitude-extent combinations rather than single point estimates (Figure 7.34). Predicted depletion magnitude-extent combinations using both these boundaries, the maximal extents of the 1% and 5% depletion halos, and the maximal depletion at farm scales (17%) all result in combinations well within the inferred 'sustainable depletion zone', based on assessments of national and international studies (Figure 7.34).

Grant *et al.* (2007) predict localised Chl-a reductions (converted from carbon units) of 5% during spring and 25% during autumn (Table 7.7, Figure 7.34), increases of ammonium by a 'factor of 2 or greater', and reduced detritus concentrations (~12%) within the Lagune de la Grande-Entrée in Québec. They concluded that these changes '*do not exhibit major effects on… ecosystem components*', that the '*current level of mussel aquaculture…does not appear to alter natural biophysical processes throughout the lagoon*', and '*that further aquaculture development could occur…even at higher stocking densities…without exhausting phytoplankton or severely compromising adjacent sites*'. The magnitudes and seasonality of their predictions are broadly consistent with those forecast within the Bay of Plenty (~6-7% Chl-a depletion during spring, and 12-17% during autumn, with localised ammonium increases of ~3%, Figure 7.28). The much coarser spatial resolution of Grant *et al.*'s (2007) box type model, however, infers these changes over a much greater spatial area

(relative to regional scales and farm size) than those within the Bay of Plenty (Figure 7.34).

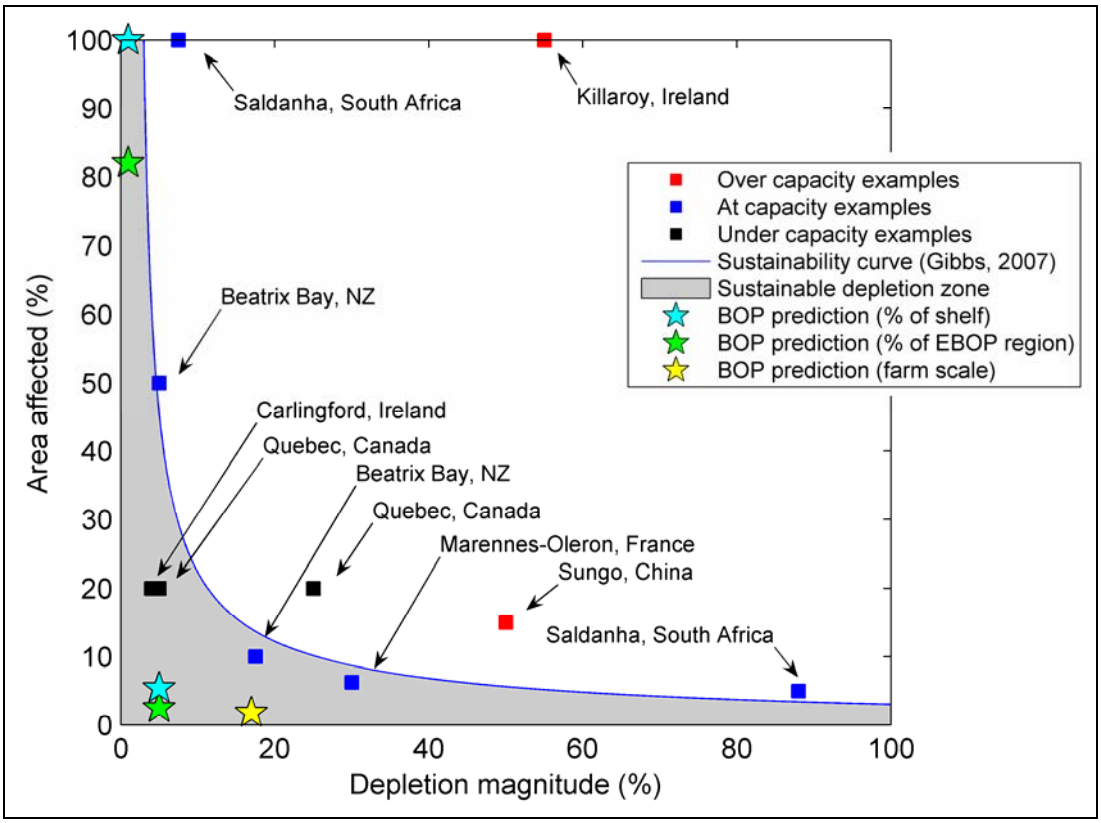

Figure 7.34 Bivalve aquaculture induced depletion magnitude-area affected combinations from published studies and maximal predictions from within the Bay of Plenty. A line of shape as that suggested by Gibbs (2007) has been fitted to those examples which were deemed to be 'near to or at' ecological carrying capacity. Depletion magnitude-extent combinations below this curve (grey area) show high potential for environmental sustainability. References for examples can be found in Table 7.7. Predictions for the Bay of Plenty consider the total area as the continental shelf (0-200 m) between Tauranga and East Cape (4500 km^2, blue and yellow stars), or for the EBOP marine area (9517 km^2: Figure 2.3, green stars).

Further supporting the case for the predicted levels of culture within the Bay of Plenty being of reduced magnitude and scale relative to those observed and predicted at other locations, is the proposition that the Bay of Plenty is likely to have a higher threshold for its ecological carrying capacity relative to the rather enclosed and restricted embayments used for comparisons (*e.g.* Quebec, Beatrix Bay, and Saldanha Bay). The open coastal morphology of the Bay of Plenty creates more favourable conditions for water exchange (Chapters 4 and 5) and renewal than enclosed embayments where water residence times are high and general hydrodynamic energy is lower. It is important to note, that while this is a clear and potentially important concept to consider (ecological carrying capacity being modulated by environmental factors), no empirical or modelled data exists to support this hypothesis and the science is not yet at a stage where comparisons of this nature can be confidently made.

7.12.2 POTENTIAL FOOD WEB CHANGES

Magnitudes of modelled phytoplankton and zooplankton changes suggest that it is unlikely that the farms, as modelled, will significantly alter the structure of zooplankton assemblages, with any impacts likely to be localised. Estimates of Chl-a concentrations at which herbivorous zooplankton growth and survival is compromised varies considerably among species. For example, many zooplankton (*e.g.* copepod and cladoceran species) have lower limits of growth (0.2-1.0 $mg.m^{-3}$, Peters and Downing 1984; Paffenhöfer and Orcutt 1986; Kleppel 1993) than cultured mussels, values that are still likely to be in existence throughout the Bay of Plenty for all seasons and depths within the euphotic zone under the modelled scenario.

Despite the comprehensive NPZD modeling, one aspect that is unknown for the present situation, and that is generally overlooked or deemed difficult to appraise in other studies, is how the proposed aquaculture activity will affect phytoplankton species composition through space and time, including potential effects this may have on production and ecosystem carrying capacity. While information on chlorophyll composition through space and time is limited for the Bay of Plenty area, studies in the Hauraki Gulf, New Zealand have demonstrated the type of seasonal fluctuations that can occur. Chang *et al.* (2003) documented seasonal changes in the nature of the phytoplankton community of the open coastal and Gulf waters thought to be driven by the seasonal changes in physico-chemical conditions. During spring, the inner-shelf region of the open coastal waters support a high biomass community of large, chain-forming diatoms. As nitrogen becomes depleted, this gives way to a community of smaller diatom species and eventually to a mixed community of small diatoms, dinoflagellates, small phytoflagellates and pico-plankton late in the summer. Farther offshore, the (relatively nutrient-poor) outer shelf waters harbour lower phytoplankton biomass (consistent with the Bay of Plenty) dominated by small, motile taxa throughout the spring and summer. Within the Hauraki Gulf, the phytoplankton community is dominated by larger, autotrophic dinoflagellates in spring, but later in the year these are replaced by smaller autotrophic and heterotrophic dinoflagellates, nanoflagellates and pico-plankton.

Modelling the phytoplankton compartment of the ecosystem as a single ‘parameter’ limits the model to a single unified growth rate, limitation factor constants *etc*, while in reality the potential for the increased dominance of more rapid growing phytoplankton is very real. Without the incorporation of additional phytoplankton groups to the present model, such predictions and insights cannot be made. However, the addition of further compartments significantly increases the complexity and computational requirements for the model and also requires an entire additional calibration dataset and set of calibration parameters (Table 7.4). Without sound data on which to base these values such additional complexity cannot be expected to improve model performance.

A weakness common to all NPZD type ecological models is their inability to simulate 'top-down' grazing effects from trophic levels higher in the food chain than zooplankton. Methodologies including such groups, however, require significant simplifications of other ecosystem aspects such as temporal variability in environmental forcing and the use of constant growth or production terms (Fulton *et al.*, 2003).

7.13 SUMMARY

The potential impacts of two large (~4000 Ha each) suspended mussel farms have been simulated within the Bay of Plenty using a calibrated ecological model. Simulated phytoplankton concentrations within the Bay of Plenty indicate high productivity potential for large scale open coast mussel culture. Coastal areas between Tauranga and Whakatane are predicted to be the most productive (year-long average) within the Bay of Plenty.

At predicted stocking densities the combined effects of the farms create low level changes to phytoplankton, zooplankton, nutrient, and dissolved oxygen concentrations. Model results indicate that maximal ($\geq$ 5%) depletion impacts of two large simulated mussel farms offshore from Pukehina and Opotiki are restricted in vertical and horizontal extent to scales of similar size to the farms themselves. Impacts vary seasonally with the largest absolute Chl-a reductions being predicted during the spring bloom. However, largest relative Chl-a reductions are predicted during autumn and winter, when ambient phytoplankton concentrations are much lower and 'recovery' rates are relatively slow. Connected to this, aquaculture induced Chl-a depletion halos also extend over greater horizontal and vertical distances during autumn and winter. Typically zooplankton depletion halos are of similar magnitudes to those of phytoplankton but extend over much greater spatial extents due to their much slower growth and recovery rates. This prediction is limited, however, by a general lack of data of zooplankton ingestion by cultured mussels.

When compared to other ecosystems, both nationally and globally where bivalve culture is present, predicted depletion levels are below that considered to be an indicator of ecological carrying capacity and applied as 'acceptable limits of change'. While it is plausible that the ecological carrying capacity within the Bay of Plenty is greater than that within more restricted embayments, there are not enough similar examples (open coastal locations) from which strong conclusions can be made.

The mussel farms simulated indicate a potential to promote primary production in specific locations due to the excretion of ammonium into a nutrient limited system following the spring bloom. This has previously been brought up (Kaiser *et al.*, 1998; Smaal *et al.* 2004) no conclusive field observations of it have been made. This addition of nutrients can lead to a succession of the spring bloom with the potential to

support faster growing phytoplankton species. In its present state, however, the current model is limited in its ability to identify the phytoplankton species response as only a single phytoplankton group is simulated.

The modelling methodology developed and applied has several key advantages over those common within the published literature dealing with aquaculture based phytoplankton depletion. Advancements include the replication of non-simplified hydrodynamics, non-generalised environmental forcings (*e.g.* winds, light, temperatures), and multiple mussel cohorts; weaknesses and over-simplification in these areas are characteristic of many published studies to date (*e.g.* Raillard and Menesguen, 1994; Ross *et al.*, 1999; Chapelle *et al.*, 2000; Dowd, 2005; Grant *et al.*, 2007). In addition to these simplifications, a typical feature of many of existing models is a coarse 2-dimensional scheme through the application of 'box model' methodologies (5-10 boxes/cells per region). The present model allows for a vastly more detailed representation through its increased spatial resolution and use of full 3-dimensional space (1751 wet cells horizontally and 10 depth layers within the Bay of Plenty).